



MARTIN-LUTHER-UNIVERSITÄT
HALLE-WITTENBERG

Somatic Functions of Bicaudal-C in *C. elegans*

Dissertation

zur Erlangung des

Doktorgrades der Naturwissenschaften (Dr. rer. nat.)

der Naturwissenschaftlichen Fakultät I – Biowissenschaften

der Martin-Luther-Universität Halle-Wittenberg

vorgelegt

von Robin Selle

Gutachter: Prof. Dr. Christian Eckmann

Prof. Dr. Stefan Hüttelmaier

PD Dr. Marco Nusch

Datum der Verteidigung: 25.03.2024

Summary

Bicaudal-C (Bic-C) proteins comprise an ancient protein family that has been found to be involved in the control of cytoplasmic post-transcriptional RNA processes in several metazoan organisms. The absence of Bic-C typically leads to embryonic mortality, underscoring the importance of these developmental regulators. However, as such severe phenotypes limit the insight into a gene or respective proteins, molecular functions and biological roles of Bic-C members known for many decades remain vague. Still, multiple lines of evidence suggest both maternal and zygotic functions. In contrast to other model species commonly utilized for studying Bic-C, worms exhibit a second locus for *bic-c*, suggesting the two to have genetically diverged from each other to fulfil complementary tasks.

The present work introduces the nematode *Caenorhabditis elegans* as a model organism to study somatic aspects of Bic-C by examining the functional characteristics of the gene *bcc-1*. Remarkably, the absence of *bcc-1* facilitated through CRISPR/Cas9 did not result in any overt deviations in either the process of development or reproductive capabilities. An initial analysis regarding spatial and temporal aspects of BCC-1 was performed utilizing genetically modified alleles of *bcc-1* encoding tagged protein variants. BCC-1 expression was revealed in somatic tissue of the hypodermis in all larval stages and adults. Furthermore, no association with the germline was detected, suggesting that *bcc-1* may have a solely somatic function. Experimental assays conducted with high concentrations of salt indicated an association between *bcc-1* and the process of osmoregulation. Moreover, using genetical studies employing RNA interference has shown a repressive effect of *bcc-1* in the process of molting. Extensive RNAi experiments using various *bcc-1* alleles encoding for proteins with altered domains showed the importance of a conserved RNA-binding motif for BCC-1 function. Finally, using a Yeast-Two hybrid approach, a potential interactor of BCC-1 in the context of molting was uncovered. Given that the putatively interacting protein, MLT-3, has homology with a suggested interactor of mammalian Bic-C, it seems likely that a molecular network revolving around Bic-C has been preserved, despite significant divergences in the biological relevances across various species. While the intricacies of *bcc-1* function remain unknown, this study contributes to the understanding of Bic-C as a regulator of transcripts in general by allowing *in vivo* insights into the importance of Bic-C protein domains.

Zusammenfassung

Bicaudal-C-Proteine (Bic-C-Proteine) stellen eine uralte Proteinfamilie dar, die an der Kontrolle zytoplasmatischer posttranskriptioneller RNA-Prozesse in vielen Metazoen beteiligt ist. Das Fehlen von Bic-C führt in der Regel zum Absterben von Embryonen, was die Bedeutung dieser Entwicklungsregulatoren unterstreicht. Da jedoch solch schwerwiegende Phänotypen den Einblick in ein Gen oder die entsprechenden Proteine einschränken, bleiben die molekularen Funktionen und biologischen Rollen der seit vielen Jahrzehnten bekannten Bic-C-Mitglieder vage. Es gibt jedoch zahlreiche Hinweise, die sowohl auf maternale als auch auf zygotische Funktionen hindeuten. Im Gegensatz zu anderen Modellorganismen, die üblicherweise für die Untersuchung von Bic-C verwendet werden, weist *C. elegans* einen zweiten Locus für *bic-c* auf, was annehmen lässt, dass sich die beiden zur Erfüllung komplementärer Aufgaben voneinander genetisch entfernt haben.

In der vorliegenden Arbeit wird der Fadenwurm *Caenorhabditis elegans* als Modellorganismus zur Untersuchung somatischer Aspekte von Bic-C etabliert, indem die funktionellen Eigenschaften des Gens *bcc-1* untersucht werden. Bemerkenswerterweise führte das Fehlen von *bcc-1*, das durch CRISPR/Cas9 ermöglicht wurde, zu keinen offensichtlichen Abweichungen im Entwicklungsprozess oder in der Fortpflanzungsfähigkeit. Eine erste Analyse der räumlichen und zeitlichen Expressionsmuster von BCC-1 wurde mit Hilfe von genetisch veränderten Allelen von *bcc-1* durchgeführt, die für getaggte Proteinvarianten kodieren. Die Expression von BCC-1 wurde im somatischen Gewebe der Hypodermis in allen Larvenstadien und bei adulten Tieren nachgewiesen. Weiterhin wurde kein Zusammenhang mit der Keimbahn festgestellt, was darauf hindeutet, dass *bcc-1* eine rein somatische Funktion haben könnte. Experimentelle Untersuchungen, die bei hohen Salzkonzentrationen durchgeführt wurden, wiesen auf einen Zusammenhang zwischen *bcc-1* und dem Prozess der Osmoregulation hin. Darüber hinaus haben genetische Untersuchungen unter Verwendung von RNA-Interferenz eine repressive Wirkung von *bcc-1* auf den Prozess der Häutung gezeigt. Weitere RNAi-Experimente mit verschiedenen *bcc-1*-Allelen, die für Proteine mit veränderten Domänen kodieren, zeigten die Bedeutung eines konservierten RNA-Bindemotivs für die Funktion von BCC-1. Schließlich wurde mit Hilfe eines Hefe-Zwei-Hybridansatzes ein potenzieller Interaktor von BCC-1 im Kontext mit Häutung aufgedeckt. Durch die Tatsache, dass das mutmaßlich interagierende Protein, MLT-3, Homologie mit einem vermuteten Interaktor von Bic-C in Säugetieren aufweist, scheint es wahrscheinlich, dass ein molekulares Netzwerk rund um Bic-C evolutionär erhalten geblieben ist, trotz

erheblicher Unterschiede in den biologischen Relevanzen in verschiedenen Arten. Während die genaue Funktion von *bcc-1* ungeklärt bleibt, trägt diese Arbeit zum Verständnis von Bic-C als Regulator von Transkripten im Allgemeinen bei, indem sie *in vivo* Einblicke in die Bedeutung von Bic-C-Proteindomänen ermöglicht.

List of abbreviations

Adenylate cyclase-6	adcy6
Amino acids.....	aa
Base pairs	bp
Bicaudal-C.....	Bic-C
Bicaudal-C-1	BCC-1
Caenorhabditis Genetics Center	CGC
Clustered Regularly Interspaced Short Palindromic Repeats.....	CRISPR
Column volume	CV
Complementary DNA	cDNA
CRISPR-associated Protein 9.....	Cas9
Dalton	Da
DAN Domain BMP Antagonist Family Member 5	DAND5
Double-stranded	ds
Drop-out	SD
Dumpy.....	DPY
Excretory canal.....	EC
Feminization of germline	FOG
Fibrillarlin.....	FIB
Full length	FL
Relative centrifugal force	g
Germline development defective-3	GLD-3
GLD-3 long	GLD-3L
GLD-3 short	GLD-3S
Germ line proliferation defective	GLP
Green fluorescent protein	GFP
High instance of male.....	HIM
Intrinsically disordered region	IDR
Isopropyl-beta-D-thiogalactopyranoside.....	IPTG
Lithium acetate	LioAc
K-homology	KH
KH-like.....	KHL

Larval stage	L
Lambda phosphatase	λ PP
Liquid-liquid phase separation	LLPS
Lysogeny broth.....	LB
Maltose Binding Protein.....	MBP
Micro RNA.....	miRNA
Molecular weight.....	MW
Molting defective	MLT
Mos1-mediated Single Copy Insertion.....	MosSCI
Nematode growth media	NGM
Never in mitosis kinase like	NEKL
Nitrocellulose	NC
Open reading frame	ORF
Optical Density	OD
PBS with Tween-20	PBS-T
Phosphate buffered saline.....	PBS
Poly(A)-specific ribonuclease	PARN
Polycystin-2.....	pkd2
Polyethylenglycol.....	PEG
Polymerase chain reaction.....	PCR
Polynucleotide Kinase.....	PNK
Ponceau S red staining solution	Ponceau
Post-translational modification	PTM
Primary transcript.....	pri-miRNA
Protein kinase inhibitor	PKI
Proteinase K	PK
Recombinant BCC-1	rBCC-1
Restriction fragment length polymorphism.....	RFLP
Reverse transcription.....	RT
Revolutions per minute	rpm
Ribonucleoprotein	RNP
RNA-binding domain	RBD
RNA-binding protein.....	RBP

RNA-induced silencing complex	RISC
RNA-interference	RNAi
RNA recognition motif.....	RRM
Roller	Rol
Sterile alpha motif	SAM
Small-angle X-ray scattering.....	SAXS
Stress granule	SG
Sodium dodecyl sulfate–polyacrylamide gel electrophoresis	SDS-PAGE
Tobacco Etch Virus	TEV
Untranslated region	UTR
Wild type	WT
Yeast Two-Hybrid.....	Y2H

Table of contents

Summary	I
Zusammenfassung.....	II
List of abbreviations.....	II
Introduction.....	1
RNA-binding proteins (RBPs) modulate cellular biology	1
RBP interaction with RNA and other proteins.....	1
Bicaudal-C is a group of RNA regulators containing KH and SAM domains separated by a disordered region	3
A conserved KH-domain of Bic-C is linked to RNA binding.....	3
The SAM domain of Bic-C is connected to polymerization	4
Functions of the IDR in Bic-C remain vague.....	5
Bic-C-mediated RNA regulation in different systems.....	5
Bic-C is essential and plays a role in the germline and the soma	7
The <i>C. elegans</i> genome encodes for two loci of Bicaudal-C, <i>gld-3</i> and <i>bcc-1</i>	8
<i>gld-3</i> is essential for germline survival	9
Putative characteristics of <i>bcc-1</i>	9
Aims of this thesis.....	12
Materials and Methods	13
Materials	13
Media, solutions, lab made buffers and plates	13
Worm work	13
Bacterial work.....	13
Western blotting solutions	13
Expressing and purifying recombinant BCC-1 (rBCC-1)	14
Affinity purification	14
Yeast media	14
Methods.....	15

General worm handling	15
Crossing	15
Genotyping of worms	15
Bleaching.....	16
Salt stress experiments.....	17
Genome editing.....	17
CRISPR/Cas9	17
MosSCI.....	18
Microscopy	19
RNA interference (RNAi) induced by feeding	20
RNAi-mediated knockdown experiments	23
Yeast Two-Hybrid (Y2H) experiments	24
Expression of recombinant(r) BCC-1	27
Protein Quantification.....	30
Bioinformatic tools	31
Results.....	33
Various alleles were generated to characterize <i>bcc-1</i>.....	33
Polyclonal rabbit serum contains antibodies with specificity against BCC-1	34
Generated BCC-1 variants can be detected using α -BCC-1	40
BCC-1 is a somatic protein expressed in the epidermis of animals	42
Loss of <i>bcc-1</i> has no effect on fertility.....	42
BCC-1 is expressed in all larval stages, but not detectable in the embryo.....	43
BCC-1 expression levels do not change significantly throughout the first larval stage	45
BCC-1 expression is unaffected by removal of germ line tissue	46
BCC-1 is expressed in the hypodermis of <i>C. elegans</i>	47
Spatial BCC-1 expression in L1 larvae resembles those of later stages	53
BCC-1 is a cytosolic protein	55
BCC-1 has a role in osmoregulation	56
Loss of <i>bcc-1</i> effects salt stress recovery rate.....	56
mCherry::BCC-1 localizes to granular foci upon stress	57
BCC-1 is not detected in the excretory canal.....	61
BCC-1 is not essential for male mating	62
BCC-1 is expressed in male tissue required for mating.....	62
<i>bcc-1</i> mutants mate no worse than wild-type males	64
<i>bcc-1</i> has a role in molting	66
BCC-1 physically interacts with the molting factor MLT-3	66

<i>bcc-1</i> genetically interacts with hypodermal molting factors	69
Discussion	81
The conserved N- and C-terminus of BCC-1 contribute to its function.....	81
The N-terminus of BCC-1 requires flexibility	81
BCC-1 likely binds RNA <i>in vivo</i> and is associated with the Ccr4-Not complex	83
BCC-1 functions likely through SAM-SAM interactions	85
<i>bcc-1</i> and <i>gld-3</i> are rather complementary than redundant genes	86
<i>bcc-1</i> has a conserved role in osmoregulation	88
Molting emerges as a role Bicaudal-C	89
Literature	95
Appendix	107
Table S1: Materials used in this study	107
Table S2: worm strains used in this study	108
Table S3: Oligonucleotides designed and used in this work	109
Table S4: List of enzymes used in this study.....	111
Table S5: Single guide (sg)RNAs and repair templates for CRISPR/Cas9-based alleles ...	112
Table S6: List of kits used in this study.....	112
Table S7: MosSCI co-injection markers.....	112
Table S8: Transgenes used to generate MosSCI-based strains	112
Table S9: Plasmids for non-genome editing used in this study	113
Table S10: Microbe strains used in this study	113
Table S11: Antibodies used in this thesis	114
Eidesstattliche Erklärung.....	115
Curriculum vitae	116

Introduction

RNA-binding proteins (RBPs) modulate cellular biology

RBPs are a highly diverse group of proteins involved in regulating gene expression at the post-transcriptional level. Such regulation is essential to ensure proper cellular metabolism, maturation, transport, stability and degradation of both coding and non-coding RNAs (Gerstberger et al. 2014). Rather than alone, RBPs often act together to regulate the fate of their targets and build up controlled networks, leading to the formation of Ribonucleoprotein (RNP) complexes (Seufert et al. 2022). Such an assembly can lead to microscopically visible membrane-less organelles, known as RNP granules, often formed through liquid-liquid phase separation (LLPS) (Ripin and Parker 2023). Some RNP granules, like the nucleolus, nuclear speckles or and paraspeckles, are constitutively seen in cells, but others, like stress granules (SGs) or processing bodies (P bodies) only get formed, or increase their size during states of translational repression (Putnam et al. 2023; Protter and Parker 2016). SGs form when translation initiation is inhibited by either chemicals or by stress response (Protter and Parker 2016). SGs therefore contain predominantly mRNAs that are stalled at translation initiation, translation initiation factors and a variety of RBPs and non-RNBs. Yet, at least concerning mammalian systems, SGs have been shown to be a highly dynamic system subjecting to fusion, fission, and flow (Kedersha et al. 2005). P bodies contain mRNAs associated with translational repressors and the mRNA decay machinery. In mammals, this repression apparatus was shown to contain decapping enzymes and the CCR4/NOT complex, making it a key player in mRNA decay (Parker and Sheth 2007; Collart and Panasenko 2012). The formation of RNP complexes of any kind is dependent on protein-RNA and protein-protein interactions which are mediated by specific functional domains (Ripin and Parker 2023). Often the presence of modularity in RBPs results in an increase of versatility in both RNA-binding capabilities and functional properties (Lunde et al. 2007).

RBP interaction with RNA and other proteins

RBPs typically contain discrete RNA-binding domains (RBD). Often a single RBP contains more than one binding domain, enhancing specific RNA-binding (Cléry and Allain 2013; Lunde et al. 2007). Moreover, linkers between domains have been shown to mediate RNA association, and their flexibility can affect whether adjacent RNA-binding domains bind independently or cooperatively (Lunde et al. 2007). Prominent RBDs include the RNA

recognition motif (RRM), the zinc-finger domain and the hnRNP K homology (KH) domains (Cléry and Allain 2013; Lunde et al. 2007).

The KH domain is about 70 amino acids in length and is often found in proteins related to transcriptional regulation and translational control (Cléry and Allain 2013). KH domains are usually found in multiple copies; however, some proteins exhibit only one (Valverde et al. 2008). While two types of KH domains exist, both are enabled to bind RNA through a minimal motif consisting of two β -sheets and two α -helices with a characteristic binding cleft in the center (Valverde et al. 2008). This loop region, consisting of four amino acids with two being flanking glycines, is called a GXXG motif and interacts with the nucleic acid of target RNAs (Nicastro et al. 2015). Interestingly, KH domains crystallize as monomers, dimers, or tetramers, which led to the proposal that the functional form of certain KH domains could be dependent on higher-order oligomers (Valverde et al. 2008).

Direct protein-protein interaction in the context of RNPs has a vital impact on cellular processes. Through specific motifs, RBPs can interact with other RBPs, for example, to jointly regulate RNA-binding partners, and with non-RBPs that are recruited to RNA by the RBP interactor (Seufert et al. 2022). One specific protein responsible for forming larger, granule-like structures through homo- and heterooligomerization is the sterile alpha motif (SAM) (Qiao and Bowie 2005). SAM domains were named after their predicted α -helical fold and their role in sexual differentiation in yeast, where they were first discovered (Ponting 1995). Yeast contains four SAM domain containing genes, which are essential for sexual differentiation and in which specific mutations induce sterility (Ponting 1995). After their initial discovery they have been found in many eukaryotes, where the number of SAM containing proteins roughly correlates with the complexity of the organism (Qiao and Bowie 2005). Structurally, SAM domains consist of about 70 amino acids usually organized in a five-helix bundle (Peterson et al. 1997). The most common interaction SAM–SAM topology is referred to as the “head to tail” or ML/EH arrangement (Mercurio et al. 2020). In this configuration, the C-terminal helix (end helix, EH) and adjacent loops of one SAM attach to central region (mid loop, ML) of another SAM (Mercurio et al. 2020). While studies have shown that SAM domains can bind RNA, they are better known as protein-protein interaction domains, able to form helical structures with other SAM domains (Green et al. 2003; Kim et al. 2002).

Bicaudal-C is a group of RNA regulators containing KH and SAM domains separated by a disordered region

Bicaudal-C (Bic-C) represents a conserved family of RNA regulators found in RNP granules and characterized by a modular structural organization containing both KH- and SAM domains (Seufert et al. 2022; Mahone et al. 1995; Wessely and Robertis 2000). Bic-C was first shown to be a vital factor of embryogenesis in *Drosophila*, associated with a double-abdomen (bicaudal) phenotype (Bull 1966; Mohler and Wieschaus 1986). Canonical Bicaudal-C members display structured features consisting of five repeats resembling (KH) domains at the N-terminus and a SAM at the C-terminus (Eckmann et al. 2002). Both are separated by a distinct region of intrinsic disorder (IDR). A graphical representation of Bic-C proteins is shown in **Figure 1**.



Figure 1: Archetypical domain structure of Bicaudal-C proteins. Five protein K homology type (KH-type) domains are separated from a Sterile Alpha Motif (SAM) by an Intrinsically Disordered Region with a Serine-rich sub region in between.

A conserved KH-domain of Bic-C is linked to RNA binding

While KH domains typically contain a GXXG motif (Valverde et al. 2008), not necessarily every domain predicted to fold in a KH-domain like manner exhibits this feature. As this is also true for Bicaudal-C proteins; corresponding domains, irrespective of a GXXG, are addressed as KH-*type* domains in this thesis. In the past, various KH-type domain boundaries and respective GXXG loops were proposed for different Bic-C proteins (Gamberi and Lasko 2012; Nakel et al. 2010). The resulting issue of conflicting boundaries was resolved by SAXS and crystallography, resulting in the so far only available crystal structure of Bic-C KH-type domains using *germline development defective-3* (GLD-3) protein in *C. elegans* (Nakel et al. 2010). The corresponding assignments also lead to a nomenclature discriminating between true KH-domains, carrying a GXXG motif, and KH-like (KHL) domains that don't (Gamberi and Lasko 2012).

Importantly, the most conserved GXXG motif in Bicaudal-C proteins appears to be in KH-type domain 2, as it is found in invertebrates (flies, worms), as well as in the vertebrate

system (zebrafish, frog, mouse). An alignment of KH-type domain 2 for several species is given in **Figure 2**.

```

Hs RVTLKMDVSHTEHSHVIGKGGNNIKKVMEEETGCHIHFPSNRNNQAEKSNQVSIAGQPAGVESARVRIR
Mm RVTLKMDVSHTEHSHVIGKGGNNIKKVMEEETGCHIHFPSNRNNQAEKSNQVSIAGQPAGVESARVRIR
Xl RVTLKMDVSHTEHSHVIGKGGNNIKKVMEEETGCHIHFPSNRNNQAEKSNQVSIAGQPAGVESARVRIR
Ce RVSLKMEELHSHLHSHIIGKGGGRGIQKVMKMTSCHIHFPDSNKYSDSNKSDQVSIISGTPVNVFEALKHLR
Dm RVIMKMDVSYTDHSYIIGRGGNNIKRIMDDTHTHIHFPDSNRSNPTEKSNQVSLCGSLEGVERARALVR
Dr RVTLKMDVSHTEHSHVIGKGGHNIKRVMEETGCHIHFPSNRHSQAEKSNQVSIAGQLTGVEAARVKIR

```

Figure 2: Sequence alignment of the KH-type 2 of Bicaudal-C proteins from selected species. Identical amino acids between human (*Hs*), mouse (*Mm*), frog (*Xl*), worm (*Ce*), fly (*Dm*) and zebrafish (*Dr*) in green, a conserved GXXG motif is indicated in teal. For *C. elegans*, only KH2 of BCC-1 but not of GLD-3 is displayed with red asterisks indicating a second GXXG motif not conserved in other species. After: (Dowdle et al. 2022).

Notably, not only the flanking glycines of the motif are highly conserved, but also the residues in between consisting of a positively charged residue (lysine in all cases except *Drosophila*) and another glycine. This constraint for positive charges hints at interactions with negatively charged molecules, such as the backbone of RNA species. Moreover, studies in the frog system have revealed that KH-type 2 is necessary and sufficient for RNA-binding, both *in vivo* and *in vitro* (Dowdle et al. 2019).

While KH-type domain is likely important for RNA-binding, it remains vague why Bic-C possesses 5 KH-type domains in all models studied (Gamberi and Lasko 2012) and has kept them throughout millions of years of evolution. Studies in frog embryos indicate a supporting effect of adjacent KH-type domains (Dowdle et al. 2019). Crystal structure analysis from the Bicaudal-C protein GLD-3 in *C. elegans* furthermore demonstrates that KH-type domains 2, 3, 4 and 5 form a globular structural unit, indicating that the domains have functions relying on a 3-dimensional topology (Nakel et al. 2010). This idea is consistent with temperature-sensitive missense mutations of Bicaudal-C in worms and flies where central glycines have been replaced with more space-occupying arginines, leading to inactive protein at higher temperatures, presumably because of disturbed globular arrangements (Rybarska et al. 2009).

The SAM domain of Bic-C is connected to polymerization

With the exception of GLD-3, all members of Bicaudal-C in model organisms contain a SAM domain at their C-terminal end (Eckmann et al. 2002; Gamberi and Lasko 2012). Human Bic-C protein (BICC1) has been demonstrated to spontaneously form polymers *in vitro* (Knight et al. 2011). Regarding SAM-SAM interaction with other proteins, Yeast-Two

hybrid studies on mammalian Bic-C proposed two interactors; the Ankyrin and SAM containing proteins ANKS3 and ANKS6, which also interact with each other (Leal-Esteban et al. 2018). In this network, BICC1 and ANKS3 bind one another through a heterodimerization of their SAM domains and through contacts involving at least the KH domains (Stagner et al. 2009; Rothé et al. 2018). ANKS6 is hypothesized to bind the SAM of ANKS3 with much higher affinity compared to BICC1 (Leettola et al. 2014). Through studies involving crystallography of a BICC1 SAM polymer, a 3D model was put forward in which ANKS3 recruited ANKS6 to BICC1, and the three proteins together cooperatively generated large, macromolecular complexes (Rothé et al. 2018). These giant scaffolds are suggested to be shaped by SAM domains, their flanking sequences, and SAM-independent protein-protein and protein-mRNA interactions (Rothé et al. 2018). Through computational predictions, yeast work and pulldowns, a model was generated in which ANKS6 facilitates the release of the BICC1 SAM from BICC1-ANKS3-ANKS6 heterooligomers through the sequestration of the ANKS3 SAM domain (Rothé et al. 2023). As ANKS3 and ANKS6 have homologs in many systems, including *C. elegans* (Lažetić and Fay 2017a), the question arises whether a corresponding interaction cluster exists outside of vertebrates.

Functions of the IDR in Bic-C remain vague

All established Bic-C members have retained an intrinsically disordered region (IDR) of variable length (Eckmann et al. 2002; Gamberi and Lasko 2012). While *C. elegans* BCC-1 exhibits the most truncated IDR, it still has a considerable length of about 160 amino acids (Eckmann et al. 2002). Additionally a strong conservation of a subregion enriched in serine residues within the IDR can be made out in Bic-C members (Eckmann et al. 2002). These observations imply that the IDR carries out a more specialized function than serving as a mere linker between the structured N- and C-terminal domains. However, literature has focused on addressing molecular or biological aspects regarding the disorder in Bic-C proteins so far.

Bic-C-mediated RNA regulation in different systems

Although Bic-C has been studied in multiple systems, surprisingly little is known about its RNA-regulating roles and its corresponding RNA targets. In flies, where the first Bic-C member (BicC) was discovered, KH-domain mutations were found to lead to *in vivo* loss-of-function, associating the BicC protein with RNA-binding (Mahone et al. 1995). Evidence that BicC functions as a translational repressor was derived from findings that BicC loss-of-function mutations affect anterior-posterior patterning as a result of ectopic and premature translation of the oskar protein, a factor determining the posterior (Saffman et al.

1998). Immunoprecipitation experiments using ovarian extracts of *Drosophila* were also the first to demonstrate that BicC associates with the NOT3/5 subunits of the CCR4-NOT complex (Chicoine et al. 2007). As the interaction of BicC with the NOT3/5 protein was also detected using a recombinant protein strategy in *E. coli*, this association was suggested to be a direct one (Chicoine et al. 2007). BicC mutations in fly embryos are reported to impact the length of the poly(A) tails of target mRNAs (Chicoine et al. 2007). In total, this lead to a model in which BicC recruits the CNOT complex to mRNAs and impacts their translation by poly(A) removal (Chicoine et al. 2007). One important RNA species being bound by BicC is proposed to be *d-myc* mRNA (Gamberi et al. 2017). Ectopic overexpression of d-Myc was shown to be lethal to flies; with few exceptions exhibiting deformations in Malpighian tubules, the kidney equivalent of flies (Gamberi et al. 2017).

In frogs, the Bic-C protein Bicc1 has been proposed as regulator of maternal mRNA translation (Zhang et al. 2009; Zhang et al. 2013). Bicc1 was demonstrated to bind *criptol* mRNA and a respective binding site of 32 nucleotides was proposed to facilitate the binding *in vivo* and *in vitro* (Zhang et al. 2013; Zhang et al. 2014; Dowdle et al. 2017). Notably, the RNA binding surface in *criptol* mRNA is predicted to form a stem-loop and both, the sequence of the loop as well as the stem properties, were found to be important for RNA binding (Dowdle et al. 2019; Zhang et al. 2014).

In mice, immunoprecipitation experiments suggest an association of the murine Bicc1 protein with mRNA species encoding for adenylate cyclase-6 (*adcy6*) and protein kinase inhibitor (PKIa) (Piazzon et al. 2012). The respective proteins are also upregulated in mouse kidney tubules of Bicc1 knockouts, substantiating the idea of Bicc1 as a repressor of translation (Piazzon et al. 2012). Further studies lead to a model hypothesizing that silencing of *Adcy6* mRNA by Bicc1 depends on the KH domains to bind the 3' UTR, and on self-polymerization of the SAM domain to concentrate Bicc1 and target mRNAs in cytoplasmic granules (Piazzon et al. 2012; Rothé et al. 2015). Recent studies also identified mouse *dand5* as a Bicc1 regulated mRNA and an important component of the Left-Right patterning pathway (Minegishi et al. 2021). Furthermore, Bicc1 has been put forward as a regulator of *Pkd2* transcript levels (Lemaire et al. 2015). Mutations in the *Pkd2* protein are associated with fluid filled cysts in kidneys (Tran et al. 2010), and Bicc1 mouse embryos were reported to exhibit lower *Pkd2* mRNA and corresponding protein. It was suggested that Bicc1 interferes with repression of *Pkd2* transcript by antagonizing the function of a miRNA (Tran et al. 2010). As *Pkd2* encodes for a member of the transient receptor potential superfamily (Tran et

al. 2010), the Pkd2 protein has orthologs in many species, even in animals without a kidney structure in the vertebrate sense, like *C. elegans* (Barr and Sternberg 1999). Whether a similar regulation in invertebrates exists is not known so far.

Furthermore, murine Bicc1 was demonstrated to co-immunoprecipitate with both the murine CNOT1 and CNOT3 proteins (Minegishi et al. 2021). These interactions were demonstrated to depend upon the KH domains, but not the SAM domain or the presence of RNA (Minegishi et al. 2021). Subsequently, a model was proposed in which Bicc1 engages with the CNOT complex to regulate *dand5* mRNA (Minegishi et al. 2021). However, Bicc1 has no effect on the poly(A) tail length of its presumed Adcy6 target mRNA in a mouse model (Piazzon et al. 2012). This suggests a different mechanism of Bic-C function compared to what has been proposed from flies.

Other experiments suggest that Bicc1 also interacts with micro RNAs (miRNAs) and related protein components to facilitate the repression of mRNA (Piazzon et al. 2012). It is hypothesized that Bicc1 is required downstream of Dicer, an enzyme processing hairpin-containing primary transcript (pri-miRNA). In this model, Bicc1 mediates an interaction between the Ago2 protein and mRNA targets (Piazzon et al. 2012). This interaction was proposed to be SAM-dependent (Piazzon et al. 2012). The Dicer enzyme was also proposed to play a role in the regulation of the *dand5* mRNA mentioned above (Maerker et al. 2021). Lastly, the interaction of both ANKS (ANKS3 and ANKS6) proteins with Bicc1 seems also important for the regulation of *dand5*, as mutations in the SAM of ANKS3 are reported to result in Bicc1-mediated decay of *dand5* mRNA (Rothé et al. 2023).

Bic-C is essential and plays a role in the germline and the soma

On the biological scale, loss of *Bic-C* genes across all metazoans usually leads to dead or severely deformed animals, as it serves important developmental roles (Wessely and Robertis 2000; Park et al. 2016; Maisonneuve et al. 2009; Tran et al. 2010). Research on Bic-C in flies suggested that the protein fulfills maternal as well as zygotic functions (Krasnow et al. 1989; Kugler et al. 2009; Snee and Macdonald 2009; Chicoine et al. 2007). Such maternal functions of Bic-C in Oo- and embryogenesis are also found in vertebrates, where endoderm formation and left/right patterning is associated with Bic-C (Park et al. 2016; Wessely and Robertis 2000). In mice, null mutations of Bic-C lead to embryonic lethality in the majority of cases, survivors have been reported to die within the first 14 days after birth (Maisonneuve et al. 2009).

Beyond the essentiality of Bic-C in embryogenesis, multiple lines of evidence also point to a somatic role of Bic-C in maintaining kidney function. *Drosophila* Bic-C is associated with maintaining the Malphigian tubules, the kidney equivalents of flies (Gamberi et al. 2017). Decreased Bic-C expression in the kidney pendants of frogs and zebrafish leads to cysts and defects in these structures (Tran et al. 2010; Bouvrette et al. 2010). Mammalian Bicaudal-C protein is found in several tissues including the neural tube epithelium as well as the pancreas primordium nephric tissue (Tran et al. 2010; Lemaire et al. 2015; Lian et al. 2014). The expression in kidney tissue is consistent with the finding that mice with mutations in Bic-C often suffer from kidney cysts (Piazzon et al. 2012). Moreover, reduced amounts of human Bic-C are connected to polycystic kidney disease and renal developmental abnormalities (Seufert et al. 2022). The reminiscent somatic functions of Bic-C in several taxa strongly indicate that the protein has –in addition to its maternal/germline function – a conserved function related to renal structures. Yet, while several data points demonstrate the importance of Bic-C for kidneys and their equivalents, underlying protein networks remain vague.

The *C. elegans* genome encodes for two loci of Bicaudal-C, *gld-3* and *bcc-1*

While Bic-C is present and highly conserved in all metazoan model organisms, studies have primarily been conducted in flies and vertebrates (Dowdle et al. 2022). However, to illuminate common biological roles and molecular functions of Bic-C in general, the invertebrate *C. elegans* also deserves attention. While all animal model systems mentioned above carry one locus for Bicaudal-C, *C. elegans* contains two: *gld-3* and *bcc-1*. A visual comparison of the gene products derived from both *bic-c* loci in *C. elegans* is given in **Figure 3**.

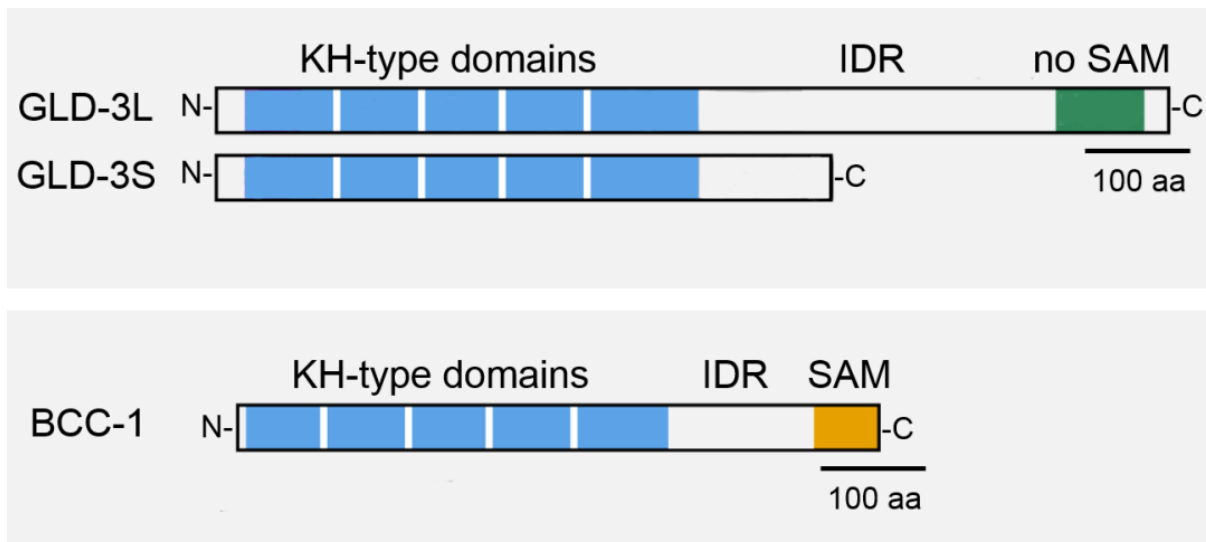


Figure 3: Stick diagrams of gene products of Bicaudal-C loci in *C. elegans*. GLD-3 exists in two alternate versions, long(L) and short(S). Both BCC-1 and GLD-3 contain 5 KH-type domains and a region of intrinsic disorder (IDR). While BCC-1 maintains the canonical SAM domain, GLD-3 possesses a different protein-protein interaction surface at the C-terminus.

***gld-3* is essential for germline survival**

gld-3 encodes for multiple variants of GLD-3, with the most abundant being two isoforms, GLD-3L (long) and GLD-3S (short) (Eckmann et al. 2002). The long and short isoforms are the result of alternative splicing of *gld-3* transcript and both contain the N-terminal KH-type domains (Eckmann et al. 2002). However, the short GLD-3 lacks the protein-protein interaction domain (which is not a SAM) and large parts of the IDR (Eckmann et al. 2002). While both isoforms are predominantly found in the germline of adult worms, GLD-3S is found most abundant in the embryo (Eckmann et al. 2002). As indicated by its spatial expression pattern, GLD-3 plays an essential role in germline survival, progression through meiosis and early embryogenesis (Eckmann et al. 2002). Molecularly, GLD-3 is a subunit of the cytoplasmic poly-A polymerase GLD-2 (Wang et al. 2002; Nakel et al. 2015; Nousch et al. 2013). GLD-3 is suggested to bind via its unfolded KH-type domain 1, which elevates low intrinsic enzymatic activity of GLD-2, resulting in a better capability to adenylate mRNA targets (Nakel et al. 2015). While this mechanism makes GLD-3 an RNA-regulator, it should be noted that none of its KH-type domains contain GXXG motifs and that the GLD-3 protein itself binds RNA poorly (Nakel et al. 2010).

Putative characteristics of *bcc-1*

Contrary to *gld-3*, very little is known about *bcc-1*. The locus of *bcc-1* resides on chromosome IV (position 4.85) and contains 15 predicted exons according to www.wormbase.org. RT-PCR has validated a predicted transcript (M7.3) corresponding to

bcc-1, therefore the gene is currently predicted to encode for a single protein, BCC-1, with a size of 644 aa and a corresponding theoretical weight of ~72 kDa (Eckmann et al. 2002). Whether *bcc-1* activity is essential for animal development and/or fertility is not known, but RNA interference (RNAi) experiments against *bcc-1* suggest a moderate reduction brood size (Haskell and Zinovyeva 2021). Moreover, how the protein domains of BCC-1 contribute to its function remains to be investigated. However, a *C. elegans* study on the receptor kinase ROL-3 used a transcriptional reporter and found *bcc-1* expressed in the major hypodermis. (Jones et al. 2013), suggesting a somatic function of the gene. The same study also showed that a deletion in the *bcc-1* genes suppresses phenotypes associated with reduced *rol-3* activity, which the authors suggest to be due to *bcc-1* being a putative translational repressor (Jones et al. 2013). The precise developmental role of ROL-3 is uncertain; nonetheless, mutations in *rol-3* have been seen to result in aberrations in overall morphology, characterized by the emergence of a roller (Rol) phenotype (Simmer et al. 2003; Brenner 1974). Furthermore, *rol-3* also plays a crucial role in development, since alleles leading to a severe reduction of its genetic activity result in a premature halt in the growth process at larval stages (Johnsen and Baillie 1991). Interestingly, the rescuing effect of *bcc-1* loss is reported to be dependent on residual ROL-3 activity (Jones et al. 2013). How the genetic connection between *bcc-1* and *rol-3* might translate to specific molecules is currently unknown.

As *bcc-1* was reported to be expressed in the hypodermis, considering the biological roles of this tissue might reveal putative functions of BCC-1 in the worm. The hypodermis of *C. elegans* consists of a small number of cells with multiple roles in physiology. The worms' body is largely covered by a single epidermal cell, called hyp7. Additional cells fuse with hyp7 in each larval stage, so that in adults hyp7 contains 139 nuclei, more than 4/5 of all epidermal nuclei (Chisholm and Hsiao 2012). The hypodermis in general performs many functions during early development, including establishing the basic body plan and can therefore be considered an important area for development (Johnstone and Barry 1996). Furthermore the hypodermis -and hyp7 in particular- carry out two essential tasks for the worm, namely osmoregulation and molting.

***bcc-1* and osmoregulation**

Maintaining the salt/water balance and facilitation of waste elimination is predominantly the role of the excretory canal (EC) cell, which has been presumed to be the *C. elegans* equivalent of excretory organs in other organisms (Nelson and Riddle 1984). While the hypodermis is to a certain extent shielded from the environment by the cuticle, the two

tissues are connected by so called hemidesmosomes (Francis and Waterston 1991). Accordingly, the hypodermis is not only connected to the EC, it also experiences hyper- or hypoosmotic stress from external sources (Iguar Gil et al. 2017). Yet, whether *bcc-1* is expressed in the EC cell or has a role in osmoregulation is currently not known.

***bcc-1* and molting**

A second essential task of the hypodermis is the secretion of the cuticle (Chisholm and Hsiao 2012). The *C. elegans* cuticle is a complex apical extracellular matrix containing proteins, lipids, and sugars. It serves several important functions including protection from the environment and pathogens (Lažetić and Fay 2017b). This barrier however needs to be shed and resynthesized in each larval developmental stage (Riddle et al. 1997). Such a molting procedure is not exclusive to *C. elegans*, but is in general an essential step of development for members of the superphylum Ecdysozoa involving other nematodes and all arthropods (Aguinaldo et al. 1997). Yet, molecular mechanisms of molting remain relatively poorly understood in general. In *C. elegans*, molting is perceived as a two-phase process, consisting of lethargus (including apolysis and synthesis) and ecdysis (Singh and Sulston 1978; Page and Johnstone 2007). During apolysis, the worm partially detaches its old cuticle, which then allows for the synthesis of an underlying new cuticle by the hypodermis. During ecdysis, a series of stereotypical movements lead to the complete detachment of the old cuticle, followed by the resumption of normal feeding and activities (Singh and Sulston 1978; Page and Johnstone 2007; Chisholm and Hsiao 2012). As molting is still a phenomenon being investigated, two genes associated with molting deficiencies, *mlt-2* and *mlt-3*, have been described (Lažetić and Fay 2017a). Interestingly, their gene products appear to encode for homologs of the mammalian proteins ANKS6 or ANKS3. However, no connection of Bic-C to either MLT protein is reported to date.

Aims of this thesis

This thesis investigates BCC-1 as a Bicaudal-C protein family member and assumes the hypothesis that both *bic-c* genes in *C. elegans*, *gld-3* and *bcc-1*, originated from the same genetic locus through a gene duplication event. As a result, the two genes might have diverged from one another, to fulfill specific tasks. As *gld-3* has been shown to fulfill essential roles in the germ line, this study focuses on the relevance of *bcc-1* in a somatic context. First, *bcc-1* expression will be verified on the protein level using western blot and by generating an affinity purified antibody solution recognizing BCC-1. Then, a basic characterization of the temporal and spatial expression patterns of BCC-1 will be conducted utilizing developmental western blots and confocal microscopy of fluorescently tagged *bcc-1* alleles. Furthermore, this study focuses on a putatively conserved role of *bcc-1* in osmoregulation by conducting experiments using high salt concentration. Moreover, a connection of *bcc-1* to the process of molting is investigated. To this end, potential physical and genetical interactors will be evaluated using either a Yeast-Two hybrid approach or an RNAi setup. Lastly, through the generation of various *bcc-1* alleles using CRISPR/Cas9, the importance of several BCC-1 domains and motifs is studied in a quantifiable way. Taken together, this thesis aims to introduce *C. elegans* as a valuable model organism for *in vivo* research of Bic-C with an emphasis on the soma and to substantiate the understanding of molecular functions and biological roles of Bicaudal-C proteins in general.

Materials and Methods

Materials

A list of consumables used in this study is given in Table S1.

Media, solutions, lab made buffers and plates

Worm work

Nematode growth media (NGM) plates: 50 mM NaCl, 0.25% Bacto Peptone, 2% agar, 0.0005% cholesterol, 1mM CaCl₂, 1 mM MgSO₄, 25 mM PBS pH 6.0.

High salt plates: 500 mM NaCl, 0.25% Bacto Peptone, 2% agar, 0.0005% cholesterol, 1mM CaCl₂, 1mM MgSO₄, 25mM PBS pH 6.0.

RNAi feeding plates: 50 mM NaCl, 0.25% Bacto Peptone, 2% agar, 0.0005% cholesterol, 1mM CaCl₂, 1mM MgSO₄, 25 mM PBS pH 6.0, 1mM IPTG.

M9 Buffer: 22mM KH₂PO₄, 42mM Na₂HPO₄, 86mM NaCl, 1mM MgSO₄.

Bleaching solution: 50% 4 M NaOH, 50% Sodium hypochlorite solution (~6-13%).

Proteinase K (PK) buffer (1x): 50 mM KCl, 10 mM Tris-HCl, 2.5 mM MgCl₂, 0.45% NP40, 0.45% Tween-20, 0.01% gelatine.

PCR buffer for genotyping (1x): 10 mM KCl, 10 mM (NH₄)₂SO₄, 20 mM Tris pH 8.8, 1.5 mM MgCl₂, 0.1% Triton X-100.

DNA loading buffer (1x): 0.025% bromophenol blue, 0.025% Xylene cyanol, 5% glycerol.

TBE buffer: 0.4 mM EDTA, 17.8 mM boric acid.

Bacterial work

LB media: 1% tryptone, 0.5% yeast extract, 86 mM NaCl.

LB agar media: 1% tryptone, 0.5% yeast extract, 86 mM NaCl, 0.5% agar.

SOC media: 2% tryptone, 0.5% yeast extract, 8.6 mM NaCl, 20 mM glucose, 25 mM KCl, 10 mM MgCl₂, pH 7.0.

Western blotting solutions

Stacking gel mix: 150 mM Tris-HCl pH 6.8, 5% acrylamide/bis-acrylamide (19:1), 0.1% SDS.

SDS running buffer (10x): 25 mM Tris-HCl pH 8.3, 192 mM glycine, 0.1% SDS.

SDS sample buffer (4x): 250 mM Tris-HCl pH 6.8, 8% SDS, 40% glycerol, 0.02% bromophenol blue, 5% 2-mercaptoethanol.

Coomassie Brilliant Blue gel staining solution: 0.1% Coomassie Brilliant Blue R-250 dye, 10% acetic acid, 50% ethanol.

Western Blotting buffer (10x): 25 mM Tris pH 8.3, 192 mM glycine.

PBS pH 7.4 (1x): 2.7 mM KCl, 137 mM NaCl, 2 mM KH₂PO₄, 10 mM Na₂HPO₄.

PBS-T: 0.05% Tween-20 in PBS pH 7.4.

Blocking solution: 5% skimmed milk powder in PBS-T.

Antibody incubation buffer: 0.5% skimmed milk powder in PBS-T.

Membrane stripping solution: 2% acetic acid, 0.5% SDS.

Expressing and purifying recombinant BCC-1 (rBCC-1)

rBCC-1 lysis/equilibration buffer: 20 mM Tris-HCl pH 7.4, 200 mM NaCl, 1 mM EDTA, 10% glycerol.

rBCC-1 washing buffer: 20 mM Tris-HCl pH 7.4, 200 mM NaCl, 1 mM EDTA, 10% glycerol, protease inhibitor cocktail.

rBCC-1 elution buffer: 20 mM Tris-HCl pH 7.4, 200 mM NaCl, 1 mM EDTA, 10% glycerol, 50 mM maltose, protease inhibitor cocktail.

Affinity purification

Acidic antibody elution buffer: 100 mM glycine-HCl pH 2.4.

Basic antibody elution buffer: 100 mM ethanolamine pH 11.5.

High salt antibody elution buffer: 50 mM Tris-HCl pH 7.4, 3 M MgCl₂.

Yeast media

YPDA medium: 2% Bacto Peptone
20 mM glucose
1% yeast extract
0.37 mM adenine

YPDA plates: 2% Bacto Peptone
2% glucose
0.5% yeast extract
0.37 mM adenine
1% agar

Drop out (SD) medium:	2.7% DOB medium 0.064% CSM –Leu-Trp dropout mix 0.74 mM adenine
SD-Leu-Trp plates:	4.4% DOB medium 0.064% CSM –Leu-Trp dropout mix 0.74 mM adenine
Transformation mix:	114 mM lithium acetate 76% Polyethylenglycol (PEG) 3350 solution 13% Freshly denatured salmon sperm DNA solution
Z-buffer (pH 7.0):	60 mM Na ₂ HPO ₄ 40 mM NaH ₂ PO ₄ 10 mM KCl 1 mM MgSO ₄
+ X-Gal	65 μM Bromo-chloro-indolyl-galactopyranoside

Methods

General worm handling

All nematode strains were kept according to standard procedures on 6 cm NGM plates spotted with OP50 *E. coli* at 20 °C, unless stated otherwise (Brenner 1974). In all experiments, Bristol N2 was used as wild type *C. elegans*. A list of worm strains used in this study is given in Table S2.

Crossing

For temperature sensitive alleles, crosses were performed at 16 °C. Hermaphrodites (2-5) were paired with up to 20 males on 3.5 cm NGM plates containing a small amount of OP50, taken from a standard spotted NGM plate. After 24 hours, hermaphrodites were individually placed on separate OP50-seeded NGM plates (=singled). During the next two days, F1 progeny was analysed for male presence to evaluate crossing effectiveness. F1 worms from successfully crossed hermaphrodites were singled again at the L4 stage. F2 worms from singled F1 mothers were again singled at the L4 stage, allowed to lay eggs, and subjected to genotype assessment (genotyping).

Genotyping of worms

To screen for animals carrying desired genotypes and to confirm homozygosity, a PCR-based approach was used unless visual markers were applicable. To this end, 8 μ l containing ≥ 12.8 mU of PK enzyme (DMC units according to manufacturer) in PK buffer were aliquoted into PCR tubes. Individual adults were then transferred into the filled PCR-tubes and frozen solid at -80 °C. Tubes were then transferred to a thermocycler (Biometra) where the samples were first heated to 65 °C for 75 minutes to allow for proper enzymatic digest and then heated to 95 °C for 15 minutes to inactivate the enzyme.

The PK-digested worm solution was used as template DNA for a standardised PCR. A 25 μ l reaction was set up containing 2 μ l template along with 100 nM forward and reverse primers (each), 10 μ M dNTP mix, and 0.5 U of Taq polymerase in PCR-buffer. The reaction mix was put into a PCR thermocycler (Biometra) and subjected to the following standard genotyping program:

Step	Time [s]	Temperature [°C]
1	240	98
2	50	95
3	45	56
4	120	72
<i>steps 2-4 are repeated 34 times</i>		
5	420	72
6	300	20

If necessary, a restriction digest was performed for genotyping. To this end, 10 μ l containing 1 U of restriction enzyme in appropriate buffer were mixed with 5 μ l of PCR result. Digests were typically incubated for 1 hour at 37 °C in a water bath, then mixed with DNA loading dye and evaluated by agarose gel electrophoresis. Running time and gel percentage varied depending on expected amplicon sizes. Primers used for genotyping are displayed in Table S3. Enzymes used for restriction digest analysis are listed in Table S4.

Bleaching

To generate a population of age-synchronized animals, a bleaching solution was applied to mixed-stage populations, resulting in only embryos surviving this procedure. Firstly, gravid worms were washed off plates using M9 buffer supplemented with 0.05% NP40 substitute (M9+NP40) and centrifuged at low speed (400 g) for 2 minutes. Supernatant was carefully removed using a plastic transfer pipette and tube was refilled to 15 ml with M9+NP40. After gently inverting the tube, this washing procedure was repeated until the

worm solution appeared visually clear of bacteria. Next, animals were harvested and resuspended in 4 ml M9+NP40. In quick succession, 400 μ l of HypoChlor solution and 400 μ l 4 M NaOH were added. Immediately thereafter, the tube was shaken vigorously and worm lysis was monitored under a stereo microscope until roughly one third of worms showed signs of rupture. The tube containing still dissolving worms was spun at 3000 g for 1 minute; its supernatant was fully removed by decantation and the tube was refilled with fresh M9+NP40 to stop the bleaching reaction. Tube was mixed well by shaking and spun again at 3000 g for 1 minute. Decanting, refilling and mixing was repeated two more times to ensure complete removal of bleaching solution. After one final spin (1 min at 3000 g) and removal of supernatant, embryos were flash frozen in liquid nitrogen to obtain embryo samples for western blotting. Alternatively, embryos were resuspended in 10 ml of M9 and allowed to hatch overnight. These L1 worms arrested by starvation were spotted onto NGM plates on the next day.

Salt stress experiments

Hand-picked young adult worms (first 24 hours after reaching adulthood) were transferred to high salt plates (500 mM NaCl). After 4 hours animals were manually transferred back to a standard NGM plate (50 mM NaCl) and allowed to recover. After 24 hours, animals were scored for survival by prodding them on the head with a metal pick. If worms did not actively move away, they were considered non-responsive.

Genome editing

To introduce stable, heritable changes in the genome of *C. elegans*, which is not achievable by regular crossing, the CRISPR/Cas9 and MosSCI techniques were utilized. Gonadal injections into the syncytial area of young adults were performed by Dr. Kathrin Patsias and Maxie Rockstroh using glass needles and an injection scope (Nikon Eclipse TS2R) with a microinjector (Eppendorf FemtoJet 4i). To reduce movement, worms were fixed onto an agar pad before injection and embedded in oil (Holocarbon 700) to aid injection processes. Final confirmations of all strains generated via CRISPR/Cas9 or MosSCI were done by amplifying the target locus via PCR and DNA sequencing (see section genotyping). Worm strains generated in this study are summarized in Table S6.

CRISPR/Cas9

The Clustered Regularly Interspaced Short Palindromic Repeats (CRISPR)-associated protein 9 (Cas9) endonuclease system was used to alter the endogenous locus of *bcc-1* in multiple ways (Ran et al. 2013). For easier evaluation of gene conversion success and

handling the screening procedure, a Co-CRISPR strategy was employed, using an additional gene conversion event at the *dpy-10* locus (Arribere et al. 2014). To obtain single guide (sg) RNAs, first a corresponding DNA sequence was cloned into sgRNA backbone plasmid pDR274 (Hwang et al. 2013).

Cloning into pDR274

To generate a plasmid for *in vitro* transcription, a designed oligonucleotide (see Table S5) was mixed with backbone-specific primer CE05207 (each 500 nM), 5 ng of pDR274 plasmid template, 200 nM of dNTP mix and 0.4 U of Phusion polymerase in HF-buffer totaling to a volume of 20 μ l. PCR result was column-purified using the Wizard® SV Gel and PCR Clean-Up System following the manufacturer's instructions and eluting in 20 μ l nuclease free water (Table S6). To re-circularize the linear PCR result, a 4 μ l reaction was set up with at least 100 ng of DNA together with 4 mM ATP, 4 U T4 Polynucleotide Kinase (PNK) and 4 U of T4 DNA ligase in T4 PNK buffer. To degrade initial template plasmid, 1 U of DpnI was added alongside. Mixture was incubated for 90 minutes at 37 °C and subsequently propagated in *E. coli* using a heat shock transformation protocol (see below). After retrieving plasmids using the Promega Wizard Plus SV Minipreps DNA Purification System kit, plasmids were identified by restriction fragment length polymorphism (RFLP) (using SspI and SpeI) and verified by sequencing. A list of purified sgRNA backbone plasmids made in this study is given in Table S5.

Single Guide plasmids (pSG) were handed to Dr. Kathrin Patsias who performed a PCR and *in vitro* transcription to obtain sgRNAs used for injection in combination with the respective repair template and Cas9 enzyme in Cas9 buffer. DNA repair templates used in this study are listed in Table S5.

F1 progeny of an injected mother were surveyed for Dumpy or Roller phenotypes, indicating a successful gene conversion event at the *dpy-10* locus. Since such animals possess an elevated chance of also exhibiting a genome editing at the locus of interest, such F1 animals were singled and their progeny was subjected to PCR-mediated genotyping (see genotyping). After final confirmation of correct target locus by sequencing, worms were backcrossed against N2 wild-type two times. All established strains are listed in Table S6.

MosSCI

All subsequently described steps based on the MosSCI technique (Frøkjær-Jensen et al. 2012) to establish ectopic expression strains were designed in collaboration with and executed by Maxie Rockstroh.

For each transgene, three different types of pDONR plasmids were generated, each carrying either inserts of a 5' regulatory region, a gene of interest's ORF, or a 3' untranslated region (UTR). Using Gateway cloning (Katzen 2007), a combination of these three pDONR plasmids was assembled into a single destination vector backbone (pDEST) that carried homologous sequences to the Mos1-tagged genomic landing site on chromosome II and a positive selection marker (*unc-119*). Together with four selection markers identifying and distinguishing from extra-chromosomal arrays (Table S7), the resulting pDEST vector (Table S8) was injected into *unc-119* deficient worms carrying a respective MosSCI landing site on chromosome II (strain no. EV1096). Alongside, a plasmid encoding the Mos transposase was injected to facilitate a double-strand break on chromosome II by excision of the Mos1 transposon. This breakage will then be repaired by incorporating sequence information from a DNA repair template with homology into the breakpoint.

Injected animals were singled and kept at 25 °C until starvation and screened for worms exhibiting normal movement, indicating a likely successful incorporation of the positive selection marker *unc-119* and the ectopic expression cassette (transgene) of interest. To exclude animals carrying extra-chromosomal plasmid arrays, animals were heat shocked (34 °C for 3 h) and non-red survivors were identified using a fluorescent microscope (Nikon SMZ18) and singled. F1 animals were then subjected to PCR-based genotyping (see genotyping). All established strains are listed in Table S6.

Microscopy

To analyse living worms using widefield or confocal microscopy, animals were immobilized on agar pads. These pads were made by squeezing freshly melted agarose (2% in M9) between two glass slides. Additional glass slides with a piece of tape are used to provide a slightly elevated surface, ensuring sufficient height of the agar on the pad. Once the agar had fully solidified, the taped slides were removed, followed by the glass slide on top, leaving behind an evenly spread agar piece on the bottom glass slide. Picked worms were transferred into a drop (~7.5 µl) of 25 mM Levamisole in M9 resting on a cover slip. The prepared agar slide was then inverted and carefully put on the cover slip without damaging the worms. To fixate the sample nail polish was added to the corners. Samples and pads were prepared immediately before analysis.

Widefield microscopy

Widefield microscopy was performed using the Leica THUNDER Imager 3D Tissue system with a DM6B microscope and a SOLA SM II light source. Animals were analysed using 10x (HC PL FLUOTAR 10x/0.32), 25x (HC PL FLUOTAR 25x/0.80 OIL) and 40x (HC PL APO 40x/0.95 OIL) objectives. For fluorescence microscopy the GFP ET filter system (Excitation at 450 ±20 nm and Emission at 525±25 nm) was used. Images were acquired with a digital camera (Leica DFC9000 GT) and LAS X premium software allowing for acquisition of multiple planes (Z-stacks) and Maximum Intensity Projections (MIP). For stitching of multiple images, the LAS X Navigator was used. If applicable, images were processed using the Thunder Station 3D DCV software plugin.

Confocal microscopy

Confocal microscopy was performed using a Leica STELLARIS 8 System with a DMi8 confocal microscope and a STELLARIS 8 white light laser. Animals were analysed using 20x (HC PL APO 20x/0.75) and 40x (HC PL APO 40x/1.10 W) objectives. For green fluorescence microscopy (GFP) the gfp HyD S detector was used (490 nm; 7% laser intensity). Red fluorescence microscopy (mCherry) was conducted using the gfp HyD X detector (587 nm; 20% laser intensity). Images were acquired with a STELLARIS 8 Tandem Scanner (8kHz) and LAS X premium software allowing for acquisition of multiple planes (Z-stacks) and Maximum Intensity Projections (MIP). For stitching of multiple images, the LAS X Navigator was used. If applicable, images were processed using the LAS X Lightning Process software plugin.

RNA interference (RNAi) induced by feeding

For experiments involving reverse genetic knockdowns, the RNAi feeding method was chosen as described (Conte et al. 2015). To utilize this method, bacterial strains expressing double stranded (ds)RNA against transcripts of interest were generated. For expression of dsRNA, complementary DNA (cDNA) sequences were generated from worm RNA, cloned into a suitable plasmid vector and transformed into an *E. coli* strain used for RNAi feeding. A list of plasmids generated is given in Table S9. Bacterial strains used are displayed in Table S10.

Generation of cDNA-based target sequences

Total worm RNA of mixed-stage wild-type worms resolubilized in water was obtained as a kind gift from Tosin Oyewale. 500 ng of total RNA were used for reverse transcription

(RT) utilizing the RevertAid kit (Thermo Fisher) with random hexamer primers. RT was conducted as recommended by the kit's manual (Table S6).

To obtain the open reading frames (ORFs) of *bcc-1*, *mlt-3*, *mlt-2*, *nekl-3* and *dpy-10*, the cDNA generated above was used as a template for PCR to amplify the locus of interest. Primers (listed in Table S3) were designed to result in amplicons possessing cleavage sites for restriction enzymes (XmaI/XhoI). A 50 μ l reaction was set up containing 2 μ l cDNA as a template along with 200 nM forward and reverse primers (each), 200 μ M dNTP mix, and 1 U of Phusion polymerase in HF-buffer. The reaction mix was put into a PCR thermocycler (Biometra) and subjected to the following program:

Step	Time [s]	Temperature [°C]
1	120	98
2	30	98
3	20	60-68*
4	300	72
<i>steps 2-4 are repeated 30 times</i>		
5	420	72
6	120	20

*variable depending on primer combination used

PCR reactions were mixed with DNA-loading sample buffer, loaded into two wells of an 8-comb agarose gel (1-2%, 11cm) and electrophoresed until sufficient band separation had been achieved. Target bands were cut using a scalpel, pooled and transferred into a fresh 1.7 ml tube. Purification of the gel fragments was performed using the Wizard® SV Gel and PCR Clean-Up System according to the manufacturer's instructions (Table S6).

Interim cloning into pJET plasmids

Purified DNA-amplicons from cDNA-templated PCR reactions were cloned into a pJET blunt-end vector using the CloneJET kit (Thermo Fisher), following the manufacturer's instructions (Table S6). These interim clonings into pJET plasmids allowed for a convenient amplification of DNA material by subsequent heat shock transformation into *E. coli* and subsequent plasmid DNA extraction. A list of generated plasmids containing the pJET backbone can be found in Table S9.

Heat shock transformation of bacteria

An aliquot of chemically competent (XL1-blue) cells (500 μ l) was thawed on ice for 30 minutes. Afterwards, 100 μ l of cells were mixed with the plasmid DNA to be propagated. After 30 minutes of incubation on ice, cells were heat shocked at 42 °C for 45 seconds and

put back on ice for two minutes. Then 300 μ l pre-warmed SOC medium (37 °C) was added and cells were incubated at 37 °C for 1 hour at 800 rpm in a thermoshaker (Eppendorf ThermoMixer C). Following incubation, cells were plated on LB plates containing appropriate antibiotics using a Drigalski spatula and allowed to grow at 37 °C. On the following day, circular DNA was retrieved by plasmid DNA extraction.

Plasmid DNA extraction

Single colonies of bacterial cells carrying plasmids of interest were transferred into 4 ml of LB medium with required antibiotic and shaken at 220 rpm overnight at 37° C. Next day, plasmids were isolated using the Wizard® Plus SV Minipreps DNA Purification System as instructed by the manufacturer and eluted DNA (20 to 100 μ l) was evaluated by agarose gel electrophoresis using RFLP. Samples showing the desired restriction pattern were subsequently submitted for DNA sequencing. Restriction enzymes used in RFLP are displayed in Table S4.

DNA Sequencing

To confirm genetic identity of plasmids or PCR products, DNA samples supplied with an appropriate sequencing primer were submitted to Microsynth, a commercial sequencing service provider. To ensure best results, concentrations were adjusted according to the service company's suggestions for "Economy runs". All sequencing primers are listed in Table S3.

Cloning of amplified DNA into RNAi feeding vectors

Following amplification using the pJET system, DNA sequences of interest were cloned into the pL4440 vector, used to express dsRNA (Timmons and Fire 1998). To generate compatible sticky ends for restriction cloning, up to 7 μ g of plasmid DNA (pL4440 backbone or insert) was supplied with 20 U of restriction enzymes (XmaI/XhoI) and rCutsmart buffer in a total volume of 50 μ l for 1 hour at 37 °C. To isolate cut DNA fragments, up to 1 μ g of DNA was mixed with DNA sample buffer, loaded into one well of an 8-comb agarose gel (11cm) and electrophoresed until sufficient band separation had been achieved. Target band was then cut using a scalpel, pooled with others and transferred into a fresh 1.7 ml tube. Purification of the gels fragments was performed using the Wizard® SV Gel and PCR Clean-Up System.

If DNA parts to be removed were very small (up to 30 bp, like multiple cloning sites), purification was conducted directly using the Wizard® SV Gel and PCR Clean-Up System (Table S6). After elution in 20-100 μ l, eluted DNA was used for plasmid ligation. In a reaction of 20 μ l, typically 50 ng of insert were mixed with 150 ng of vector backbone and 30 U of T4 DNA ligase (Thermo Fisher) in supplied T4 DNA Ligase Buffer. To allow for

optimal ligation, the reaction was incubated at 16 °C overnight. Ligated plasmids were transformed into *E. coli* utilizing transformation by electroporation. Plasmids used and generated for RNAi feeding are listed in Table S9.

Transformation by electroporation and preparation of RNAi plates

One aliquot of electrocompetent HT115 bacterial cells (100 µl) was thawed on ice for 30 minutes and supplied with 900 µl of water. A cuvette was filled with 100 µl of the diluted cells, 100-200 ng plasmid DNA and placed into an Eporator (Eppendorf). Electroporation was conducted at 2500 V and pre-warmed (37 °C) SOC was added to rescue the cells in the cuvette. SOC medium and cells were transferred to a 1.7 ml tube and incubated at 37° C for 1 hour at 800 rpm in a thermoshaker (Eppendorf ThermoMixer C). Following incubation, cells were plated on LB plates supplemented with ampicillin and tetracycline using a Drigalski spatula and incubated at 37 °C shielded from light. On the next day, individual colonies were used to inoculate 4 ml of LB containing 100 µg ampicillin. Following overnight growth, the culture was harvested in 50 ml Greiner-Tubes by spinning 8 minutes at 2900 g. The supernatant was decanted and the pellet resuspended in 20 ml of LB for washing. After spinning down again the pellet was solubilized in 2 ml of LB containing ampicillin.

Induction of dsRNA production was triggered by spotting 3x 40 µl cell suspension onto NGM plates containing carbenicillin (25 µg/µl) and 1 mM Isopropyl-beta-D-thiogalactopyranoside (IPTG). After spots had dried, plates were incubated at 25 °C overnight. If not used on the next day, plates were kept at 4 °C for up to seven days. The plates were accommodated to 20 °C before use and supplied with either hand-picked L4-staged worms or spotted with L1 arrested worms generated from bleaching experiments.

RNAi-mediated knockdown experiments

Male mating assay

HT115 cells transformed with pL4440 carrying the ORF of *fog-1* were grown and spotted onto NGM plates (see transformation using electroporation and preparation of RNAi plates). A few young adult worms were manually placed on these plates resulting in self-sterile (feminized) F1 animals due to reduction of *fog-1* (Barton and Kimble 1990). Next, a single feminized animal was put onto a 3.5 cm NGM plate with a little scrap of OP50 as food source. Then one adult male was added and the plate was incubated for 24 hours at 20 °C. Afterwards, the male was removed and the remaining female worm scored for amount of cross-progeny until egg laying stopped. To allow for proper progeny counting, the mother animal was transferred to a fresh standard NGM plate every 24 hours.

Molting assays

HT115 cells transformed with pL4440 carrying the ORF of *mlt-2*, *mlt-3* or *nekl-3* gene were grown and spotted onto NGM plates (see transformation using electroporation and preparation of RNAi plates). L4 worms carrying genotypes of interest were transferred onto the plates allowed to lay a sufficient number of eggs and removed. Alternatively, L1 worms synchronized by bleaching (see above) were directly spotted. Plates were incubated either at 20 °C or 25 °C and animals were scored using a stereo microscope (Nikon SM800) after three or two days, respectively. Worms either not having matured into adults or adults showing signs of rupture or excessive cuticle parts were classified in a combined category as “Cuticle Defective”.

Dumpy assay

HT115 cells transformed with pL4440 carrying the ORF of *dpy-10* gene were grown and spotted onto NGM plates (see transformation using electroporation and preparation of RNAi plates). Synchronized L1 larvae (see bleaching) were spotted on the plates and incubated at 25 °C for two days. Worms exhibiting a significantly shorter and thicker phenotype were scored as Dumpy (Dpy).

Yeast Two-Hybrid (Y2H) experiments

To investigate putative protein-protein interactions, the Y2H system was utilized in this thesis (Fields and Song 1989). To generate shuttle vectors for Y2H analysis, previously generated pJET or pL4440 plasmids were used as a ORF sequence source for *mlt-2*, *mlt-3*, *bcc-1* and *nekl-3* (see chapter RNA interference induced by feeding). The ORF of human *Bicc1* was provided by Dr. Andreas Fischer through a vector-based plasmid and it was further cloned into a shuttle vector. Using this plasmid, a 50 µl reaction was set up containing 3 ng DNA as a template along with 200 nM forward and reverse primers (each) adding restriction sites for XmaI/XhoI, 200 µM dNTP mix and 1 U of Phusion polymerase in HF-buffer. The reaction mix was subjected to the following program in a PCR thermocycler (Biometra):

Step	Time [s]	Temperature [°C]
1	120	98
2	30	98
3	20	62
4	300	72
<i>steps 2-4 are repeated 30 times</i>		
5	420	72
6	120	20

PCR result was mixed with DNA sample buffer, loaded into two wells of an 8-comb agarose gel (1-2%, 11cm) and electrophoresed until sufficient band separation had been achieved. Target bands were cut using a scalpel, pooled and transferred into a fresh 1.7 ml tube. Purification of the gels fragments was performed using the Wizard® SV Gel and PCR Clean-Up System according to the manufacturer's instructions (Table S6). Purified DNA was cloned into pJET plasmids and propagated using heat shock transformation (see interim clonings into pJET plasmids/ heat shock transformation).

Cloning into yeast shuttle vectors

Following amplification using the pJET system, DNA sequences of interest were cloned into pLexKn2 or pAct2 vectors prior to combined yeast co-transformation. To generate compatible sticky ends for restriction cloning, up to 7 µg of plasmid DNA (either backbone or insert) was supplied with 20 U of restriction enzymes (XmaI/XhoI) and rCutsmart buffer in a total volume of 50 µl for 1 hour at 37 °C. To isolate digested DNA fragments, up to 1 µg of DNA was mixed with DNA sample buffer, loaded into one well of an 8-comb agarose gel (11cm) and electrophoresed until sufficient band separation had been achieved. Target band was then cut using a scalpel, pooled with others and transferred into a fresh 1.7 ml tube. Purification of the gels fragments was performed using the Wizard® SV Gel and PCR Clean-Up System. If to be removed DNA fragments were very short (up to 30 bp, like multiple cloning sites), the purification occurred directly using the Wizard® SV Gel and PCR Clean-Up System. After elution in 20-100 µl water, eluted DNA was used for plasmid ligation.

Plasmid DNA ligation into yeast shuttle vectors

In a reaction of 20 µl, typically 50 ng of insert were mixed with 150 ng of vector backbone and 30 U of T4 DNA ligase (Thermo Fisher) in supplied T4 DNA Ligase Buffer. To allow for optimal ligation, reaction was incubated at 16 °C overnight. Ligated plasmids were propagated by heat-shock transformation (see heat shock transformation) and subsequently used for transformation into yeast. Generated plasmids used for Y2H are listed Table S9.

Yeast transformation

Plasmids carrying putative protein interactors were transformed into yeast using the lithium acetate/single-stranded carrier DNA/polyethylene glycol method (Gietz and Woods 2006). To this end, a solitary L40 yeast colony grown on YPD plates was dissolved in 20 ml YPDA and grown overnight shaking at 180 rpm at 30 °C. On the following day, a volume of

$V=8.3/[\text{Optical Density (OD600) value}]$ was transferred into 50 ml YPDA medium to inoculate a larger and actively dividing yeast culture.

Upon reaching an OD600 of 0.6, the culture was pelleted at 3220 g for 3 min, washed by resuspension in 25 ml H₂O and pelleted again. Subsequently, cells were resuspended in 1 ml 0.1 M lithium acetate (LioAc) and transferred to a 1.7 ml tube. After centrifugation (3000 g for 15 s) and removal of supernatant, yeast cells are mixed with 400 µl of 0.1 M LioAc and aliquoted (50 µl) into fresh 1.7 ml tubes. After removing excess 0.1 M LioAc, yeast aliquot pellets were covered by 326 µl transformation mix. Subsequently, 35 µl water containing 250 ng of (each) plasmid was added to initiate the co-transformation procedure. After vigorous racking to mix all components well, yeast cells were incubated at 30 °C and afterwards heat shocked at 42 °C for 30 minutes each to facilitate plasmid uptake. Excessive liquid was removed after spinning (6000 g, 15 sec) and yeast pellets were gently resuspended in 500 µl H₂O. To select for cells having taken up both plasmids, 200 µl of yeast suspension was plated on double drop out plates (SD-Leu-Trp) using glass beads. After growth for three to four days at 30 °C, single colonies were picked for a β-galactosidase blue/white reporter assay.

β-galactosidase reporter assay

Putative protein interactions were analyzed by a blue-white reporter test. Single yeast colonies were streaked onto a nitrocellulose (NC) membrane disk layered on a SD-Leu-Trp plate and additionally on a second empty SD-Leu-Trp replica plate for later western blot analysis. Following overnight incubation at 30 °C, NC membranes were submerged into liquid nitrogen for 15 seconds and transferred onto a chromatography filter paper pre-soaked in Z-buffer + X-gal. In the sealed petri dish, color development was monitored during fixed intervals at 37 °C. Images were taken using a flatbed color scanner (Epson Perfection V700 Photo). Experiments were terminated by membrane removal before negative control showed blue color development.

Yeast protein extraction

To validate the expression of fusion proteins, corresponding yeast colonies were subjected to western blot analysis. Single colonies from replicate SD-Leu-Trp plates were inoculated in 12 ml of SD drop out medium overnight at 30 °C. A volume corresponding to 4 OD600 units was pelleted (4 min, 1800 g) and resuspended in 100% TCA. Solution was transferred to 1.7 ml tubes, centrifuged (1500 g for 4 min) and the pellet resolubilized in 20% TCA after the supernatant has been discarded. To break open yeast cell walls, 200 µl of glass

beads were added and cells lysed using a bead mill (Retsch MM301) for 5 min at 30 Hz. Proteins were rescued from the solution by briefly spinning down the tube and transferring the supernatant carefully to another tube using gel well tips while avoiding glass beads. To increase protein yield, the lysis procedure was repeated using 5% TCA and the glass beads remaining in the tube. After pooling both proteins fractions, sample was spun for 10 min at 845 g and supernatant discarded. To resolubilize the pellet and to adjust its pH, 200 µl 2x SDS sample buffer and 50 µl unbuffered 1 M Tris were added. Sample was then mixed in a thermoshaker (Eppendorf ThermoMixer C) at 95 °C at 1000 rpm. To prepare sample for loading on SDS gels and to avoid transfer of insoluble fractions, the tube was spun at 21,000 g for 10 minutes and 80% of the supernatant was transferred to a fresh 1.7 ml tube.

Expression of recombinant(r) BCC-1

To affinity purify polyclonal sera containing antibodies against BCC-1 and to evaluate the running behaviour of BCC-1 in western blots, recombinant BCC-1 was expressed in *E. coli*. To this end, the ORF of *bcc-1* was fused to the coding sequence of Maltose Binding Protein (MBP) in a vector for recombinant protein expression, transformed by electroporation into *E. coli*, expressed and purified.

Cloning into pETmm41

To introduce a compatible restriction site (KpnI), a previously generated pLexKn2 plasmid containing the ORF of *bcc-1* (and already a restriction site for XhoI) was used as a PCR template. A 50 µl reaction was set up containing 3 ng plasmid DNA along with 200 nM forward and reverse primers (each), 200 µM dNTP mix and 1 U of Phusion polymerase in HF-buffer. The reaction mix was subjected to PCR-mediated amplification in a thermocycler (Biometra) using the following program:

Step	Time [s]	Temperature [°C]
1	120	98
2	30	98
3	20	62*
4	300	72
<i>steps 2-4 are repeated 30 times</i>		
5	420	72
6	120	20

PCR result was digested with 100 U of KpnI and 40 U of XhoI (1h at 37°C), mixed with DNA sample buffer, loaded into two wells of an 8-comb agarose gel (1-2%, 11cm) and electrophoresed until sufficient band separation had been achieved. Target bands were excised

using a scalpel, pooled and transferred into a fresh 1.7 ml tube. Purification of the gels fragments was performed using the Wizard® SV Gel and PCR Clean-Up System according to the manufacturer's instructions (Table S6). The preexisting backbone vector, pETmm41 (4 µg), was digested with 100 U of KpnI and 40 U of XhoI in rCutsmart buffer (1 h at 37 °C) and column purified using the same kit to remove the excised MCS fragment.

To ligate insert and backbone, a reaction of 20 µl was set up using 150 ng of insert and 50 ng of vector backbone together with 30 U of T4 DNA ligase in T4 DNA Ligase Buffer. To allow for optimal ligation, the reaction was incubated at 16 °C overnight. Ligated plasmids were transformed into BL21(DE3) cells utilizing transformation by electroporation (see transformation using electroporation). After overnight growth on a LB plate, a single colony was transferred into LB+kanamycin medium and grown overnight shaking at 37 °C. To generate glycerol stocks, cells were pelleted (2900 g 10 min), resuspended in 2 ml LB+kanamycin, mixed thoroughly with an equal amount of 50% glycerol and stored at -80 °C.

Protein expression procedure

To express MBP::BCC-1 fusion protein, 5 ml of LB+kanamycin medium was inoculated with a small fraction of above prepared bacterial cryo stocks and shaken at 180 rpm overnight at 37 °C. The next day, a small fraction was taken into fresh LB+kanamycin medium and grown to a target OD600 of ~0.6. Once this bacterial culture had been cooled down on ice, protein expression was induced by addition of 1 mM IPTG. Following overnight incubation at 16 °C and 180 rpm, bacteria were pelleted, mixed with equal amount of 4x SDS sample buffer and evaluated using SDS-PAGE followed by Coomassie staining (see protein quantification). To expand biomass volume for larger-scale expression, a one litre culture was set up and induced from the glycerol stock showing best expression of recombinant fusion protein according to Coomassie analysis. After overnight expression, bacterial cells were cooled on ice, harvested at 4 °C and stored as pellets at -20 °C until further use.

Purification of rBCC-1

To initiate the extraction process, 40 ml of rBCC-1 lysis buffer were used to resuspend a frozen bacterial pellet made from one litre culture. Cells were lysed on ice using a sonicator (Bandelin Sonoplus GM 70) over the course of four cycles (4 min, 50% pulse) interrupted by a one min pause to prevent overheating. To retrieve soluble MBP::BCC-1, the supernatant was taken, filtered through a 0.45-micron syringe PVDF Filter and frozen until column

purification. For usage in affinity antibody purification, pellet-containing MBP::BCC-1 inclusion bodies were further purified from bacterial leftovers. To this end, pellets were resolubilized in 500 mM NaCl with 1% Triton X-100 and subjected to one cycle of sonication and centrifugation as described with the supernatant being discarded. Purification was repeated three times, cleaned inclusion bodies stored at -20 °C and used for affinity purification of antibody sera.

Column Purification

A one ml column (Pharmacia Biotech) packed with amylose resin was received as a kind gift from Oleksandr Sorokin. After installation into a NGC chromatography system (Bio-Rad), the system was equilibrated using rBCC-1 washing buffer until conductivity, pH curves and absorption rates were stable at a flow rate of 1 ml/min. A pressure restriction was set to 386 mbar, as recommended by the manufacturer. While all chromatography steps took place at room temperature (RT), MBP::BCC-1-containing supernatant was kept on ice during loading. Column was washed with 10 column volumes (CV) of rBCC-1 washing buffer and bound protein was eluted using 5 CV of rBCC-1 elution buffer. Three fractions of one ml each were collected using a fraction collector. Bradford assay (Bradford 1976) and SDS followed by Coomassie staining (see protein quantification) was used to determine protein concentration and purity of each fraction. Remaining volume of fractions deemed acceptable was further processed to remove MBP tag.

TEV cleavage

After evaluating amount and purity of eluted MBP::BCC-1, relevant fractions were treated with a protease to split the fusion protein from its affinity tag MBP, using a TEV cleavage site that is present in the linker sequence joining the two protein parts. In a 150 μ l reaction volume, \sim 20 μ g of eluted protein was mixed with 10 U of AcTEV™ protease in supplied TEV buffer and 1 mM DTT. After incubation at 37 °C for 1 hour, 10% of the reaction was subjected to SDS-PAGE and analyzed using Coomassie staining (see protein quantification). After verifying successful cleavage, sample was tested in western blotting to determine appropriate loading amount when probed with α -BCC-1 antibody solution.

Affinity purification of sera containing α -BCC-1 antibodies

To obtain antibodies with specificity against BCC-1, two pre-existing polyclonal sera obtained from rabbits injected with GST-tagged parts of BCC-1 (aa 1-400) were affinity purified using insoluble MBP::BCC-1 fusion protein (see Purification of inclusion bodies). To this end, the frozen pellet was resolubilized in 3 ml SDS sample buffer and mixed at 800 rpm

and 95 °C in a thermoshaker (Eppendorf ThermoMixer C). Recombinant MBP::BCC-1 protein (250 µl) was then loaded onto each of four SDS-Gels using a Prep-well comb and transferred onto a NC membrane (see protein quantification). The running height of the fusion protein band was determined by staining with Ponceau solution and respective areas were cut into narrow strips which were placed into a 15 ml tube. After blocking for 30 min using 25% horse serum in PBS-T, strips were stored in PBS-T. To bind antibodies, 200 µl of raw serum (second bleed) were added to the membrane strips in a 14 ml solution containing 25% horse serum in PBS-T. After overnight incubation at 4 °C, strips were washed 3 times for 15 minutes on a rocker using PBS-T. Antibody elution was performed in a 3-step manner.

In the first elution step, strips were incubated for 1 minute in 1.5 ml acidic antibody elution buffer and thereafter immediately neutralized using 200 µl of Tris pH 8.8. Prior to the next elution, strips were washed with PBS-T three times for 5 minutes. Second elution was conducted by incubating strips for 1 minute in 1.5 ml basic antibody elution buffer which was subsequently neutralized by addition of 200 µl Tris pH 6.8. After another washing cycle (3 times, 5 minutes) with PBS-T, the third elution step was performed by adding high salt antibody elution buffer to strips for 1 minute. Eluted solutions were pooled and dialyzed overnight in the cold room against 1x PBS with 50% glycerol using a Slide-A-Lyzer dialysis cassette (Thermo Fisher) system. After removal from cassettes, affinity purified antibody solution was stored at -20 °C.

Protein Quantification

SDS-PAGE

To characterize proteins in a solution regarding identity, amount or purity, sodium dodecyl sulfate–polyacrylamide gel electrophoresis (SDS-PAGE) was utilized. Samples were mixed with hot (> 90 °C) SDS-sample buffer to a final concentration of more than 1x SDS buffer. For mixed-stage worm samples, typically the estimated volume of settled worm pellet was mixed with an equal amount of SDS-sample buffer and 10 µl were loaded. Manually picked worms were collected in 10 µl of M9 and mixed with an equal volume of SDS-sample buffer and the complete solution was loaded. Shearing of nucleic acids was achieved by sonication for 15 min at 80 °C using an ultrasonic water bath (Bandelin Sonorex). After 15 min of additional shaking in a thermoshaker (Eppendorf ThermoMixer C) at 800 rpm and 95°C, samples were spun at 21,000 g for 10 minutes before being loaded. For SDS-PAGE, 10% polyacrylamide gels were prepared using the Bio-Rad Mini-PROTEAN system and electrophoresed at 25 mA until desired resolution was achieved. Typically, no less than

10 µl per sample were loaded alongside a pre-stained marker (Thermo Fisher, PageRuler Prestained Protein Ladder) for size reference. After PAGE, gel was removed from glass plates, stacking gel discarded and protein analysis was conducted using either Coomassie staining or western blotting.

Coomassie staining

To evaluate protein amounts and/or purity, gels were stained with Coomassie solution on a rocker for 20 minutes at RT, followed by destaining with water until desired contrast was achieved. Images of gels were taken using a flatbed color scanner (Epson Perfection V700 Photo).

Western blotting

For antibody-based detection for proteins following SDS-PAGE, western blotting was used. To this end, proteins on the gel were immobilized on a NC membrane using a blotting sandwich tank transfer system (Bio-Rad Mini-Protean Tetra System). Blots were subjected to 400 mA for 2.5 h in the cold room to prevent overheating. After blotting, efficient protein transfer was verified using Ponceau S red staining solution (Ponceau) by covering the membrane with Ponceau and destaining with water until desired level of contrast was reached. After Ponceau removal in excess water, membrane was blocked for 10 minutes at RT on a shaker in a 5% non-fat milk solution in PBS with 0.05% Tween-20 (PBS-T) added. Following blocking, membranes were sealed with primary antibodies (Table S11) using a plastic pouch overnight at 4 °C. To remove residual primary antibody, membranes were washed 3 times for ~10 minutes on a shaker in PBS-T. Subsequently, secondary antibodies (Table S11) were diluted 1:10,000 in 0.5% milk (in PBS-T) for 150 minutes on a shaker at RT, shielded from light. After repeating the washing procedure, detection was conducted using an Odyssey Fc imaging system (LI-COR) and Image Studio Lite V2 software. Membranes were typically exposed for 10 minutes to allow for maximum signal detection and afterwards stored in the fridge if needed again.

Membrane stripping

To allow for re-probing, NC membranes were rinsed with water and antibodies removed by incubation with stripping solution at 55 °C overnight. After washing away residual stripping solution with water, membranes were transferred into PBS-T and evaluated for residual antibody signals before being reused.

Bioinformatic tools

Prediction tools

In silico structure predictions for proteins were generated using the Robetta prediction algorithm (rosetta.bakerlab.org). Obtained .pdb files were analyzed using UCSF Chimera (www.softpedia.com/get/Science-CAD/UCSF-Chimera.shtml)

Prediction of putative phosphorylation sites in BCC-1 was conducted using Phospho Support Vector Machine (PhosphoSVM) available online (sysbio.unl.edu/PhosphoSVM) (Dou et al. 2014).

Results

Various alleles were generated to characterize *bcc-1*

To characterize BCC-1's molecular and biological roles, various alleles of *bcc-1* were generated that may produce predicted BCC-1 protein variants as summarized in **Figure 4**.

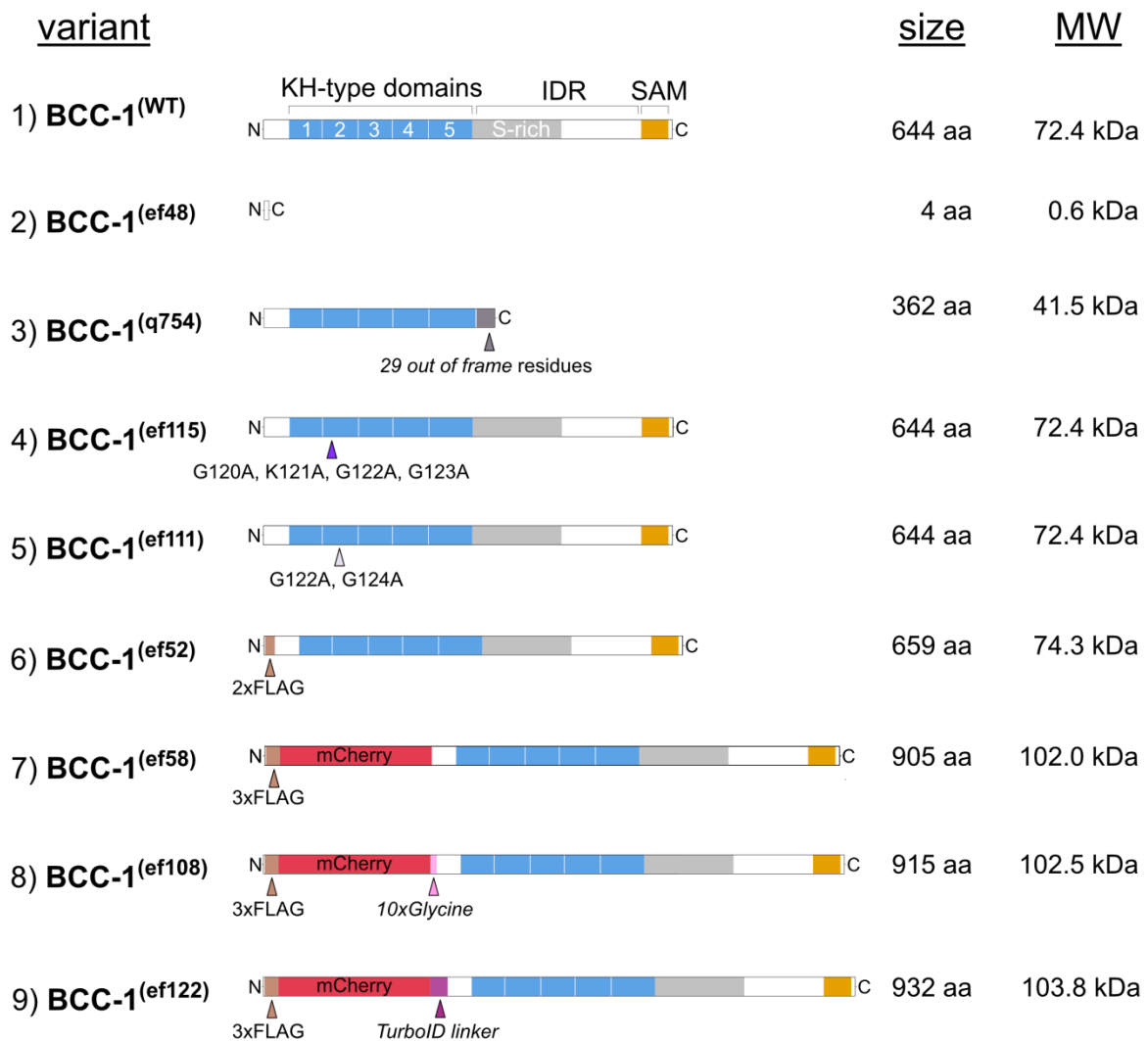


Figure 4: Overview of BCC-1 variants used in this study. Displayed are predicted protein products encoded by various *bcc-1* alleles. BCC-1 variants are named according to their respective genomic alleles written in bold brackets and superscripted. Lengths in amino acids (aa) and theoretical molecular weights (MW) are indicated. (1) Wild type (WT) BCC-1 with annotated protein domains: hnRNP K (KH) homology folds, intrinsic disordered region (IDR) with a subregion enriched for Serines (S), sterile alpha motif (SAM). (2) Protein-null mutant limited to the first 4 aa of BCC-1. (3) C-terminal deletion variant exhibiting all 5 KH-type domains and 29 extra aa, novel to BCC-1. (4) Glycines (G) and lysine (K) residues of KH-type 2 domain exchanged to alanines (A). (5) Flanking glycines of the second putative RNA-binding motif substituted with alanines. (6) BCC-1 tagged with 2xFLAG tag at the N-terminus. (7) BCC-1 with N-terminal 3xFLAG and mCherry protein tags. (8) Identical to (7), but with 10 additional glycine residues following the mCherry tag. (9) Resembling (7), but with a 27 aa Turbo ID linker (Artan et al. 2021) fused to the mCherry tag. Strains expressing (1), (2), (3) and (6) were already established before this study, (7) was provided by Dr. Kathrin Patsias; all variants other than (1) and (3) were generated using the CRISPR/Cas9 technique.

All generated strains were confirmed to carry correct alleles by genotyping and DNA sequencing. To assess whether the respective gene product is expressed at the protein level, antibodies against BCC-1 were generated.

Polyclonal rabbit serum contains antibodies with specificity against BCC-1

To study BCC-1 expression in a native background, two polyclonal sera from rabbits were obtained that had been challenged with a GST::BIC-1(aa1-400) fusion protein (rb 27.420 and rb 7BF5; produced by the MPI-CBG antibody facility). To evaluate whether detection of BCC-1 is feasible using raw serum, wild-type and *bcc-1* null mutant worms were washed off from NGM plates and protein extracts were subjected to western blot analysis using one of the two α -BCC-1 raw sera rb 27.420 together with actin as a loading control.

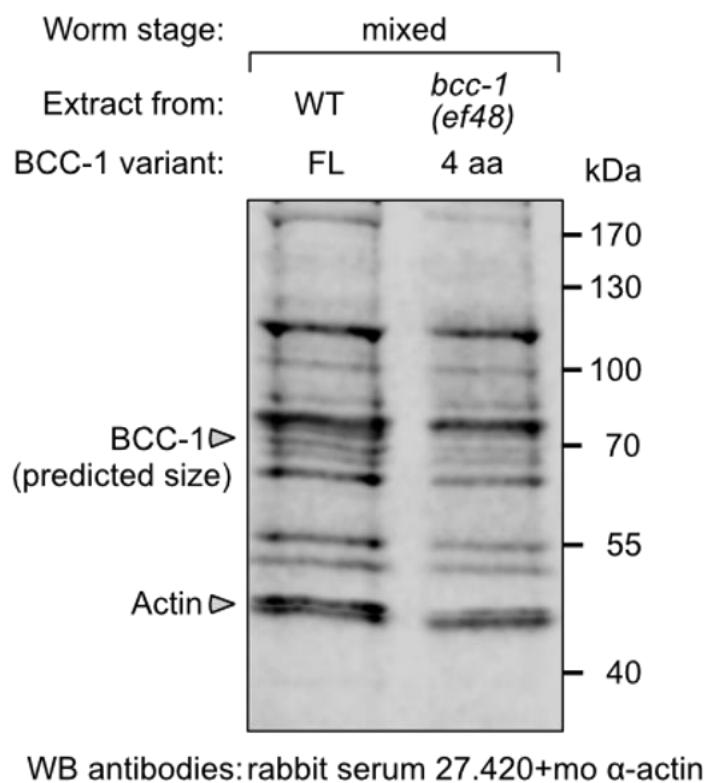


Figure 5: Western blot (WB) using unpurified polyclonal rabbit serum does not reveal bands specific to BCC-1. Raw rabbit serum 27.420 was used to probe a nitrocellulose membrane blotted with wild-type (WT) or *bcc-1*(*ef48*) protein extracts of mixed-stage animals along with mouse (mo) α -actin as a loading control. Animals expressed either full-length (FL) BCC-1 or a truncated version of just 4 amino acids (aa), respectively. Marker bands in kilodaltons (kDa) are indicated.

A comparison of band patterns from wild-type worms to animals expressing a BCC-1 variant of only 4 amino acids in length indicates the presence of many antibodies recognizing

epitopes other than BCC-1. Multiple signals corresponding to the theoretical molecular weight of BCC-1 (~72 kDa) were detected in protein extracts of either genotype, putatively veiling potentially weaker bands corresponding to BCC-1. In conclusion, the raw serum is not considered to be appropriate for BCC-1 detection in a mixed-stage population of worms. Western blot analysis using the second obtained serum rb 7BF5 unpurified was not attempted, as the results for serum 1 rb 27.420 were discouraging. To improve specificity of either serum and thereby revealing potential BCC-1 specific signals, both were subjected to blot-based affinity purification. To this end, recombinant BCC-1 protein N-terminally fused to Maltose Binding Protein (MBP) was expressed in *E. coli*, size-fractionated on SDS-gels and blotted. The membrane area containing the fusion protein was excised, incubated with raw serum and absorbed antibodies were eluted using three conditions: high pH, low pH and high salt eluents. The three elution fractions containing immune-purified antibodies were pooled, rebuffered in PBS with 50% glycerol and tested for specificity against BCC-1 in western blotting experiments.

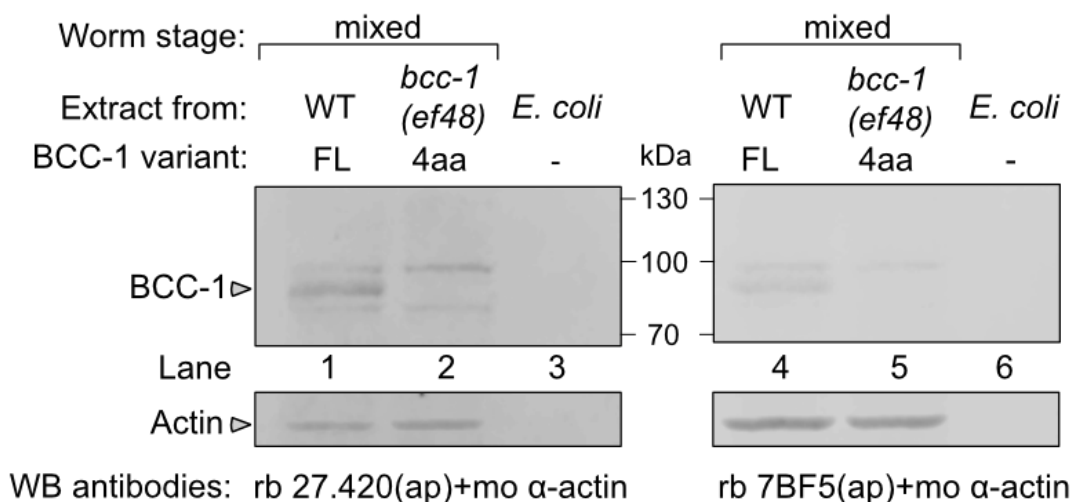


Figure 6: Polyclonal sera contain antibodies against BCC-1. Affinity-purified (ap) sera rabbit (rb) 27.420 and 7BF5 along with mouse (mo) α-actin, as a loading control, were used in western blot (WB) detection of wild-type (WT) and *bcc-1*(*ef48*) worm extracts of mixed stage. Animals expressed either full-length (FL) BCC-1 or a truncated version of just 4 amino acids (aa), respectively. An amount of *E. coli* visible in Ponceau staining scratched from seeded NGM plates served as a control for cross-reactivity with bacterially-derived proteins. Marker bands in kilodaltons (kDa) are indicated. Signal detection of left and right membranes was conducted simultaneously.

Following affinity purification, fewer signals appeared using affinity-purified rabbit sera compared to the raw serum (compare to **Figure 5**). Moreover, when comparing WT with *bcc-1*(*ef48*) protein extracts, a somewhat diffuse band between 70 and 100 kDa became visible only in WT (**Figure 6**). The same sized band could be seen with either purified antibody in WT but not in *bcc-1*(*ef48*) samples (**Figure 6**, compare lanes 1 and 4 with 2 and

5), arguing for a signal specific to BCC-1. Alongside this band, additional seemingly unspecific signals were detected on either membrane for WT and *bcc-1(ef48)*. Signal intensity of the actin loading control demonstrated that WT and *bcc-1(ef48)* samples were comparable in terms of loaded protein amount. A very similar banding pattern was observed for both sera; however, a better ratio of specific to non-specific signal was achieved with rabbit serum 27.420. Therefore, this purified antibody solution was selected to be used in further experiments and will from here onwards be referred to as α -BCC-1. As background bands were reduced and a signal corresponding to BCC-1 appeared on both membranes, affinity purification was considered a success despite remaining impurities limiting the usage of the purified antibody solution.

To further clarify the running behavior of BCC-1 in western blots and to investigate the to some degree diffuse nature of the presumed BCC-1 signal, resolution of polyacrylamide gels was optimized by prolonging their running time.

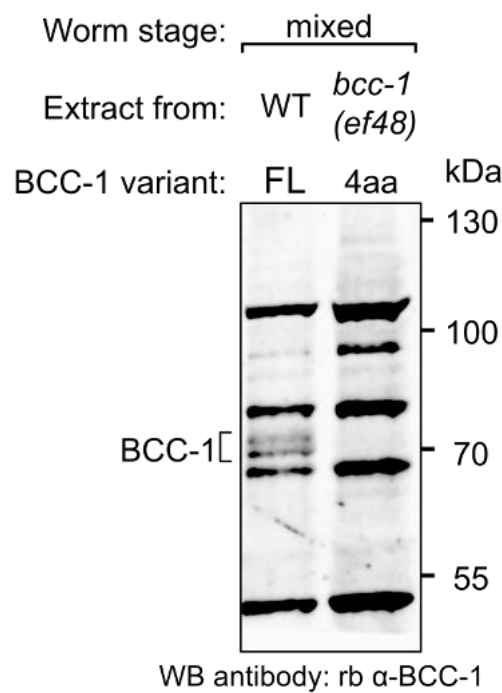


Figure 7: Wild-type (WT) worms express multiple variants of BCC-1. Purified rabbit serum 27.420 (α -BCC-1) was used to probe mixed-stage protein extracts of either wild-type animals expressing full-length (FL) protein or *bcc-1(ef48)* mutants expressing BCC-1 protein truncated to 4 amino acids. Marker bands in kilodaltons (kDa) are indicated.

After increasing resolution, WT and *bcc-1(ef48)* extracts show a similar signal patterning of unspecific bands (**Figure 7**). However, multiple bands corresponding in size to

the calculated BCC-1 height became visible in WT protein extracts that are absent in *bcc-1(ef48)* animal extracts (**Figure 7**). Although these bands are less intense than the unspecific signals, this result suggests that WT contains at least two variants of BCC-1.

Two likely explanations for multiple BCC-1 variants detected in western blots could be envisioned, post-translational modifications (PTMs) or different isoforms of BCC-1 protein. To evaluate both possibilities, it is necessary to analyze which –if any– signal is corresponding to unmodified, full-length BCC-1 protein. For this reason, recombinant soluble MBP::BCC-1 generated in *E. coli* was purified using an amylose column (**Figure 8**). Eluted protein fractions were then analysed using SDS-PAGE and Coomassie staining (**Figure 8, A**). An evaluation of the maltose elution fractions for protein concentration and purity disclosed that the MBP::BCC-1 fusion protein was present in all eluted fractions (**Figure 8, B**). As fraction 1 exhibited a strong band at the theoretical size of maltose binding protein only (~44 kDa), it was concluded that the majority of the sample is not consisting of fusion protein (**Figure 8, B**). For this reason, only fractions 2 and 3 were chosen for further downstream processing.

Eligible fractions (2 and 3) were further processed to separate BCC-1 from MBP to obtain untagged recombinant rBCC-1 protein using a commercially available AcTEV kit. Incubation with Tobacco Etch Virus (TEV) protease allows for specific cleavage of the MBP::BCC-1 fusion protein at the TEV recognition site (ENLYFQG) located between MBP and BCC-1, producing a N-terminally extended BCC-1 protein by 7 additional amino acids (due to cloning reasons). Cleaved fractions were supplied with SDS sample buffer and evaluated using SDS-PAGE and Coomassie staining (**Figure 8, B**). In both fractions after TEV cleavage, three bands appeared at the height of the three proteins expected (MBP, rBCC-1 and TEV). Furthermore, no signal corresponding to uncleaved protein (~117 kDa) was visible (**Figure 8, B**). Therefore, TEV cleavage appears to have been successful making both fractions applicable for usage in western blotting experiments. The ratio of MBP to rBCC-1 was favourable in fraction 3. Thus, in further experiments, only fraction 3 was used for the sake of consistency.

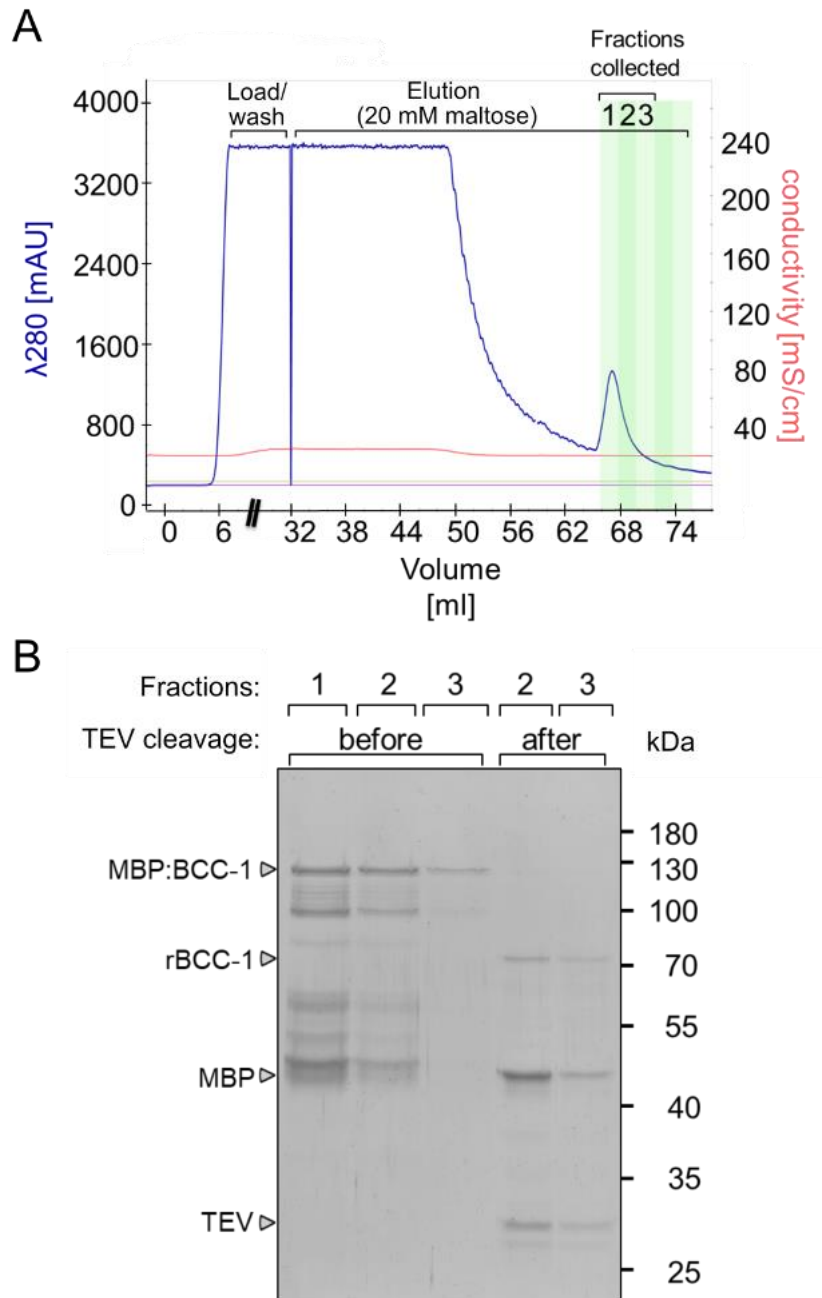


Figure 8: Amylose-mediated purification and subsequent Tobacco Etch Virus (TEV) protease cleavage yields tag-free full-length recombinant (r)BCC-1. (A) Amylose column purification run of *E. coli* extracts showing absorption values at 280 nm (λ_{280} , blue graph) and conductivity (red graph). Column was equilibrated using equilibration buffer and loaded with protein extract containing soluble MBP::BCC-1. After elution using maltose, the single peak appearing between volumes 67-69 was collected in three fractions of 1 ml each. (B) Coomassie staining of fractions eluted in (A) before and after TEV cleavage. Equal volumes of eluted fractions were loaded onto an SDS gel. Expected bands and their sizes are indicated. Marker bands in kilodaltons (kDa) are indicated. Solely fractions 2 and 3 were subjected to TEV cleavage, as fraction 1 was deemed too impure.

After recombinant tag-free BCC-1 was obtained, the wild-type specific signal pattern previously observed in **Figure 7** was investigated further. As BCC-1 might be phosphorylated (Zielinska et al. 2009), it was investigated whether additional bands can be attributed to a phosphorylation status of BCC-1. For this experiment, snap-frozen worms of mixed stages

were thawed and treated with lambda phosphatase (λ PP) at 30 °C before being loaded on a SDS-PAGE gel and western blot detected using α -BCC-1 antibody solution (**Figure 9**). As a reference for unmodified BCC-1, the recombinant protein solution generated above was included (**Figure 9**, lane 4).

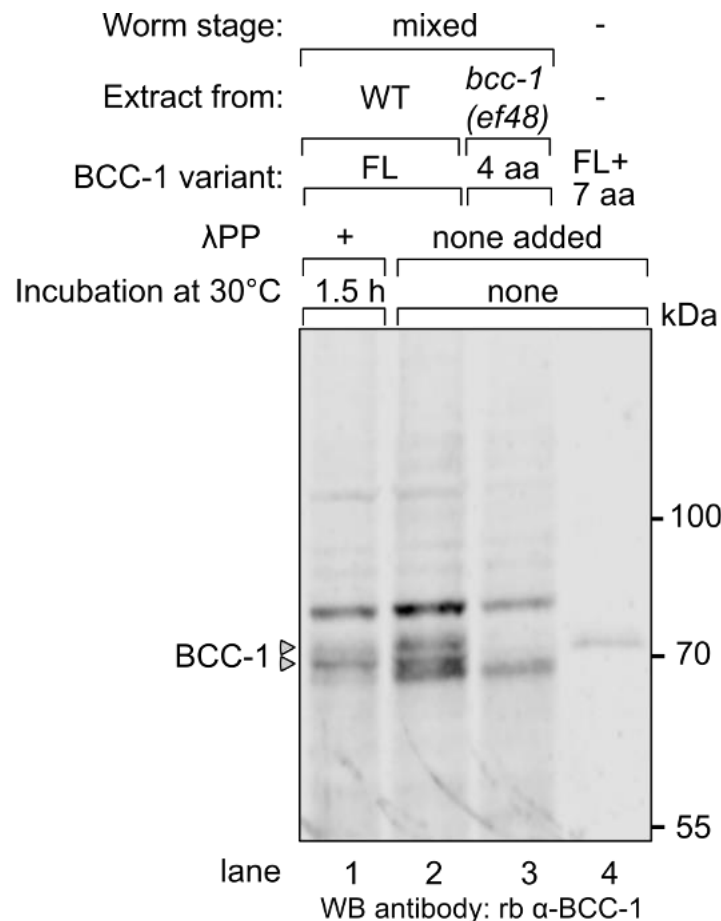


Figure 9: BCC-1 is likely phosphorylated in wild-type (WT) worms. Rabbit (rb) α -BCC-1 antibody solution was used to probe a nitrocellulose blot containing wild-type (WT) and *bcc-1(ef48)* protein extracts alongside recombinant BCC-1 which is 7 amino acids (aa) longer than the full-length (FL) variant. Lane 1 was treated with 200 units of lambda phosphatase (λ PP) and incubated for 90 minutes before applying SDS-sample buffer. All other samples were processed immediately. Marker bands in kilodaltons (kDa) are indicated.

When untreated WT extract was compared to mutant *bcc-1* extract (**Figure 9**, lane 2 and 3) protein bands of similar size to rBCC-1 were detected (**Figure 9**, lane 4), arguing that these bands are BCC-1 specific and similar to the observation made in **Figure 7**. However, it was challenging to attribute the signal of rBCC-1 to one of the bands in lane 2 due to the close proximity of BCC-1 signals (**Figure 9**, lanes 2 and 4). Furthermore, the recombinant protein is slightly larger (7 aa) compared to WT BCC-1, potentially resulting in a slight upshift in size. In addition, the running behavior of total lysates (lanes 1-3) might differ from a diluted non-complex protein solution containing mostly rBCC-1 (lane 4). Incubation of WT total

lysate with λ PP for 90 minutes (lane 1) lead to a loss of BCC-1 specific and unspecific signals with at least one specific signal remaining constant (lanes 1, 2). While this data would support the idea of BCC-1 being phosphorylated, it should be noted that this experiment only demonstrates BCC-1 signal selectively vanishing over time, but not necessarily due to the addition of λ PP. Endogenous phosphatases in the lysate might alone be sufficient to facilitate de-phosphorylation of BCC-1 as well. In addition, BCC-1 signal(s) not being stable over time might also be attributed to different PTMs but phosphorylation seems the most likely as the protein was suggested to be phosphorylated *in vivo* (Zielinska et al. 2009).

A different explanation for the presence of multiple BCC-1 variants considers the existence of locus-derived isoforms. In the past, isoforms have been reported for the *C. elegans* Bicaudal-C ortholog, GLD-3 (Eckmann et al. 2002). However, alternative transcripts have neither been predicted nor experimentally suggested for *bcc-1* according to www.wormbase.org WS290). In addition, when examining the genomic sequence of *bcc-1*, it was concluded that incorporation of entire introns to increase the size of the open reading frame is not possible without introducing premature stop codons into the ORF. Therefore, it seems unlikely that multiple BCC-1 signals observed in western blotted are due to protein isoforms (**Figure 7, Figure 9**).

Generated BCC-1 variants can be detected using α -BCC-1

Multiple alleles of *bcc-1* producing different protein variants of BCC-1 were generated (**Figure 4**) and allow a further analysis of BCC-1 products (**Figure 4**). To assess whether animals actually express their respective protein variation, worms of mixed stages were collected in M9, supplied with SDS sample buffer and subjected to SDS-PAGE followed by western blotting (**Figure 10**).

By comparing extracts of wild-type to *bcc-1* null mutants (lanes 1 and 2), bands specific to BCC-1 were detectable at the height of ~ 70 kDa, similar to what has been observed previously (**Figure 6, Figure 7, Figure 9**). Similarly sized BCC-1 specific bands were seen in extract of missense mutated *bcc-1* worms, arguing that these animals express KH-domain 2 mutated but otherwise full-length BCC-1 changed only in two different GXXG motifs (lanes 3 and 4). In extracts of animals expressing the N-terminally-tagged 2xFLAG::BCC-1 fusion protein (lane 5), a single band slightly increased in size when compared to WT BCC-1 seems in line with the added molecular weight resulting from the FLAG tag. It remains unclear whether lane 5 also exhibited multiple BCC-1 signals, as such might have been veiled by unspecific bands above.

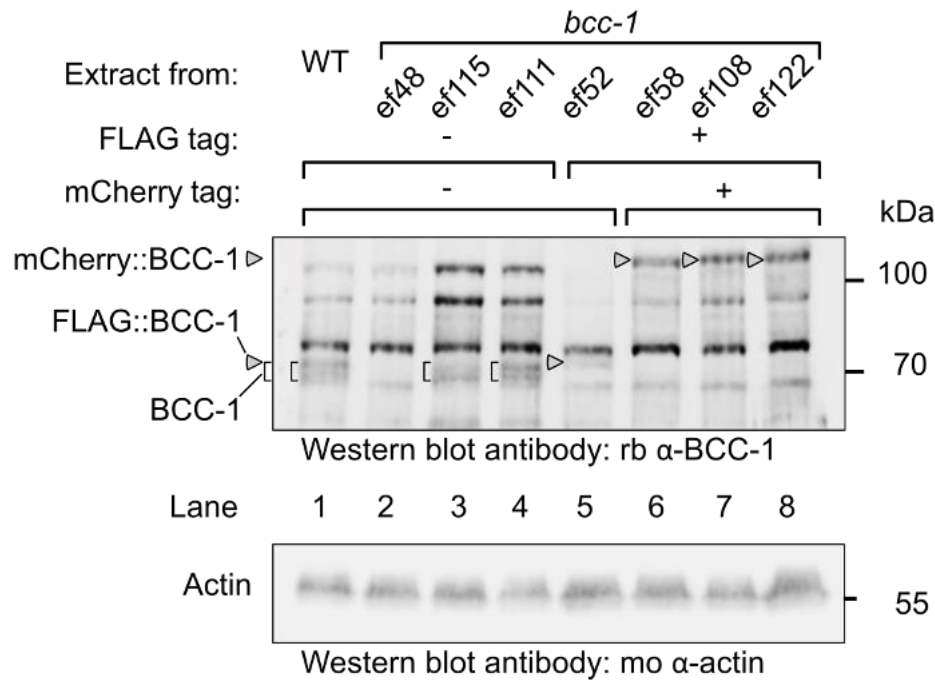


Figure 10: Generated worm strains express desired BCC-1 variants. Rabbit (rb) α-BCC-1 (top membrane) was used to probe a blot containing protein extracts of mixed stage animals carrying various *bcc-1* alleles. Corresponding BCC-1 protein stick diagrams and theoretical molecular weights are listed in Figure 4. Mouse (mo) α-actin (bottom membrane) was used as loading control. Marker bands in kilodaltons (kDa) and expected heights for native [brackets] and tagged BCC-1 species (arrow heads) are indicated.

Worm extracts examined in lanes 6, 7 and 8 of **Figure 10** are derived from alleles predicted to express endogenous BCC-1 N-terminally extended by mCherry and 3xFLAG, shifting the size of these fusion proteins beyond 100 kDa. Unfortunately, lanes 1-4 also exhibit unrelated bands to BCC-1 of similar sizes, however, these bands run slightly lower and vary in intensity, compared to the intense bands correlating with mCherry::FLAG::BCC-1 fusion protein sizes (compare lanes 6-8 with lanes 1-4). The more intense specific signal compared to FLAG::BCC-1, either derives from a detection efficiency difference pertaining to the FLAG antibody, or because the higher molecular weight mCherry::FLAG::BCC-1 bands contain multiple variants not being separated from each other due to insufficient resolution. Such a merging of bands would also explain the absence of multiple individual BCC-1 specific bands at ~70 kDa from lanes 6, 7 and 8, as observed in lane 1, 3 and 4. As the actin loading control indicates roughly equal protein amounts in each lane, the data demonstrates that all full-length BCC-1 variants are comparably expressed in abundance.

This allows for further use of the strains in actual experiments. By contrast, multiple attempts failed to detect the protein expressed by deletion allele *bcc-1(q754)* (not shown). This could either be due to low BCC-1 protein amount or because the polyclonal serum only

recognizes epitopes not present in this mutant. As the antibody serum was generated using a fusion protein of GST and the first 400 aa of BCC-1, it is unlikely to assume the latter. If detection failed due to protein abundance, it cannot be clarified whether degradation happens at RNA or protein level, but as proteins expressed by other *bcc-1* alleles seem to be detectable and therefore stable at RNA level, the data hints at the C-terminal half of BCC-1 being important for protein stability.

BCC-1 is a somatic protein expressed in the epidermis of animals

Loss of *bcc-1* has no effect on fertility

As the two loci of Bicaudal-C are likely the result of a gene duplication event in *C. elegans*, *bcc-1* and *gld-3* may still have redundant functions. Alternatively, the genes could have evolved already to fulfill different, exclusive tasks. The activity of *gld-3* is essential for germ line development and homozygous *gld-3* mutants are reported to have strongly reduced broods and the few generated die during embryogenesis (Eckmann et al. 2002).

Therefore, it was first investigated whether loss of *bcc-1* has a similar effect. To this end, individual L4 worms of wild-type (N2) and *bcc-1* null mutants *bcc-1(ef48)* were grown at 20 °C on NGM plates and transferred every day to a fresh plate until egg laying stopped. Two days after each passage, the living brood was assessed and summed up to calculate the total living brood size for 10 worms of both genotypes. Only hatched, moving larvae were scored; non-viable embryos were therefore not considered (**Figure 11**).

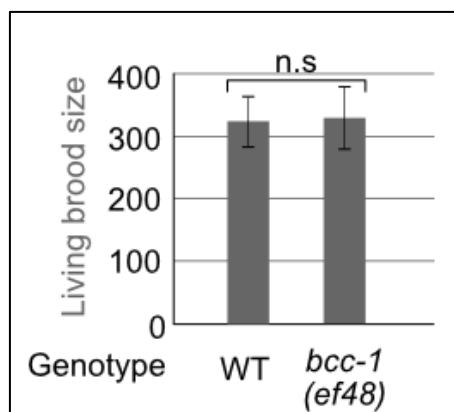


Figure 11: Loss of *bcc-1* does not affect fertility. Living brood of mothers (n) of given genotypes were counted (wild-type, WT). Worms were grown at 20°C. Error bars indicate standard deviation. Student's *t*-test suggests no statistically significant (n.s.) difference among the two groups. Experiment performed with the help of Jacqueline Pinheiro.

Wild-type worms exhibited an average total living brood size of 329 progeny with a standard deviation (SD) of 42 (n=10; **Figure 11**). This type of fertility is typical to other

findings, e.g. Hodgkin and Barnes reported a total progeny count of 327 (\pm 28) in a similar assay (Hodgkin and Barnes 1991). Loss of *bcc-1* resulted in an average living brood of 335 (n=10). Student's *t*-test analysis showed no significant difference between wild-type and *bcc-1*(*ef48*), as both averages are close to each other. The data shows that, at least under standard lab conditions, loss of *bcc-1* has no impact on animal fertility. This finding could be explained either by *bcc-1* having a biological role completely different from *gld-3* or –on the contrary– by a strong genetic redundancy of both genes. In this case, the presence of *gld-3* would be enough to compensate for missing *bcc-1*. However, regarding brood size, the presence of *bcc-1* is not sufficient to make up for loss of *gld-3* (Eckmann et al. 2002), making the converse scenario less likely.

BCC-1 is expressed in all larval stages, but not detectable in the embryo

To further elude on a potentially different character of *bcc-1* and *gld-3*, the temporal expression pattern of BCC-1 and GLD-3 were investigated, as redundantly functioning genes would be expected to exhibit at least overlapping expression. To elucidate in which larval stages either protein is expressed, worms possessing the *bcc-1*(*ef52*) allele, encoding for an N-terminally 2xFLAG tagged BCC-1, were utilized for developmental western blotting. Worms were synchronized using bleaching solution and collected as either embryos or allowed to hatch overnight, spotted on plates and collected in different larval stages by washing off and snap freezing in liquid nitrogen. Adult worms (n=100) were manually picked into 10 μ l of M9. Once all samples were collected, proteins were extracted in SDS sample buffer and subjected to western blotting using mouse α -FLAG to detect the FLAG::BCC-1 fusion protein (**Figure 12**). Detection with α -BCC-1 was not attempted due to known strong background signals (**Figure 10**). Furthermore, a mouse monoclonal pan- α -GLD-3 antibody (preexisting in the lab) to follow expression of GLD-3 isoforms, and one against α -tubulin was used to control for loading, were applied. A mixed-stage population of wild-type worms was included as a specificity control for the mouse α -FLAG antibody. Only one antibody was applied at a time and the membrane was stripped after each individual detection event (see materials and methods).

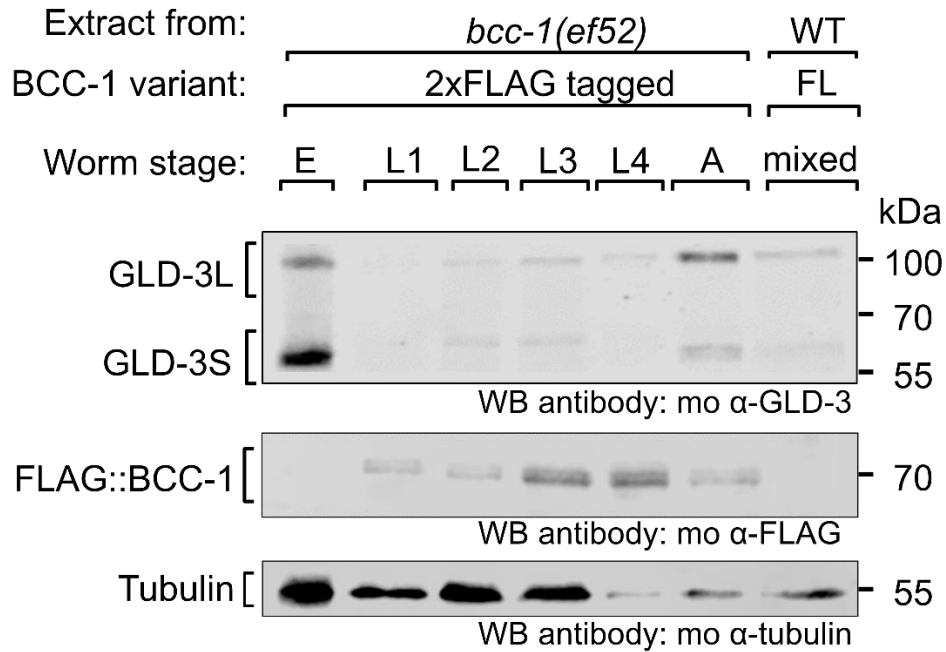


Figure 12: Developmental western blot (WB) reveals BCC-1 expression in all stages but embryos. Mouse (mo) α -GLD-3, α -FLAG, and α -tubulin were used to probe a blot containing protein extracts of wild-type (WT) and *bcc-1(ef52)* worms of different stages expressing either full length (FL) or N-terminally FLAG tagged BCC-1. Synchronized worm stages are: E – embryos, L – larval stages, A – young adult worms. Marker bands in kilodaltons (kDa) as well as signals corresponding to tubulin, tagged BCC-1 and the long (L) as well as short (S) isoform of GLD-3 are indicated. Two independent experiments performed.

gld-3 is reported to encode for 2 major protein isoforms, GLD-3L and GLD-3S (Eckmann et al. 2002). Both proteins were found to be predominantly expressed in embryos and adults, with GLD-3S being most abundant in embryos (Eckmann et al. 2002). In addition, either isoform of GLD-3 is not detected in adult worms expressing an only rudimentary germ line tissue (Eckmann et al. 2002), demonstrating that GLD-3 is primarily a protein expressed in the germ line. Consistent with these published findings, this study found GLD-3 signals predominating in embryos and adults (**Figure 12**), with the vast majority of GLD-3S appearing in embryo samples, indicating that embryos developing within the adult mothers contribute to signal intensity. In larvae, GLD-3 expression can barely be detected; however, for GLD-3L there seems to be an increase with larval stages, correlating with progressive germ line development. When comparing extracts of adults and mixed stage animals, the latter seem to show identical, but weaker GLD-3 bands, which can be explained by the sample consisting of more larval worms, diluting GLD-3 amounts in the extract. Together, the data matches the published expression pattern of GLD-3 as maternally donated germ line protein involved in embryogenesis (Eckmann et al. 2002).

Bands corresponding to FLAG::BCC-1 were detected in extracts of all larval stages and adults, but not in extracts of embryos (**Figure 12**). Furthermore, an absence of signal in wild-type demonstrates specificity of the monoclonal mouse antibody. Observing the signals for tubulin revealed that similar amounts of protein were loaded with the exception of L4 and adult extracts. When normalized to their tubulin loading controls, lanes containing L4 extracts displayed stronger bands specific to FLAG::BCC-1 than lanes of other larval stages and adults. Also, the detected signal appears to be at least a duplet, which is consistent with results using α -BCC-1 antibodies (**Figure 7**, **Figure 10**), arguing that the appearance of additional bands is independent of a native N-terminus of BCC-1. As abundance of FLAG::BCC-1 is not correlating with germ line development and FLAG::BCC-1 is not detectable in embryos, these data does neither support a strict coexpression of BCC-1 with GLD-3 nor does it suggest that BCC-1 is maternally donated and may playing a role in embryogenesis like GLD-3 (Eckmann et al. 2002). These conclusions are consistent with the previous finding that loss of *bcc-1* does not impact fertility (**Figure 11**) and, therefore, would rather indicate non-redundant roles of *bcc-1* and *gld-3*.

BCC-1 expression levels do not change significantly throughout the first larval stage

After establishing that BCC-1 is present in all larval stages, but not detectable in the embryo, the question arises when BCC-1 expression actually starts and whether it changes in abundance within developmental stages. Transcript levels of *bcc-1* have been reported to oscillate (roughly 2.4 fold) within a period of 8 hours at 20 °C (Hendriks et al. 2014). This suggests a potential difference in BCC-1 protein abundance within a single larval stage, as these last for 7-14 hours (Byerly et al. 1976).

To examine whether BCC-1 amount changes in the first larval stage, wild-type L1 worms were synchronized by bleaching and collected at different time points after being spotted on NGM plates with food. To make sample collection more convenient while allowing for maximum growth, worms were grown at 25 °C. Collected worms were snap-frozen, mixed with SDS sample buffer and subjected to western blotting using affinity purified α -BCC-1 antibody solution. A previously generated mixed-stage extract of worms carrying the null allele *bcc-1(ef48)* was loaded as a specificity control (**Figure 13**).

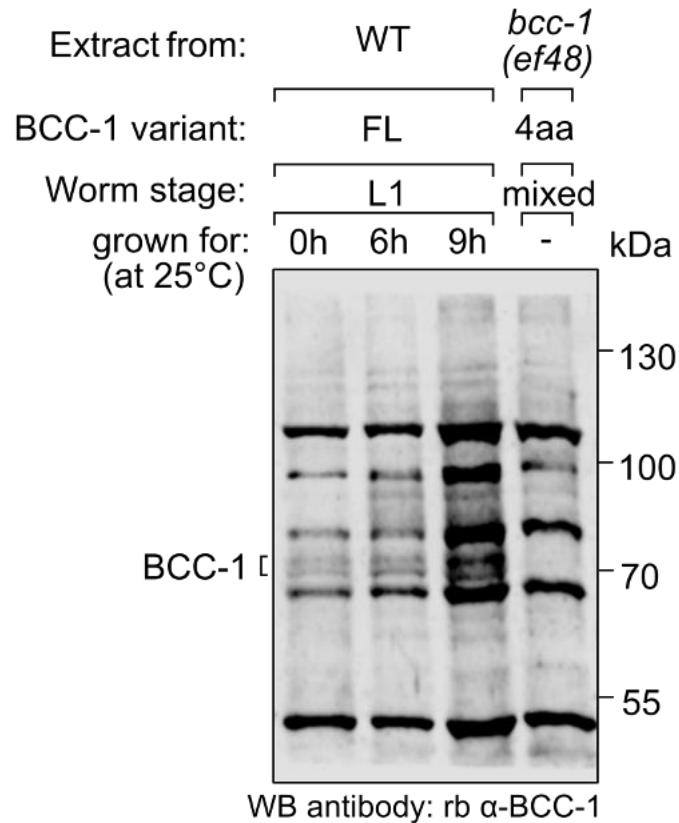


Figure 13: Wild-type express multiple BCC-1 variants throughout the first larval (L1) stage. Rabbit (rb) α-BCC-1 was used to probe a blot containing extracts of wild-type (WT) worms expressing full-length (FL) BCC-1. Animals were spotted on plates with or without (0h sample) bacterial food, removed after indicated amount of time at 25 °C and subjected to western blotting (WB). A previously generated mixed-stage extract of *bcc-1(ef48)* animals expressing BCC-1 truncated to its first 4 amino acids (aa) was loaded alongside. Dash indicates that mixed-stage animals were not grown for a defined amount of time. Marker bands in kilodaltons (kDa) are indicated.

When comparing extracts of WT animals to *bcc-1(ef48)* null mutants, BCC-1 specific signals appeared as at least a duplet on the blot, as it was seen in previous blots (**Figure 7**, **Figure 9**, **Figure 10**). Both bands were comparable in terms of intensity regardless of animal age (**Figure 13**, L1 lanes). While only the 9h sample visually differed in intensity, this sample also seemed to have more protein loaded overall, as indicated by the more intense unspecific protein bands. This data argues that BCC-1 is already present in freshly hatched animals and that expression of BCC-1 variants remains somewhat constant within the first larval stage. Why the mRNA of *bcc-1* oscillates as reported by Hendriks et al. 2014 remains elusive.

BCC-1 expression is unaffected by removal of germ line tissue

To assess whether BCC-1 is present in germ cells, like GLD-3, worms carrying a 2xFLAG tag introduced to the endogenous locus of *bcc-1* [*bcc-1(ef52)*] were crossed into a temperature sensitive *glp-4* mutant strain. As adults, these animals possess only rudimentary germ line tissue when raised at 25 °C, while exhibiting a wild type-like germ line tissue when

grown at 16°C (Rastogi et al. 2015). Hence, animals grown at different temperatures were used for western blotting. To generate protein extracts, 50 worms were manually picked into a minimal amount of M9, mixed with SDS sample buffer and subjected to SDS-PAGE. Western blots were conducted using mouse α -FLAG and α -actin antibody.

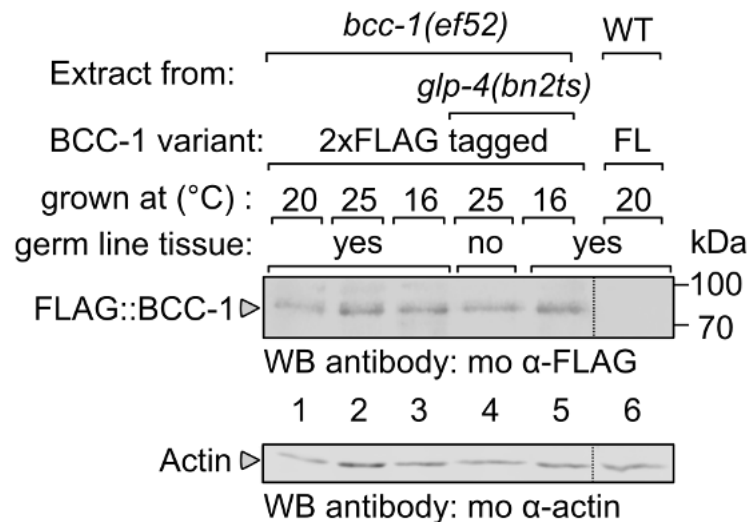


Figure 14: BCC-1 expression is independent of temperature and presence of a germ line tissue. Adult worms of indicated genotypes were grown at indicated temperatures and hand-picked in groups of 50 for western blotting (WB) analysis. Worms expressed full-length BCC-1 either from a wild-type (WT) locus or the *bcc-1(eF52)* locus encoding 2xFLAG::BCC-1. Additionally, *bcc-1(eF52)* worms carrying a temperature sensitive *glp-4* mutation (*bn2ts*) were picked. These worms possess only a rudimentary germ line when raised at 25 °C. WB membrane was probed with mouse (mo) α -FLAG and α -actin as loading control. Marker bands in kilodaltons (kDa) are indicated. Two independent experiments performed.

In **Figure 14**, all but wild-type derived extracts exhibited distinct bands corresponding to the molecular weight of FLAG::BCC-1. As these signals were similar in lanes 1 to 3, it can be concluded that expression of BCC-1 is not affected by the temperature in which animals were grown. Furthermore, a comparison of lane 4 to 5 shows no apparent difference, indicating that BCC-1 expression is independent of germ cells. As BCC-1 is expressed in both adults containing or not containing a germ line tissue, the data suggest that BCC-1 is –unlike GLD-3– a predominantly somatically expressed protein in adult worms.

BCC-1 is expressed in the hypodermis of *C. elegans*

While the results displayed in **Figure 11**, **Figure 12**, and **Figure 14** indicate that BCC-1 is a protein expressed in the soma, it remained unanswered in which tissue(s) BCC-1 is expressed. To tackle this question, transcriptional reporter strains expressing a FLAG::GFP fusion protein mediated by the presumed *bcc-1* promoter were generated using the Mos1-mediated Single Copy Insertion (MosSCI) technique (Frøkjær-Jensen et al. 2008) (**Figure 15**,

A). The strains were made with the help of Maxie Rockstroh and Dr. Kathrin Patsias and analyzed using widefield fluorescence microscopy. Based on a similar transcriptional GFP reporter driven by the putative promoter region of *bcc-1* incorporated as a transgene of an extrachromosomal array, Jones et al. suggested *bcc-1* to be expressed in the hypodermis (Jones et al. 2013). For this reason, additional transcriptional reporter strains were constructed, expressing FLAG::GFP under the control of the *dpy-7* promoter that is reported to be expressed in the same tissue (Gilleard et al. 1997) (**Figure 15, A**).

Prior to microscopical experiments, all generated strains carrying reporter constructs were assessed regarding their FLAG::GFP expression levels. Protein analysis was done by hand-picking 50 adult worms into a minimal amount of M9, mixing with SDS sample buffer and subsequent SDS-PAGE followed by western blotting using mouse α -FLAG antibody (**Figure 15, B**). In this western blot analysis, only protein extracts from transgenic strains contained a single band correlating with the theoretical molecular weight of the GFP fusion protein reporter (**Figure 15, B**). However, one of the two *bcc-1* reporter strains (i.e., EV1114) exhibited a much weaker signal, compared to the other *bcc-1* reporter strain (i.e., EV1115). However, its expression level was comparable to the two *dpy-7* reporter strains (**Figure 15, B**), suggesting that EV1114 reflects upon a lower promoter activity than seen in EV1115. A molecular reason for this difference remains unclear.

Next, the generated strains were compared regarding their *in vivo* GFP expression pattern by immobilizing on agar pads mounted animals with levamisole for widefield fluorescence microscopy (**Figure 15, C**). Above noted expression differences at the western blot level among the two *bcc-1* reporter strains were recapitulated by observing GFP autofluorescence differences by widefield microscopy; EV1114 showed a less intense GFP fluorescence signal than the other reporter strains (**Figure 15, C**). Nonetheless, all animals share a comparable expression pattern of GFP in the peripheral cells of the organism, spanning the whole animal with the exclusion of head, tail, and vulva areas. As the GFP expression pattern driven by the *dpy-7* promoter looks similar to a *bcc-1* promoter driven one, it seems likely that the (presumed) *bcc-1* promoter is active and that *bcc-1* is expressed in the hypodermis.

In future experiments, the lower expressing transcriptional *bcc-1* reporter strain was not used anymore, as the signal intensity was deemed too low. Instead, the *bcc-1* reporter EV1115 was used for further microscopic characterization.

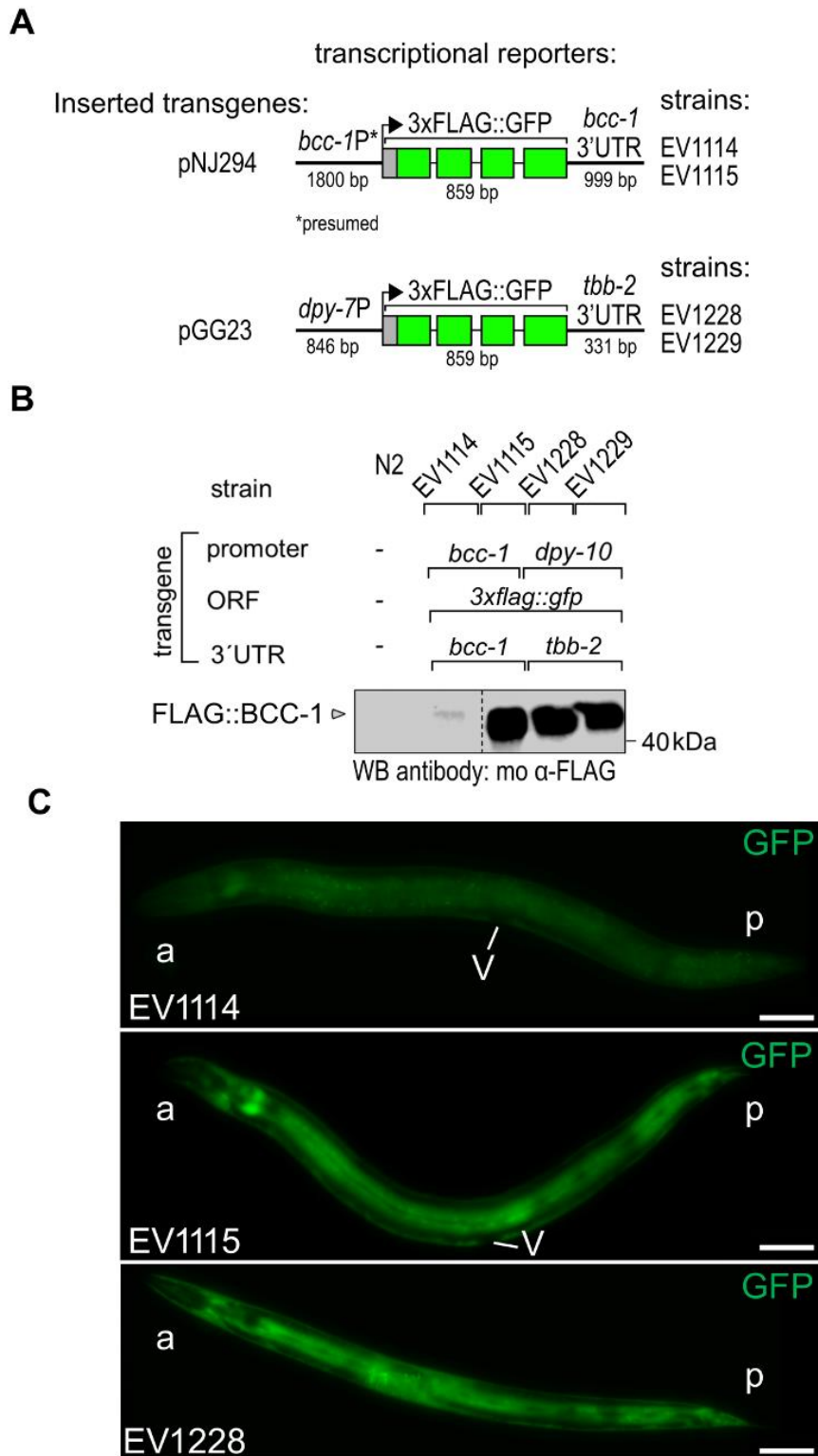


Figure 15: The *bcc-1* promoter is predominantly active in the epidermis. (A) Schematic representation of plasmid-derived integrated transgenes. Respective strains were constructed by Maxie Rockstroh. An intronized open reading frame (ORF) encoding a 3xFLAG::Green fluorescent protein (GFP) fusion sequence is downstream of *bcc-1* or *dpy-7* promoters (P), followed by 3' untranslated regions (UTR) of *bcc-1* or *tbb-2*, directing translational control. (B) Western blot (WB) detection of FLAG::GFP fusion protein via mouse (mo) α-FLAG antibody; 50 adults per lane. (C) Exemplary widefield fluorescent microscopy maximum intensity projections of transgenic adults; anterior (a) and posterior (p) ends are indicated; position of vulva (V) indicated if visible. Pictures were taken with identical acquisition settings to allow for comparison of intensity; $n > 5$ worms per strain. Scale bars represent 50 μm .

To improve the level of cellular detail in describing *bcc-1* promoter activity, confocal microscopy was conducted. High resolution images of young adult worms revealed a homogenous GFP signal in the epidermis of adult worms (**Figure 16**). GFP signal intensities appeared to be equally strong across the animal and in the cytoplasm of the multinucleated hyp7 epidermis. However, GFP signal accumulated also in round structures being deprived of signal in its center. The number, localization and signal-devoid central areas of these rounded structures indicate them being nuclei, consistent with GFP's molecular mass to pass through the nuclear pore complexes by diffusion while being unable to enter the nucleoli. Seam cells extending along the lateral lines of hyp7 were found to be devoid of GFP signal. Seam cells extending along the lateral lines of hyp7 were found to be devoid of GFP signal. Consistent with widefield microscopy (**Figure 15, C**), GFP signal was absent in other epithelial parts like parts of the head, the tail and the vulva. Together, this suggests that *bcc-1* activity might be confined to hyp7.

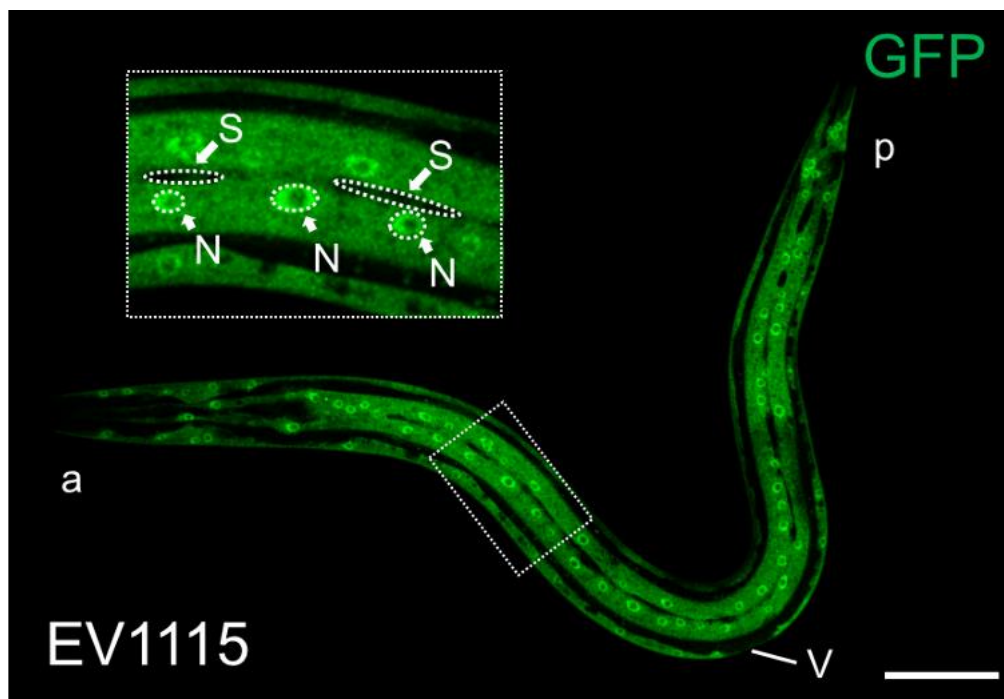


Figure 16: The *bcc-1* GFP reporter reveals transcriptional activity primarily in the syncytial hypodermis. Confocal microscopy of living transgenic adults immobilized on agar pads and detected in the GFP channel. Multiple apical planes were merged into a maximum intensity projection spanning 21 μm . Anterior (a) and posterior (p) region as well as the position of the vulva is indicated. A blow up (dotted rectangular region) indicates the position of two highlighted seam cells (S, longer arrows) and three nuclei (N, shorter arrows). $n > 5$ worms analyzed.

To further corroborate the insights from the transcriptional *bcc-1* GFP reporter strain and to gain insights into the expression dynamics of endogenous BCC-1 protein, CRISPR/Cas9 was used to introduce a sequence that encodes 3xFLAG::mCherry into the endogenous locus of *bcc-1*. The generated N-terminally tagged BCC-1 fusion protein

encoding allele, *bcc-1(ef58)*, was made by Dr. Kathrin Patsias and analyzed using confocal microscopy. Larval worms were immobilized on agar pads using levamisole and mCherry::BCC-1 expression detected using a mCherry microscopy channel. As this strain does not express any GFP, the GFP channel is used to visualize the worms' general outline by making use of its' autofluorescence.

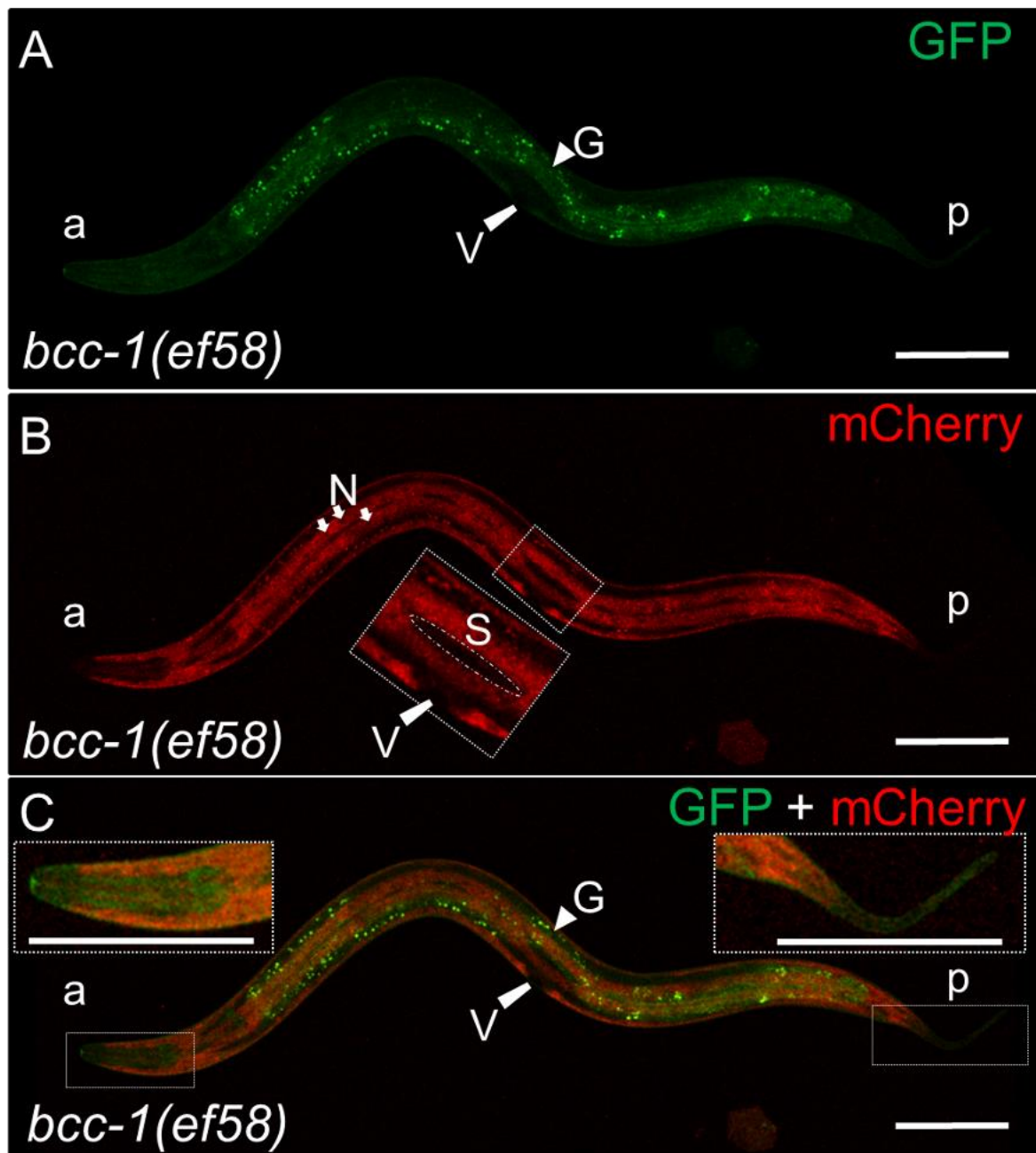


Figure 17: mCherry::BCC-1 fusion protein is homogenously distributed throughout hyp7. Confocal microscopy images of living L4 larvae immobilized on agar pads. Displayed are maximum intensity projections totaling to 39 μm in thickness. Anterior (a) and posterior (p) orientations are indicated; the extent of the gut (G) is well visible in the green GFP channel; the developing vulva (V) in the center of the animal is marked. (A) GFP and (B) mCherry channel; (C) overlay of both fluorescent channels. Images of zoomed in areas, outlined by dashed lines, were increased in brightness and

lowered in contrast in (C). Arrows indicate positions of selected nuclei (N) and a seam cell (S) is highlighted by a dashed ellipsoid. Scale bars represent 50 μm . $n > 10$ worms analyzed.

Figure 17 shows an example of a larval stage 4 hermaphroditic animal imaged for general shape in the GFP channel (**Figure 17, A**), and for tissues expressing the mCherry::BCC-1 fusion protein (**Figure 17, B**). Intense autofluorescence emitted primarily from intestinal lysosomal-related gut granules is visualized in the GFP channel. This phenomenon enables to mark the position of the gut, as reported before (Pincus et al. 2016). The mCherry::BCC-1 signal (**Figure 17, B**) exhibited a pattern very similar to what has been observed in **Figure 16** for the transcriptional *bcc-1* reporter. mCherry::BCC-1 is expressed homogeneously in hypodermal tissue, displaying four characteristic bands of *hyp7*, but is excluded from seam or vulval cells (**Figure 17, B and C**). Subcellularly, round objects deprived of mCherry::BCC-1 can be spotted, which likely represent nuclei (**Figure 17, B**), indicating that mCherry::BCC-1 localizes primarily to the cytoplasm. By overlaying the red and green channels, it became apparent that the GFP signal from the animals' gut and mCherry::BCC-1 are different (**Figure 17, C**). Furthermore, the tips of head and tail are not showing any mCherry::BCC-1 signal. The presence of these boundaries therefore indicates that endogenous BCC-1 might be predominantly expressed in the main syncytium of the epidermis, which is *hyp7*. By taking together data of **Figure 17** and **Figure 16**, it can be concluded that *bcc-1* is an epidermally active gene, driving the production of a cytoplasmically localized protein, expressed abundantly in the *hyp7* cell.

To further ascertain the specificity of the fluorescence signal of mCherry::BCC-1, an RNAi feeding clone against the ORF of *bcc-1* was constructed. Then L1 *bcc-1(ef58)* worms were fed bacteria expressing dsRNA against *bcc-1* or *xfp* that served as a negative control. Confocal microscopy was applied to examine how the feeding RNAi alters signal intensities (**Figure 18**).

Animals fed with *xfp* control or *bcc-1* RNAi did not display any overt phenotypical anomalies at the morphological level and had wild type-like appearance in DIC microscopy (**Figure 18, A and B**), arguing that neither tagging nor downregulation of *bcc-1* does have severe consequences on animal development. However, by comparing *xfp* to *bcc-1* RNAi-treated animals, the fluorescent signal vanished almost to completion only upon *bcc-1* RNAi (**Figure 18, compare A' to B'**). This shows that the constructed RNAi clone is functional and that the signals obtained in the mCherry channel are to a very large degree not artificial, but related to *bcc-1* gene products derived from the endogenous transgenic locus.

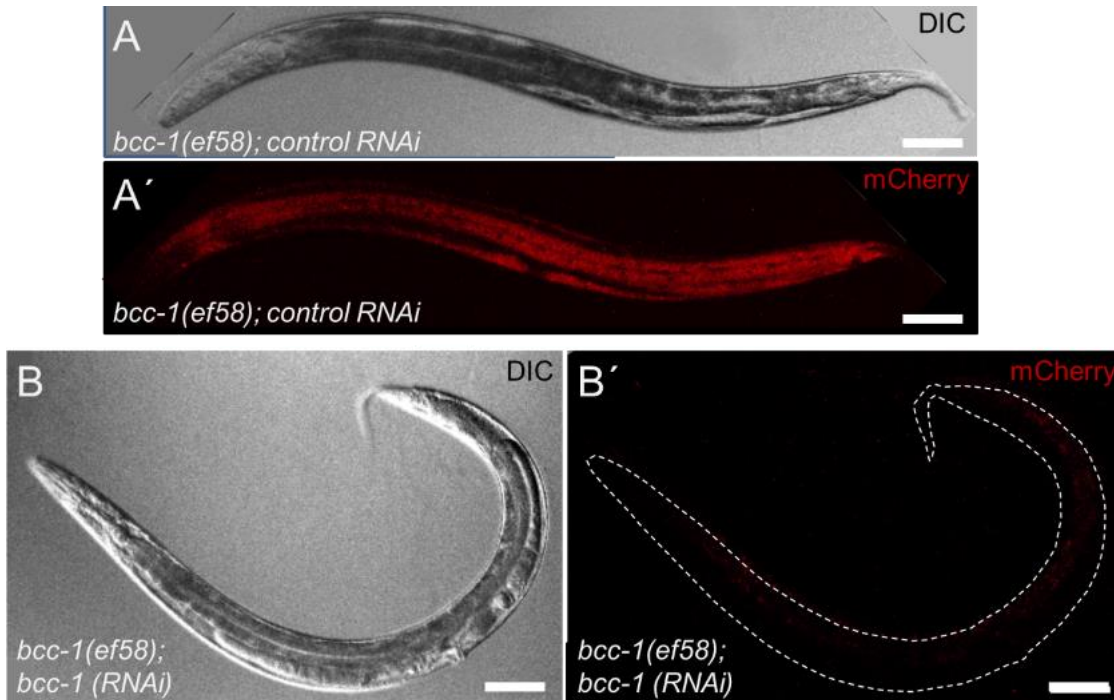


Figure 18: *bcc-1* RNAi strongly reduces mCherry::BCC-1 signal intensities. L1 worms containing the sequence of mCherry fused to the endogenous locus of *bcc-1* (allele *ef58*) were fed dsRNA against *bcc-1* or *xfp* for two days. Young adults were then immobilized on agar pads and subjected to confocal microscopy. Displayed are single plane differential interference contrast (DIC) images (A, B) and maximum intensity projections (A', B') of 39 μm in the mCherry channel processed equally. Dashed line in B' indicates the worms outline from B. Scale bars represent 50 μm .

Spatial BCC-1 expression in L1 larvae resembles those of later stages

After finding mCherry::BCC-1 in the hypodermis of L4 animals (**Figure 17**), it was investigated whether in earlier stages other tissues might show expression of BCC-1. To answer this question, adult *bcc-1(ef58)* animals were bleached and surviving embryos were allowed to hatch into M9 medium overnight. Freshly hatched larvae (L1 worms) halt development in “L1 arrest” or until sufficient food is supplied (Baugh 2013). On the next day, starvation arrested L1 worms were spotted onto empty plates before being mounted for confocal microscopy, using levamisole and agar pads to immobilize <5 living animals per pad. An example is given in **Figure 19**.

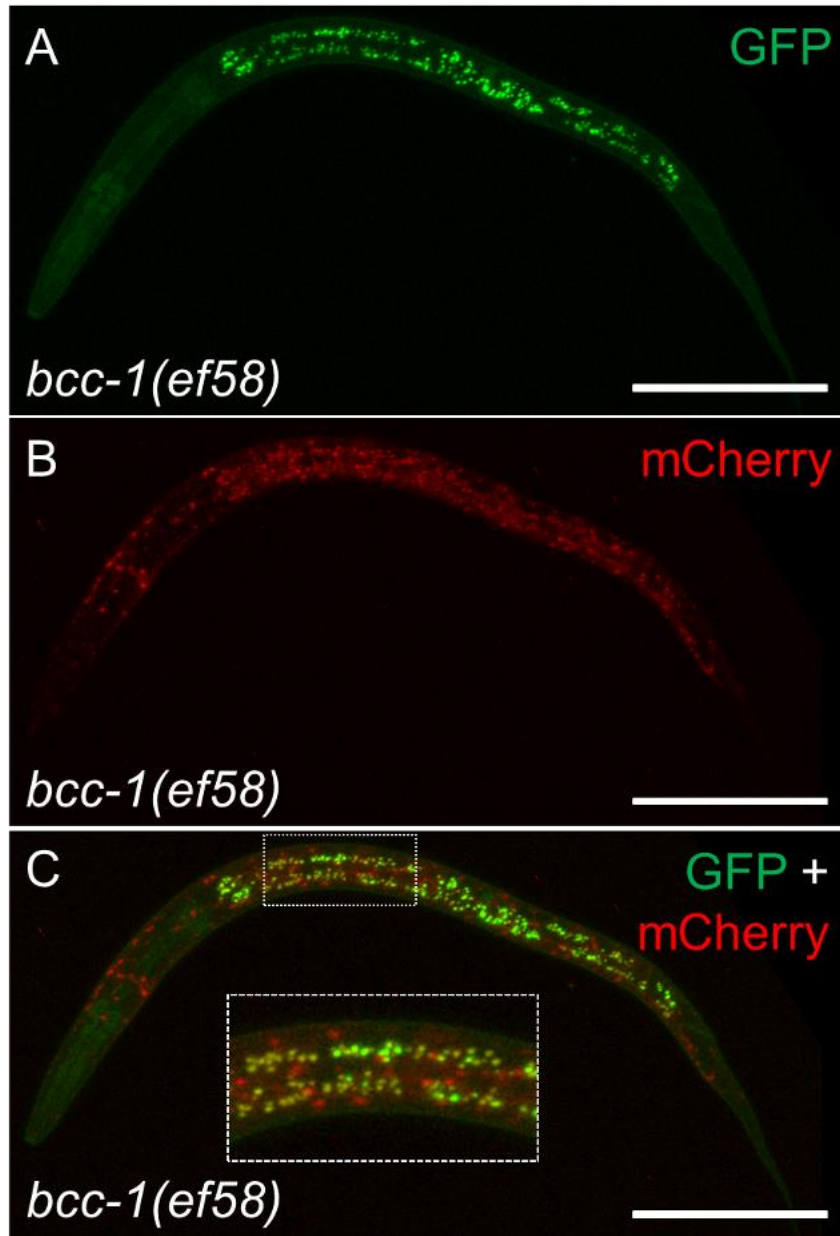


Figure 19: Starvation-arrested larval stage 1 (L1) worms express BCC-1 in hyp7. Hatched worms without access to food were immobilized on agar pads and subjected to confocal microscopy. Displayed are maximum intensity projections (17 μ m) showing (A) mCherry and (B) GFP channel as well as an overlay (C). Autofluorescent gut area was zoomed in (dashed lines) to better visualize that GFP and mCherry signals are different. Also, note granular appearance of mCherry::BCC-1 signals throughout hyp7. Scale bars represent 50 μ m. $n > 5$ worms analyzed.

Looking at the mCherry channel, confocal microscopy of transgenic L1 worms (**Figure 19, B**) revealed mCherry::BCC-1 signals spanning large parts of the worm with head and tail being excluded, indicating the same tissue expression pattern as in L4 worms (**Figure 17, B**) and adults (**Figure 18, A**). Nonetheless, starvation-arrested L1 transgenic worms exhibited a mCherry::BCC-1 signal distribution less homogenous and more granular (**Figure 19, B**) than previously seen in **Figure 17, B** and **Figure 18, A**. Furthermore, an overlay of the

mCherry with the autofluorescence (GFP) channel revealed that the vast majority of red signal is exclusive to the mCherry channel and absent in the GFP channel, indicating that red signal is specific to mCherry::BCC-1 (**Figure 19, C**). The more granular expression pattern might be due to the worm's age or its physiological condition, as it did not have access to food. The data suggests that BCC-1 is already synthesized in freshly hatched L1 worms and expressed in the hyp7 syncytium of the hypodermis.

BCC-1 is a cytosolic protein

The major subcellular difference observed in confocal microscopy using a transcriptional GFP reporter strain (**Figure 16**) and an endogenously mCherry-tagged strain (**Figure 17**) affected round objects in the multinucleated syncytium of hyp7 that accumulated GFP but not mCherry::BCC-1. As GFP has a tendency to translocate to nuclei (Seibel et al. 2007), it was tested whether the structures in question represent indeed nuclei. To this end, the endogenously tagged mCherry allele *bcc-1(eF58)* was combined with the chromosomally integrated transgene *knuSi221* that expresses an eGFP::FIB-1 fusion protein. Fibrillarin (FIB)-1 is a protein involved in nucleogenesis and enriches in the nucleolus (Lee et al. 2012). Therefore, the fusion protein eGFP::FIB-1 can be used to highlight the position of nucleoli within a nucleus. The strain containing both marked genes, *knuSi221; bcc-1(eF58)*, was generated by crossing and its progeny was analyzed using confocal microscopy using levamisole and agar pads (**Figure 20, n>5**).

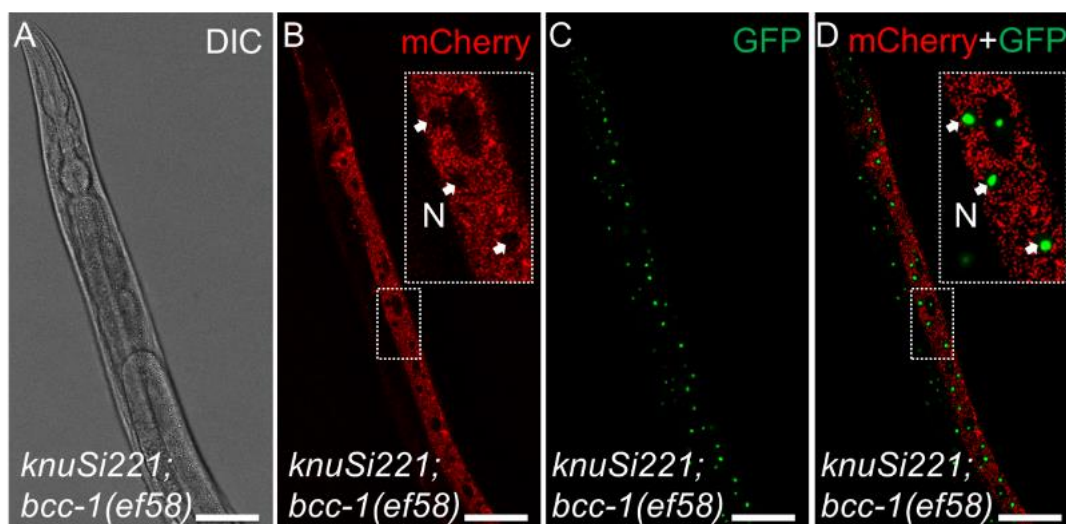


Figure 20: BCC-1 is expressed in the cytosol. Young adult expressing eGFP::FIB-1 and mCherry::BCC-1 were imaged on agar pads. Displayed is an image of a single plane from an anterior region. (A) Differential interference contrast showing the entire head region and parts of the gut and a gonadal arm. (B) mCherry and (C) GFP channel and (D) an overlay of the two fluorescent channels is shown with a selected epithelial area (dashed lines) being zoomed in. Arrows indicate positions of selected nuclei (N). Scale bars represent 50 μm . $n>5$ worms analyzed.

By comparing DIC with the mCherry channel in the top head region, an exclusion of mCherry::BCC-1 signal was seen (**Figure 20**, A and B), similar to what had been observed before (**Figure 17**). Furthermore, mCherry::BCC-1 signal seemed absent from visible gonadal regions. Images of higher magnification than given in **Figure 17** clearly displayed round areas deprived of mCherry::BCC-1 signal (**Figure 20**, B). Images of the GFP channel revealed the position of nucleoli (**Figure 20**, C). An overlay of both red and green channels (**Figure 20**, D) demonstrated that most of the signal-holes in the mCherry channel contained intense eGFP::FIB-1 signal. Conversely, nucleolar eGFP::FIB-1 signals did not appear to overlay with mCherry::BCC-1 signals, arguing they are spatially distant from each other. Notably, the green signal does not only appear within the areas devoid of signal in the mCherry channel, it also does not completely fill them, sparing a small area, due to FIB-1 only being localized in the nucleoli, leaving the rest of the nucleus deprived of either fluorescent signal (**Figure 20**, D). Taken together this data strongly argues that, at the subcellular level, BCC-1 is predominantly a cytosolic protein.

BCC-1 has a role in osmoregulation

Loss of *bcc-1* effects salt stress recovery rate

After establishing BCC-1 as a somatic protein of the *C. elegans* hypodermis (**Figure 16**, **Figure 17**, and **Figure 20**) putative biological functions of *bcc-1* were investigated next. One main function of the hypodermis is osmoregulation (Rohlfing et al. 2011). This is well in line with proposed kidney-related functions of Bicaudal-C proteins, which are associated with cystic renal structures in many systems like flies, zebrafish, frogs and mice (Gamberi et al. 2017; Bouvrette et al. 2010; Tran et al. 2010; Bouvrette et al. 2008; Gamberi et al. 2017).

To investigate, whether also *bcc-1* is related to salt and water balance, the ability of *bcc-1* mutants to recover from salt stress was tested using a slightly adapted published salt stress recovery assay (Hahn-Windgassen and van Gilst 2009). Young adult worms grown on regular NGM plates at 20 °C were manually transferred to a high salt plate containing 500 mM NaCl. Worms were transferred back manually (unlike Hahn-Windgassen and van Gilst, who washed worms from plates) to regular NGM plates after 4 hours. 24 hours later, recovery was checked by prodding worms with a metal pick. Worms actively moving away from the pick were scored as recovered; worms not responding or moving while staying in place were counted as non-recovered. A graphical representation of the assay is displayed in **Figure 21**, A.

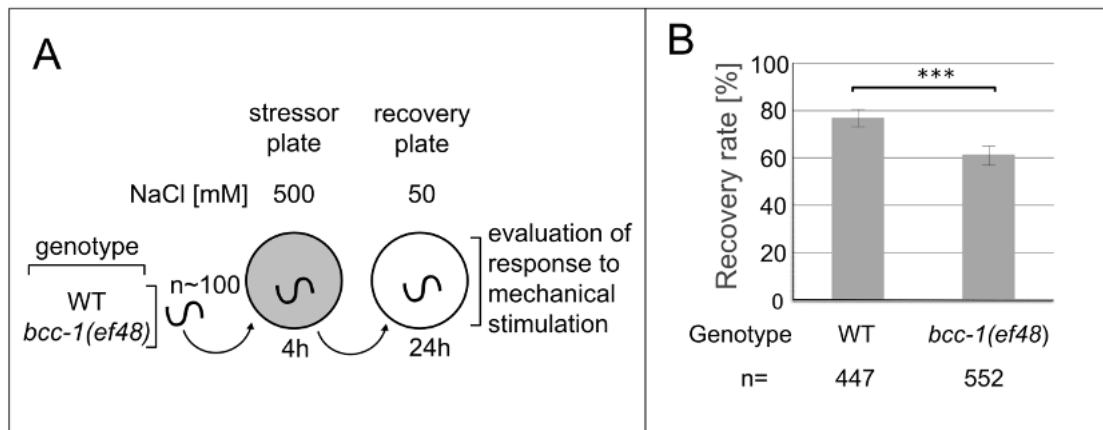


Figure 21. Loss of *bcc-1* reduces recovery rate after salt stress. (A) Schematic overview of the salt stress assay. Young adult wild-type (WT) or *bcc-1(ef48)* protein null mutant animals were placed onto high NaCl NGM agar plates for 4 hours before being transferred back to regular NaCl NGM plates. Worms were scored after 24 hours for recovery. (B) Quantified results of the assay performed 4 times at 20 °C. Recovered fractions of total worms (n) are displayed for both genotypes investigated. Animals not actively crawling away after prodding were scored as not recovered. Error bars represent 95% confidence intervals. Groups were compared using Fisher's exact test and showed significant differences at $p < 0.001$.

After salt stress, more than three quarters (77%, $n=447$) of wild-type worms were able to recover (**Figure 21, B**). In a similar assay, higher rates of survival (~90%) were reported after the same time (Hahn-Windgassen and van Gilst 2009). This might be attributed to methodological differences, as the van Gilst lab did not manually transfer worms to recovery plates but used M9 solution to wash them off. This may result in less physical stress and thus higher survival rates. In contrast to wild-type, variant *bcc-1(ef48)* animals showed a reduced recovery rate of less than two thirds (61% $n=552$). While statistical testing confirms a significant difference compared to wild-type, the absolute decrease in recovery appears to be moderate (**Figure 21, B**). For comparison, RNAi against the osmoregulatory gene *nhr-31*, a HNF α homolog mediating excretory tube function, has a reported survival rate below 20% compared to ~90% in WT (Hahn-Windgassen and van Gilst 2009). Nonetheless, the presented data in **Figure 21** suggests that *bcc-1* plays a role in salt stress recovery, although this is not its main function, as a more drastic change in recovery would otherwise be expected.

mCherry::BCC-1 localizes to granular foci upon stress

As compared to wild-type, salt stress recovery in *bcc-1* mutants was significantly reduced (**Figure 21**), the role of *bcc-1* in salt stress recovery was further explored. In particular as Bicaudal-C homologs are associated with stress-induced RNA granules (stress granules) in other species (Estrada Mallarino et al. 2020), a putative sub-cellular reorganization of BCC-1 upon salt stress was investigated. Animals expressing the transcriptional *bcc-1* GFP reporter (strain EV1115) and those expressing endogenously

mCherry-tagged BCC-1 (*bcc-1(ef58)*) were age-synchronized and grown on either regular (50mM) NGM plates or plates containing elevated levels of salt (100 mM NaCl). As a positive control for stress induction and cellular reaction, animals grown on regular NGM plates were subjected to 1 hour of 35 °C heat exposure, which is reported to induce stress granule formation (Sun et al. 2011). Animals (n>5) were mounted on agar pads in 5 mM levamisole followed by confocal microscopy. To first control for BCC-1 independent subcellular changes in GFP fluorescent signal localization upon either stressor, the worm strain EV1115 was analyzed using confocal microscopy (**Figure 22**).

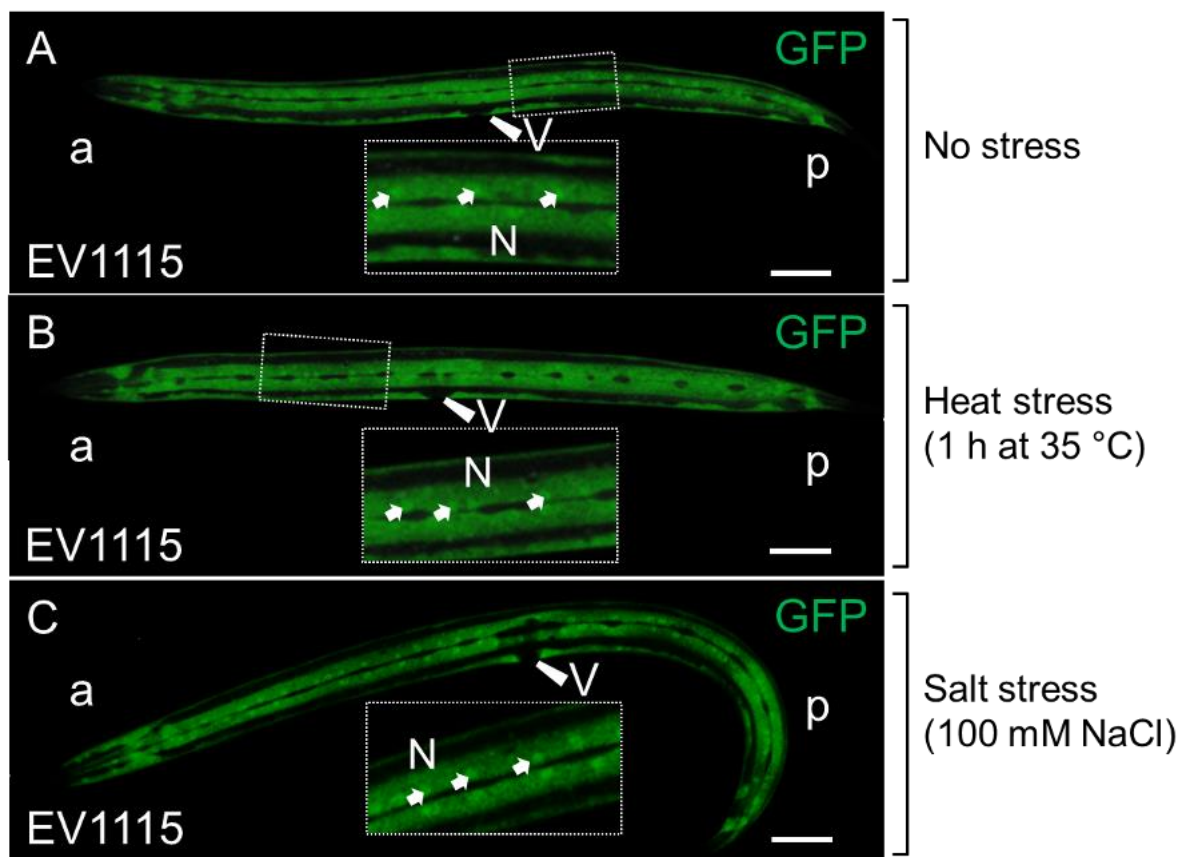


Figure 22: GFP expression and localization is unaffected by stress in EV1115 worms. Transgenic L4 animals expressing GFP under the control of the presumed *bcc-1* promoter were grown at (A) regular (50 mM) or (C) elevated (100 mM) NaCl concentration. (B) As a reference for stress reaction, animals were subjected to 35 °C heat shock for 1 hour. Multiple planes spanning 24-34 μm were merged into a maximum intensity projection. Anterior (a) and posterior (p) regions as well as the localization of the developing vulva (V) are shown. Arrows indicate selected GFP-enriched nuclei (N). Scale bars represent 50 μm.

An evaluation of worm strain EV1115 revealed that irrespective of heat (**Figure 22, B**) or salt stress (**Figure 22, C**), neither GFP expression intensities nor its subcellular localization changed with respect to unstressed animals (**Figure 22, A**). Moreover, GFP signals remained in all cases restricted to *hyp7* and were found distributed smoothly and homogenous in the

cytoplasm with some enrichment in nuclei (**Figure 22**, B and C). As neither salt nor heat stress lead to relocalization of GFP, the same stress analysis setup was repeated for animals expressing endogenously tagged mCherry::BCC-1 fusion protein (**Figure 23**).

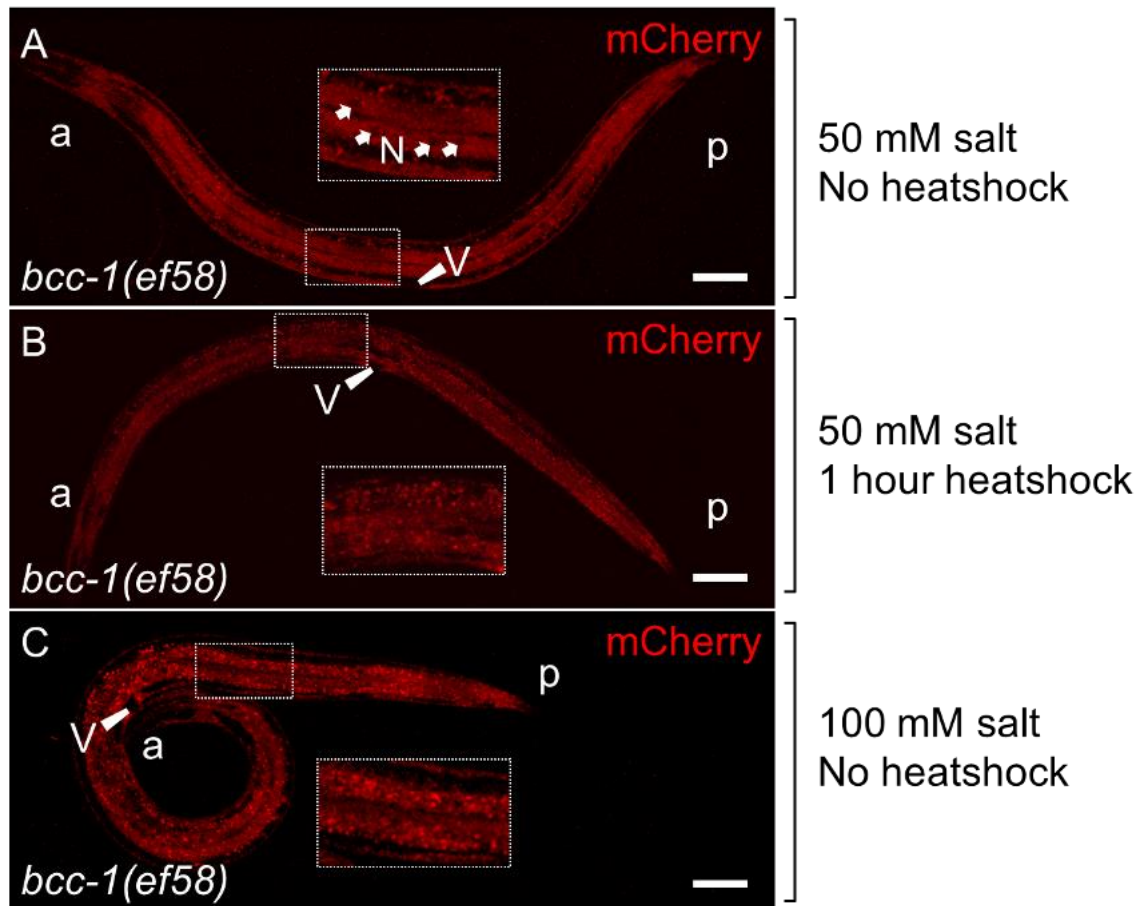


Figure 23: mCherry::BCC-1 localizes to granular foci upon salt and heat stress. (A-C) L4 animals carrying the sequence of mCherry fused to the endogenous locus of *bcc-1* (allele *ef58*) were grown at regular (50 mM) or elevated (100 mM) NaCl concentration. (B) As a reference for stress reaction, animals were subjected to 35 °C heat shock for 1 hour. Maximum intensity projection planes spanning 32-41 μm were merged. Anterior (a) and posterior (p) regions as well as the localization of the vulva (V) are shown. Arrows indicate selected mCherry::BCC-1 deprived nuclei (N). Scale bars represent 50 μm. Per condition, n>5 animals were analyzed.

If worms are not subjected to stress, an epidermal, smooth and homogenous mCherry::BCC-1 signal can be observed, where the position of nuclei can be inferred by lack of mCherry::BCC-1 signal (**Figure 23**, A). However, after subjecting animals to heat stress (**Figure 23**, B) or growing them on elevated salt concentrations (**Figure 23**, C), mCherry::BCC-1 signal appeared less homogeneously diffuse and more granular in the hyp7 cytoplasm. Moreover, it was difficult to pinpoint the positions of nuclei as they became less distinct (**Figure 23**, B and C). Together with the observation that GFP alone, controlled by the *bcc-1* promoter (**Figure 22**), does not relocalize upon stress, it can be concluded that

mCherry::BCC-1 is undergoing a subcellular change in distribution upon salt and heat stress, indicating that endogenous BCC-1 could also be a part of a general stress response.

mCherry::BCC-1 foci formed upon stress are reversible

To further explore the nature of the stress-related foci observed in **Figure 23**, it was investigated whether induced granular structures containing mCherry::BCC-1 are themselves dynamic as aggregation of mCherry::BCC-1 might be either static or reversible. As salt and heat stress showed comparable subcellular changes in mCherry::BCC-1 localization (**Figure 23**), only heat stress was used for following experiment shown in **Figure 24**. To test for reversibility, $n > 5$ L4 *bcc-1(ef58)* worms expressing mCherry::BCC-1 fusion protein were subjected to confocal microscopy either before, directly after, or 4 hours after heat shock exposure (1 hour at 35 °C). Animals mounted for analysis were not reused; different worms from the same plate were used for each time point. To evaluate homogeneity of mCherry::BCC-1 signal, the visibility of nuclei was qualitatively assessed in **Figure 24**.

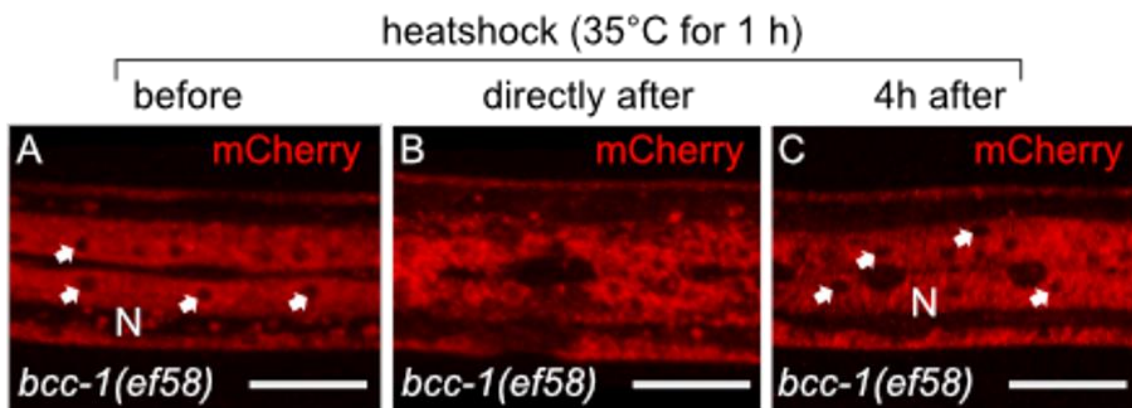


Figure 24: Stress induced mCherry::BCC-1 foci are reversible. (A-C) Different L4 animals expressing the mCherry::BCC-1 fusion protein were analyzed (A) before and (B) after heat shock. (C) After heat treatment, animals were allowed to recover at 20 °C for 4 hours before being analyzed. For confocal microscopy, worms were immobilized on agar pads using 5 mM levamisole. Multiple planes (11-21 μm) were merged into a maximum intensity projection. Arrows indicate position of selected nuclei (N). Scale bars represent 25 μm. Per stage, $n > 5$ worms analyzed.

Similar to previous experiments, untreated animals showed an even distribution of mCherry::BCC-1 signal in the cytoplasm, allowing to spot the position of nuclei (**Figure 24**, A). After heat treatment the signal appeared less diffuse and more granular; nuclei became difficult to discern (**Figure 24**, B). However, after four hours of recovery, nuclei were apparent again in a homogeneously diffuse cytoplasmic mCherry::BCC-1 signal (**Figure 24**, C). Therefore, the fusion protein mCherry::BCC-1 changed subcellular localization reversibly upon heat stress. Given the results documented in **Figure 23**, it is further conceivable that this behavior might extend to other stresses, such as high salt concentrations.

BCC-1 is not detected in the excretory canal

Since a role in osmoregulation was found for *bcc-1* (Figure 21) and Bicaudal-C is generally associated with renal structures in mice, frogs, flies and zebrafish (Cogswell et al. 2003; Tran et al. 2007; Maisonneuve et al. 2009; Bouvrette et al. 2010), it was investigated whether BCC-1 is not only expressed in *hyp7* (Figure 17), but also in other tissues related to osmoregulation. The largest cell of the secretory-excretory system reported to be involved in osmoregulation is the excretory canal (EC) cell (Nelson and Riddle 1984). To test whether BCC-1 is expressed in this bifurcated cell, *bcc-1(ef58)* animals carrying mCherry-tagged *bcc-1* were crossed into a strain possessing an integrated transgene that leads to the expression of GFP under the control of the *vha-1* promotor, which is predominantly active in the EC cell (Mattingly and Buechner 2011). The obtained EV1123 strain (*qpIs11;bcc-1(ef58)*) was investigated by confocal microscopy and analyzed regarding co-localization of GFP and mCherry::BCC-1. An example image is given in Figure 25.

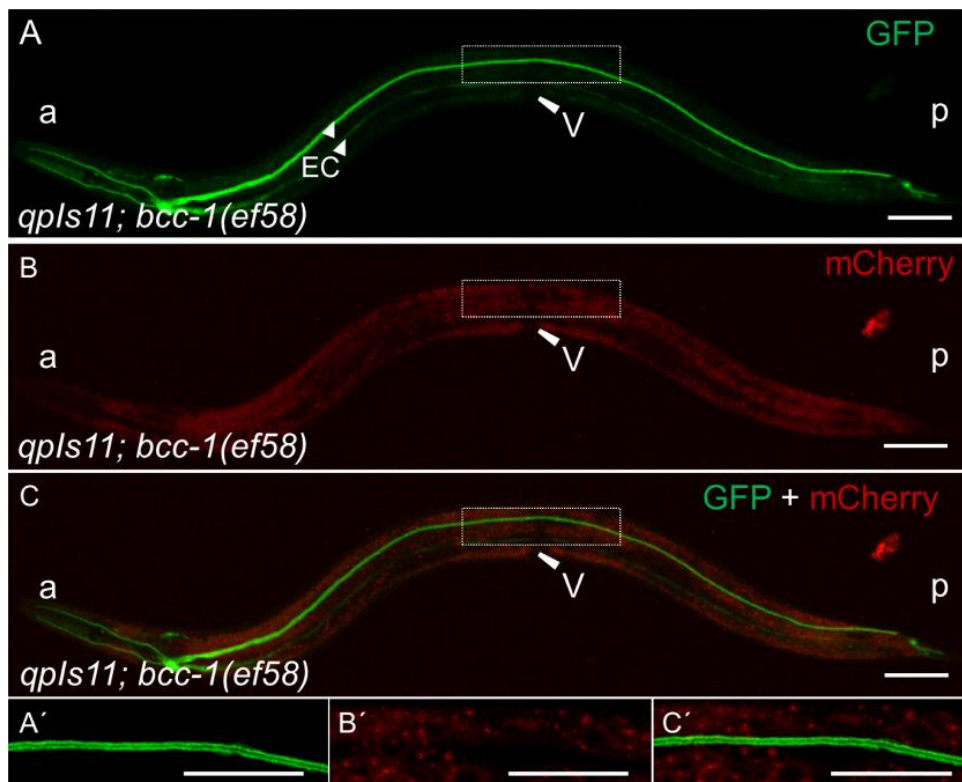


Figure 25: mCherry::BCC-1 is not detected in the excretory canal (EC). L4 animals expressing both EC-driven GFP under the control of a *vha-1* promotor and mCherry::BCC-1 were imaged. Maximum intensity projections of selected confocal planes covering 26 μm. (A, A') GFP, (B, B') mCherry and a merge (C, C') are shown with a single plane being zoomed in (A', B', C'), represented by dashed lines. For orientation, anterior (a), posterior (p), the developing vulva (V), and excretory canals branches are indicated. Scale bars represent 50 μm.

The EC cell was found to extend throughout the animals' body, adopting an H-like shape, with two extensions in the head region and two long lateral extensions posterior towards the animal's tail (**Figure 25, A**). Its cell body was seen to contain a single nucleus located in the bridge connecting both EC branches near the pharyngeal bulb. Presumably, due to technical reasons of image analysis, one of the two posterior canals is more prominently marked by GFP expression. Both shorter anterior canals showed equal GFP signal intensities (**Figure 25, A**). A comparison of GFP and mCherry signals revealed no overt overlap (**Figure 25, C**). In the focal planes the excretory cells are located, less mCherry::BCC-1 signal is obtained, resulting in a weaker signal requiring additional contrasting (**Figure 25, B and C**). Consistent with a more interior position of the EC branches, the typical hyp7 band-like structure and its nuclei devoid signal were barely detectable (**Figure 25, B and C**). In merges of GFP and mCherry channels, no colocalization of both signals, displayed in yellow, was visible (**Figure 25, C**). To further scrutinize this finding, a single plane corresponding to one EC branch was analyzed at higher magnifications (**Figure 25, A' to C'**). However, the chosen plane did not reveal a colocalization of GFP with mCherry signals either, suggesting that BCC-1 is predominantly expressed in the hypodermis, but either below detection level or not at all in the EC. Taken together, these data argue that while *bcc-1* has a role in osmoregulation (**Figure 21**) its function might not be directly associated with an organismal salt-water balance but rather with a cellular general stress response in the hypodermis.

BCC-1 is not essential for male mating

BCC-1 is expressed in male tissue required for mating

A likely role of *bcc-1* in osmoregulation (**Figure 21**) is in line with established connection of Bicardal-C to renal tissue (Dowdle et al. 2022). In vertebrates one of the associations of Bic-C with kidneys is the suggested upregulation of polycystin-2 (*pkd2*) RNA (Tran et al. 2010; Rothé et al. 2020). Mutations in *pkd-2* are casually linked to polycystic kidney disease in human (Deltas 2001). As *pkd2* has an ortholog in the nematode, it was investigated whether the *C. elegans* pendant *pkd-2* might be regulated by BCC-1. In nematodes, however, *pkd-2* has neither been linked to kidney function nor osmoregulation to date. Instead, the derived protein product, PKD-2, was found expressed in male tail structures and its function is connected to a male's ability to localize the vulva of a mating partner (Barr and Sternberg 1999; Barr et al. 2001).

To evaluate whether the two genes *bcc-1* and *pkd-2* could be functionally connected, it was first established whether expression of BCC-1 in males is different from the established

expression pattern in hermaphrodites (Figure 16, Figure 17, Figure 20), as *hyp7* has been reported to contain the bulks of male rays, a vital part of the male reproductive system (Chow et al. 1995). To this end, L4 animals carrying a mCherry-tagged endogenous *bcc-1* locus (*bcc-1(ef58)*) were subjected to heat stress to generate males. These males were propagated further as a stock and more than 10 animals were used to confocal microscopy to evaluate the expression pattern of mCherry::BCC-1 (Figure 26).

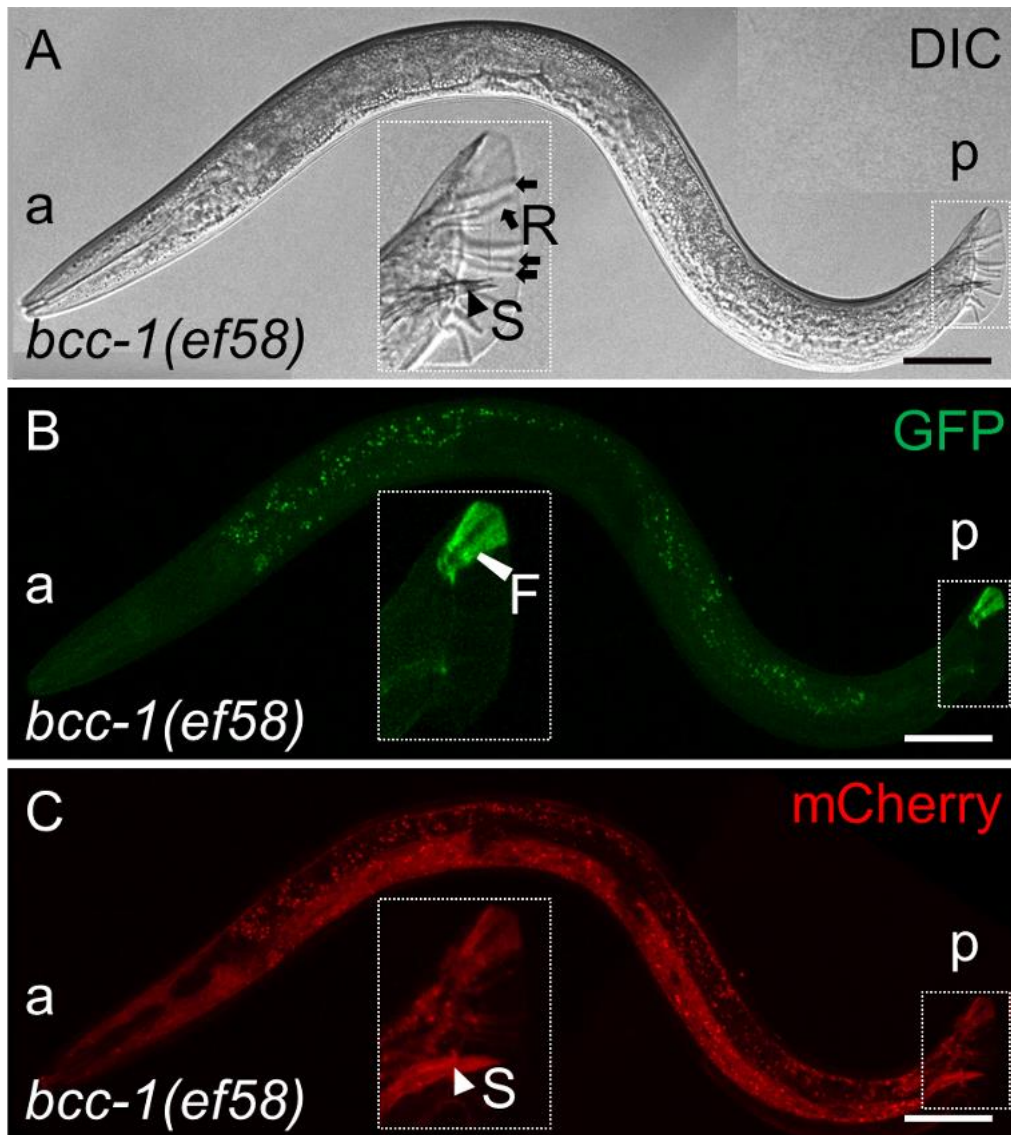


Figure 26: mCherry::BCC-1 is expressed in the spiculum of male *bcc-1(ef58)* worms. (A) Single differential interference contrast (DIC) plane of an agar pad-mounted mCherry::BCC-1-expressing male, with a focus on tail structures (inset). Selected rays (R) and the spiculum (S) are shown. Anterior (a) and posterior (p) regions are indicated. (B) Maximum intensity projection spanning 35 μm in the GFP channel revealing autofluorescence of dorsal fan structures (F). (C) The same MIP as in (B) showing mCherry::BCC-1 signals. Next to an expression in the hypodermal *hyp7* syncytium a red signal emerges from the spiculum (S). Scale bars represent 50 μm.

Copulatory tail structures of males are well distinguishable in DIC microscopy (**Figure 26**, A). In healthy males, eight rays necessary for vulva location are visible, as the last two rays (8 and 9) are usually fused together (Nguyen et al. 1999) (**Figure 26**, A; zoomed in area). Autofluorescent artefacts were detected in the GFP channel in the gut and the tip of the animal's tail (**Figure 26**, B). In the mCherry channel, BCC-1 fusion protein spanned almost throughout the entire worm in a band-like manner (**Figure 26**, C) similar to what has been observed in hermaphrodites (**Figure 17**), suggesting that BCC-1 is also predominantly expressed in the hypodermis in males. Different from what was seen in hermaphrodites, the mCherry::BCC-1 expression includes in males the tail tip (**Figure 26**, C). Furthermore, the spiculum, but not the rays in males show mCherry::BCC-1 expression. While it appeared as BCC-1 might be expressed in the fan region as well (**Figure 26**, C) comparison with the GFP channel (**Figure 26**, B) suggests artificial fluorescence unrelated to mCherry::BCC-1.

Together, confocal data shows expression of mCherry::BCC-1 in *hyp7* and the spicules of male worms. As these male-specific structures are important to probe for vulva openings and aiding in sperm transfer (Liu and Sternberg 1995; Garcia et al. 2001), the results would support a role for *bcc-1* in male mating.

***bcc-1* mutants mate no worse than wild-type males**

As BCC-1 was found in male structures related to vulva location (**Figure 26**), a connection between *bcc-1* and *pkd-2* seemed increasingly likely. To investigate whether loss of *bcc-1* has similar effects to loss of *pkd-2* *in vivo*, which would suggest a shared genetic pathway, the ability of male worms to locate the vulva of hermaphrodites upon *bcc-1* loss was investigated in mating assays. To this end, wild-type and *bcc-1(ef48)* males were generated using a heat shock procedure. As a control for reduced *pkd-2* gene activity, a strain from the Caenorhabditis Genetics Center (CGC) was obtained that carries a deletion in the *pkd-2* gene (*pkd-2(sy606)*) and produces males more frequently than wild-type due to a high instance of male (*him*) mutation (*him-5(e1490)*). This double mutant is reported to have a reduced responsiveness of males to hermaphrodites (Piasecki et al. 2017).

Furthermore, L1 wild-type worms were subjected to feeding RNAi against *fog-1*, to suppress sperm development in such hermaphrodites. As a consequence, *fog-1* RNAi animals are females which depend on external sperm to propagate and lay embryos. For the assay, single *fog-1* RNAi feminized L4 animals were individually paired with a single male on 6 cm NGM plates containing only a minimal amount of food. After 24 hours, each feminized worm

was transferred to a regular NGM plate. The transfer was repeated on a daily basis until egg laying stopped and total broods could be assessed (summarized in **Figure 27**).

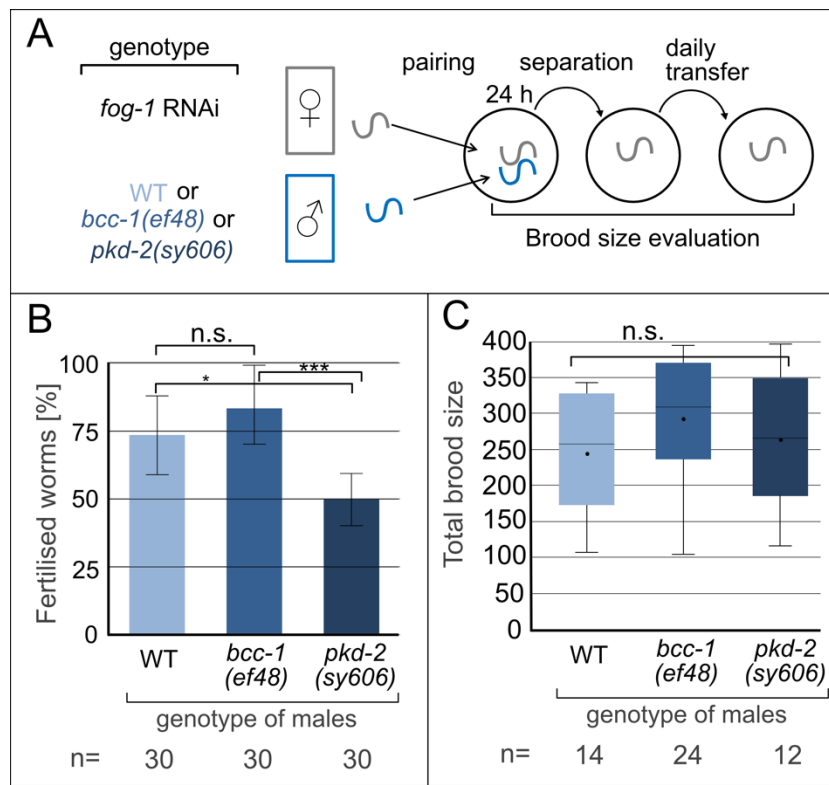


Figure 27: Loss of *bcc-1* does not resemble loss of *pkd-2* phenotypes. (A) Graphical representation of the mating assay. One animal with a feminized germ line tissue (*fog-1* RNAi) was combined with one male of indicated genotype; wild-type (WT). After 24 hours, worms were separated and cross progeny was scored over the following days. If no male was added, no brood was seen in *fog-1* RNAi animals, confirming feminization (n=10). Experiments were performed at 20 °C and repeated two times with 10 worms per genotype. (B) Bar chart of mating effectiveness. Plates (n) were checked for presence of embryos which is interpreted as a successful copulation event. Error bars represent 95% confidence intervals. Groups were compared using Fisher's exact test showed significant differences at p<0.001 (***) or p<0.05 (*) respectively. (C) Box-Whisker plot showing living brood size of inseminated females by *bcc-1* or *pkd-2* mutant males. Total living broods (n) were scored by daily counting until egg laying stopped. One sided Students t-test did not reveal statistical differences (n.s.).

Under the conditions of the assay, wild-type males mated successfully in roughly 75% of the time (**Figure 27, B**). Males carrying the protein null allele of *bcc-1* showed a slightly higher but not significantly different mating success rate compared to wild-type (**Figure 27, B**). However, fertilization events drop significantly to 50%, when males were mutant for *pkd-2* (**Figure 27, B**), validating the assay itself. As mCherry::BCC-1 was found expressed in the spicules of males (**Figure 26**), which function in sperm transfer (Garcia et al. 2001), the total brood resulting from this assay was also assessed to evaluate whether *bcc-1* mutants might exhibit compromised sperm transfer resulting in lower cross fertilized brood numbers (**Figure 27, C**). Mating with wild-type worms resulted in an average brood of 242 ± 125 (n=10). This

is not significantly different from the brood size obtained by mating with *pkd-2* mutants (225 ±118, n=10) and somewhat lower than the brood resulting from *bcc-1* mutant males (314±90, n=10). Therefore, this mating assay suggests that *bcc-1* has no role in male reproduction efficiency. Furthermore, it does not support the hypothesis that *bcc-1* and *pkd-2* are genetically or biologically connected in *C. elegans*.

While the results from **Figure 26** suggest otherwise, the data in **Figure 27** does not argue for a role of *bcc-1* in vulva location, sperm transfer or a connection to *pkd-2* regulation. This is in line with the general observation that male stocks of *bcc-1(ef48)* could be generated and kept without elevated effort. While a genetical or physical connection between gene products of *pkd-2* and *bcc-1* is still possible, it seems at least unlikely that *bcc-1* promotes the expression of *pkd-2*, as it was suggested by homologs in a different animal system (Tran et al. 2010).

***bcc-1* has a role in molting**

BCC-1 physically interacts with the molting factor MLT-3

The SAM domain of mammalian Bicaudal-C is reported to form polymers *in vitro* and to mediate localization to cytoplasmic foci in cultured cells (Rothé et al. 2015; Maisonneuve et al. 2009). Furthermore, Bicaudal-C has been suggested to directly physically interact in a SAM-dependent manner with two Ankyrin and SAM domain containing proteins, ANKS3 and ANKS6 (Rothé et al. 2018). The worm homologs of ANKS3/ANKS6, molting defective (MLT)-3 and MLT-2, are expressed in the same tissue as BCC-1 and contain –at least in parts– structural similarities to their vertebrate counterparts (Lažetić and Fay 2017). It was therefore explored whether a physical interaction network analogous to the mammalian system might exist in the worm for BCC-1, MLT-3 and MLT-2.

To this end, yeast was chosen as a heterologous protein interaction test system. Plasmids containing the full open reading frame of *bcc-1*, *mlt-3*, *mlt-2*, and human Bicaudal-C (*bicc1*) fused to an N-terminal DNA-binding domain or a Gal4 Activation domain were constructed and used in a Yeast-Two Hybrid assay (Fields and Song 1989). In this technique, two plasmids encode one fusion protein each; the first protein of interest is combined with a DNA-binding domain and the second protein of interest is fused to a RNA polymerase II-recruiting transcription factor. If both proteins of interest interact with each other, a functional transcription factor is reconstituted and a *LacZ* reporter gene (encoding β-Galactosidase) engineered into the genome of a designated yeast strain can be expressed. Thus, reporter gene activity can be visualized by a colorimetric change after the addition of X-Gal. A colony color

change from white to blue can therefore be interpreted as a physical interaction of the two proteins in question.

The known and established interaction of the two proteins GLD-2 and GLD-3 served as a positive control (Eckmann et al. 2004). First it was investigated whether BCC-1 binds itself, indicating a behavior similar to the mammalian homolog. Next, it was also investigated whether human BICC1 protein might be able to bind BCC-1, which would suggest an evolutionary conserved molecular mechanism (**Figure 28**). Lastly, potential interactions of BCC-1 with MLT-2 and MLT-3 were investigated (**Figure 29**).

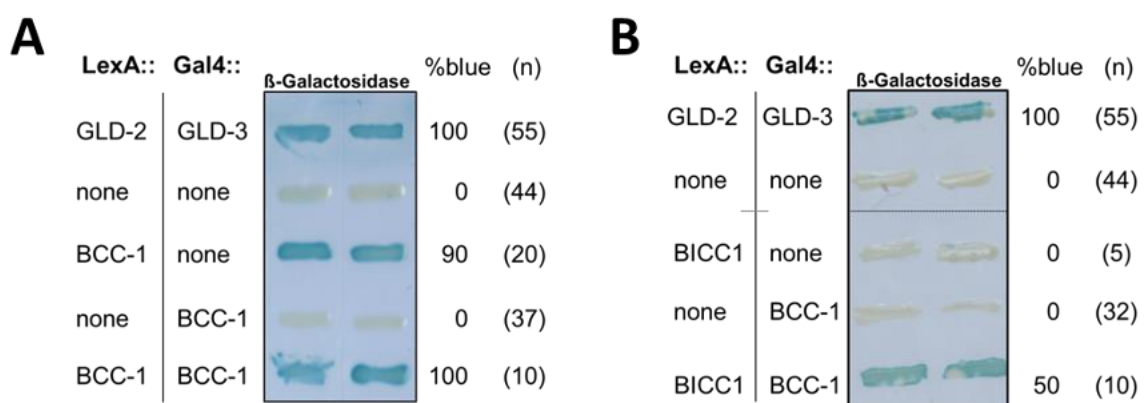


Figure 28: BCC-1 interacts with its mammalian homolog BICC1. Displayed is the activity of β -galactosidase (in %blue) of yeast colonies (n) coexpressing indicated fusion proteins; 'none' means no fusion to the DNA-binding domain (LexA::) or the Gal4 activation domain (Gal4::). Membranes of streaked out colonies were incubated for 2 hours at 37°C to test for β -galactosidase reporter activity. (A) BCC-1 exhibits strong autoactivation when fused to LexA. (B) The mammalian homolog of BCC-1, BICC1, physically interacts with BCC-1. β -galactosidase assays were conducted in collaboration with Richard Sacasa Petzsch.

While positive and negative controls show the expected blue/white behavior, BCC-1 fused to the DNA-binding domain alone is sufficient for a blue color to appear (**Figure 28**, A). This strong autoactivation veiled a putative interaction of BCC-1 with itself, rendering this test inconclusive. As BCC-1 cannot be used in a fusion with the DNA-binding domain, a fusion construct containing LexA::BICC1 was tried instead. While the positive control turned always blue, neither BICC1 fused to the DNA-binding domain, nor BCC-1 fused to the Gal4 domain induced by themselves a blue color change. This makes the observed color change in colonies of both in combination, LexA::BICC1 with Gal4::BCC-1, interpretable as it indicates an interaction between the proteins (**Figure 28**, B). However, it should be noted that only 50% of the analyzed colonies actually turned blue. This might be due to the nature of interaction, technical issues or reasons of varying protein expression. Nonetheless, expression of fusion proteins in total lysate was confirmed by Richard Sacasa Petzsch.

The result that human BICC1 and nematode BCC-1 seem to interact with each other suggests that also BCC-1 may bind to itself, as both proteins contain the putatively important SAM domain. While a self-interaction of BCC-1 could not be tested due to autoactivation, the result further supports the idea that SAM domain containing proteins bind each other. Next, it was investigated whether a physical network between BCC-1, MLT-3 and MLT-2, corresponding to the human interaction network of BICC1, ANKS6 and ANKS3, might exist (Figure 29).

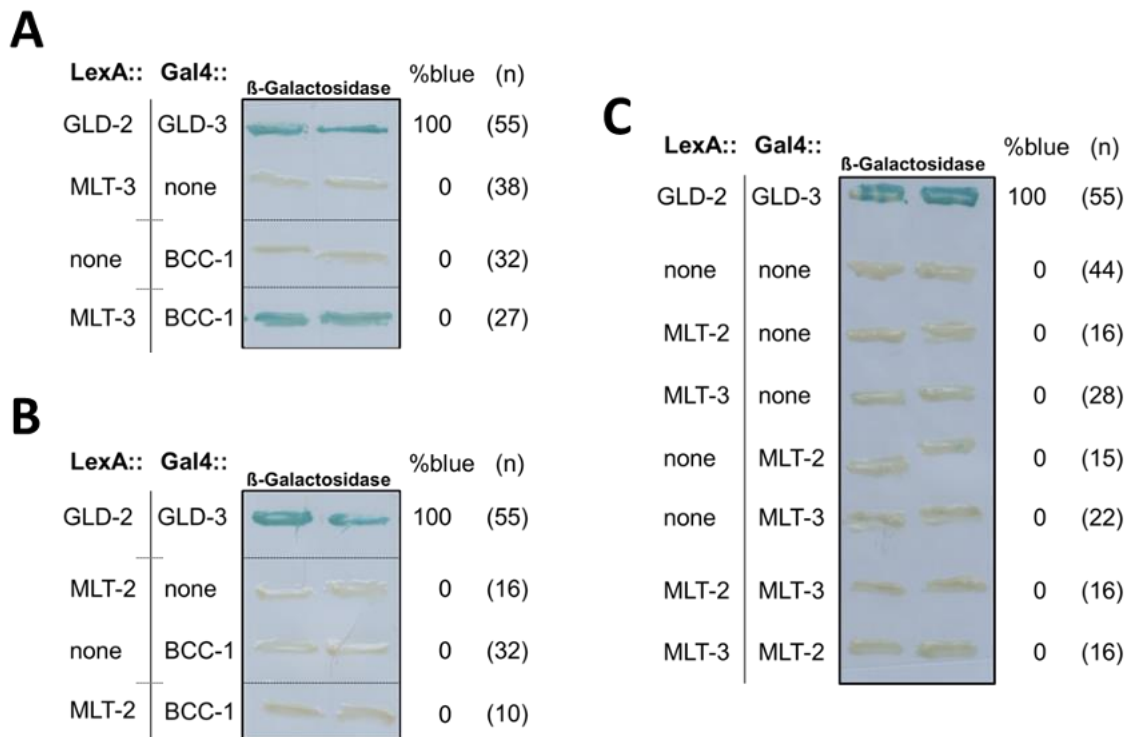


Figure 29: MLT-3 and BCC-1 physically interact with each other, but not with MLT-2. Displayed is the activity of β -galactosidase (in %blue) of yeast colonies (n) coexpressing indicated fusion proteins; 'none' means no fusion to the DNA-binding domain (LexA::) or the Gal4 activation domain (Gal4::). Membranes of streaked out colonies were incubated for 2 hours at 37 °C to test for β -galactosidase reporter activity. (A) BCC-1 interacts with MLT-3, the homolog of ANKS3. (B) No interaction is detected of BCC-1 with MLT-2, the homolog of ANKS6. (C) MLT-2 and MLT-3 show no interaction with each other. β -galactosidase assays were conducted in collaboration with Richard Sacasa Petzsch.

As BCC-1 cannot be used when fused to the DNA-binding domain due to autoactivation (Figure 28, A), only combinations with LexA::MLT-3 (Figure 29, A) and LexA::MLT-2 (Figure 29, B) were investigated. As LexA::MLT-3 and Gal4::BCC-1 without an interaction partner did not show a change in color but colonies turned blue when expressing both together (Figure 29, A), it can be concluded that BCC-1 and MLT-3 may physically interact with each other in yeast, similar to what is shown for their human counterparts BICC1 and ANKS3 (Rothé et al. 2018). On the contrary, tests between MLT-2

and BCC-1 did not reveal that a binding between the two proteins is likely (**Figure 29**, B). Moreover, tests to investigate whether MLT-2 and MLT-3 interact with one another, as it would be suggested by their mammalian counterparts (Rothé et al. 2018), turned out negative (**Figure 29**, C). As neither MLT-2 nor MLT-3 showed autoactivation, both orientations were tested. However, while positive controls turned blue, neither coexpression of MLT-2 with MLT-3 did (**Figure 29**, C). Therefore, an interaction of the worms' homologs of ANKS3/ANKS6 could not be recapitulated.

Taken together, these data indicate a physical interaction of BCC-1 with two SAM domain containing proteins, MLT-3 and BICC1. Furthermore, MLT-2 was not demonstrated to interact with BCC-1 or MLT-3. As the interaction of the mammalian proteins ANKS3 and ANKS6 is suggested to be SAM based (Delestré et al. 2015) and the ANKS6 homolog, MLT-2, does not possess a SAM domain, above results collectively argue for SAM domain-mediated binding of BCC-1 and MLT-3.

***bcc-1* genetically interacts with hypodermal molting factors**

Loss of *bcc-1* suppresses molting defective phenotypes caused by knockdown of *mlt-3*

After revealing a potential physical interaction between BCC-1 and the molting factor MLT-3 (**Figure 29**), the questions arose whether this connection could be exploited to unveil a functional role of *bcc-1* in the hypodermis related to synthesis and/or shedding of the cuticle. *mlt-3* was found to be an essential gene for correct molting as a loss-of-function allele leads to worms arresting in their development (Lažetić and Fay 2017). Furthermore, such molting defects were also inducible by RNAi against *mlt-3* when pre-sensitized strains of *C.elegans* were employed (Lažetić and Fay 2017). As such pre-sensitized strains were unavailable, the penetrance and expressivity of *mlt-3* RNAi in wild-type animals were first investigated. To this end, the full open reading frame of *mlt-3* was amplified from cDNA and cloned into the RNAi feeding vector pL4440. Wild-type worms in their first larval stage were spotted onto RNAi plates against *mlt-3* and analyzed by mounting on agar pads and subsequent DIC microscopy after three days at 20 °C, after which animals under standard condition are expected to have grown into adults. A summary of observed phenotypes is given in **Figure 30**.

All investigated control-treated animals developed into wild type-like adult hermaphrodites displaying normal length and diameter, a vulva and embryos inside their uterus (**Figure 30**, A, D, E). However, when wild-type animals are fed dsRNA against *mlt-3*,

different phenotypes were seen in 50% of the cases (**Figure 30 B, C**). Animals either arrested in larval stages being apparently unable to shed their cuticle (**Figure 30, B**) or developed into adults with severe skin defects (**Figure 30, C**). Such defects manifested in stacked embryos in the animals' uterus through a blocked vulva, unshed cuticle parts, and a stiffer and less sigmoidal body movement.

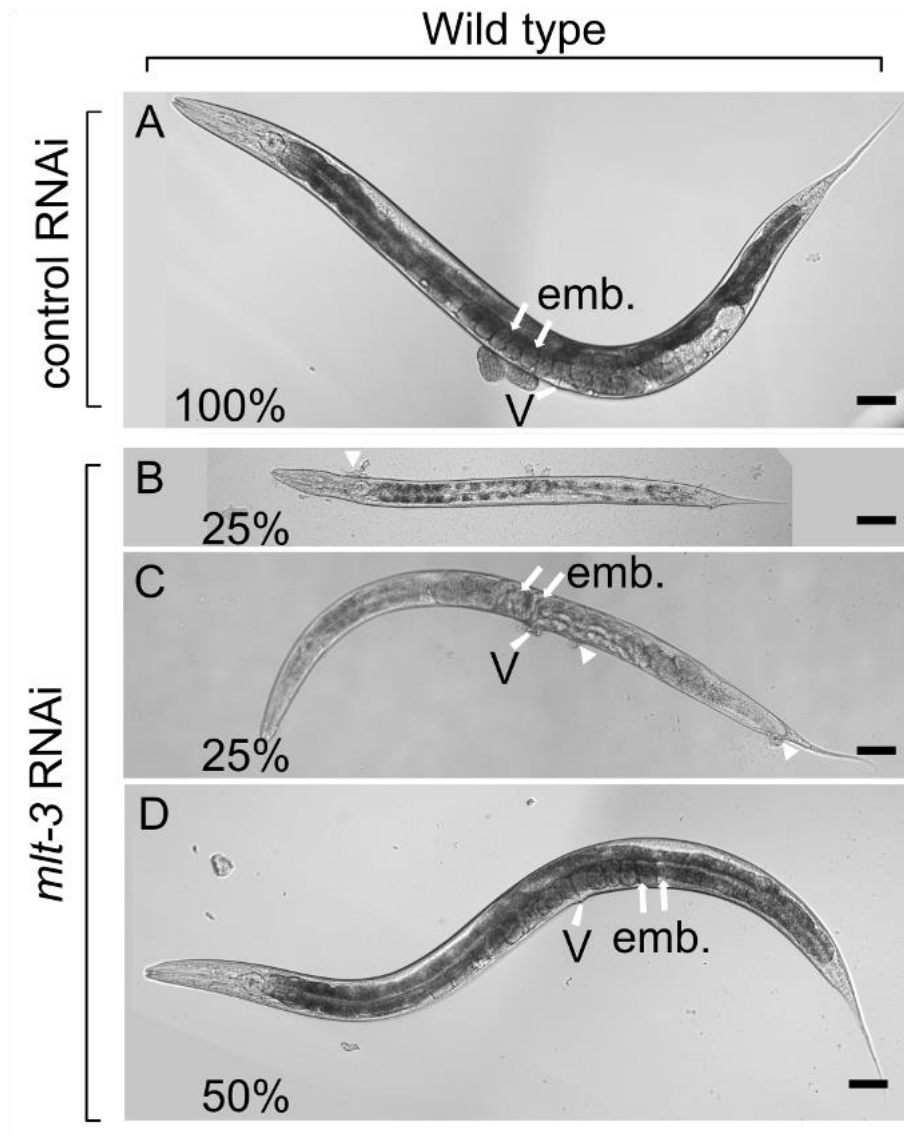


Figure 30: RNAi knockdown of *mlt-3* induces molting related phenotypes. Wild-type L1 animals fed for three days with dsRNA against *xfp* (control RNAi) and the molting factor, *mlt-3*. Penetrance in % is indicated; n= 10 animals analyzed. Anterior is to the left; scale bar represents 50 μ m. (A and D) Wild type-looking adult exhibiting regular size, normal vulva development (V) and embryos (emb.) in their uterus. (B) Animal arrested as a not further defined larvae. Development of vulva is not apparent and excessive cuticle parts are visible (arrowheads). (C) Adult animal with present vulva and embryos but smaller in size and with unshed vulva cuticle parts attached to its body exterior (arrowheads). Note accumulated embryos in the worm indicating an egg laying defect.

As these phenotypes are similar to what has been described for *mlt-3* mutants (Lažetić and Fay 2017), it can be concluded that the generated *mlt-3* feeding RNAi clone is functional

and that molting phenotypes also occur in genetic backgrounds that have not been pre-sensitized for RNAi treatment although they are not seen in every animal and therefore less penetrant.

Nonetheless, this partial penetrance regarding overt molting phenotypes upon *mlt-3* knockdown enables the assessment of *bcc-1* loss in a molting compromised system. If *bcc-1* and *mlt-3* were operating in a combined pathway, as it could be suggested by their physical interaction, removing *bcc-1* activity in a *mlt-3* compromised background might enhance the effect and/or penetrance of *mlt-3* knockdown.

To test for such a putative genetic interaction, wild-type and *bcc-1* protein null mutant (*bcc-1(ef48)*) worms were synchronized by bleaching, allowed to hatch overnight without liquid and spotted as L1-starved animals onto RNAi plates targeting *mlt-3* or derivatives of *gfp* ('*xfp*') as a control. After three days at 20 °C worms were visually analyzed using a stereomicroscope (**Figure 31, A**). If worms arrested or showed signs of skin abnormalities in adults, animals were classified as “cuticle defective”.

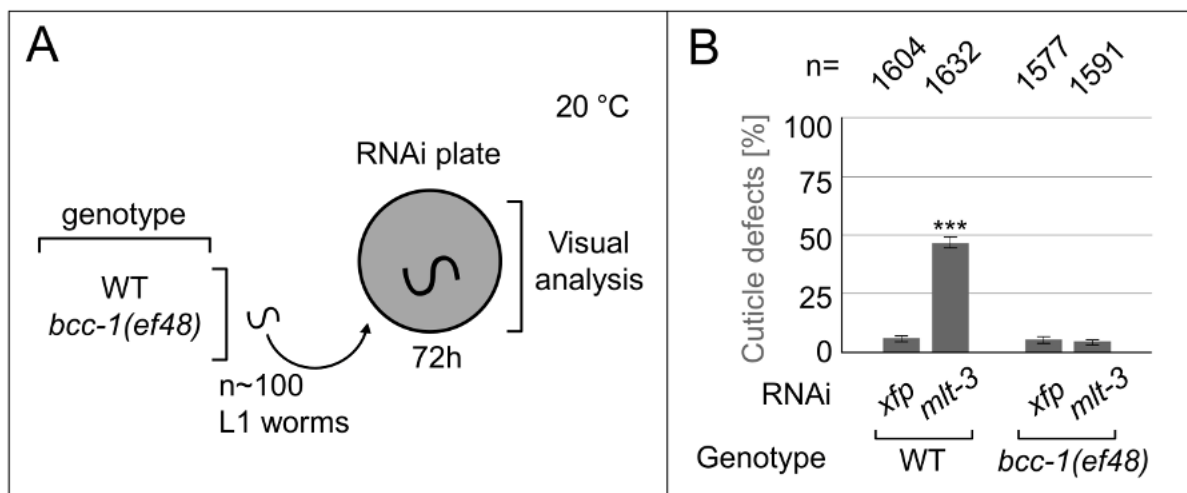


Figure 31: Loss of *bcc-1* suppresses phenotypes caused by *mlt-3* RNAi knockdown.

(A) Schematic overview of the molting assay. Wild-type (WT) or *bcc-1(ef48)* worms of the first larval stage (L1) were spotted onto plates with dsRNA against *mlt-3* or *xfp* (RNAi plates). Worms were scored after 72 hours for cuticle defects. (B) Quantification of the molting assay results. Experiment was conducted three times in which multiple RNAi plates were used each time to increase animal (n) number. Fisher's exact test shows significant difference ($p < 0.001$) between WT worms being fed *mlt-3* dsRNA and all other groups.

In this set of experiment, *mlt-3* RNAi induced cuticle defects in ~48% animals of wild-type background compared to ~5% caused by *xfp* RNAi (**Figure 31, B**). While this validates the assay it also demonstrates that not every dsRNA treatment leads to molting defects, demonstrating that the increased effects for *mlt-3* are specific. Moreover, *xfp* control RNAi

did not lead to a higher percentage of affected animals in the background of *bcc-1(ef48)* (**Figure 31, B**), arguing that loss of *bcc-1* does not lead to increased molting deficiency rates either. Surprisingly, *mlt-3* RNAi fails in *bcc-1(ef48)* animals to induce cuticle defects above background levels, as its penetrance rate (~4%, n=1591) is comparable to control RNAi feeding (**Figure 31, B**). This genetic suppression effect strongly argues for a connection of *mlt-3* and *bcc-1* and indicates a potential role of *bcc-1* in molting unseen in *bcc-1* mutants under standard conditions.

Loss of *bcc-1* does not suppress somatic RNAi phenotypes in general

Loss of *bcc-1* suppresses phenotypes caused by knockdown of *mlt-3* (**Figure 31**). However, this observation has so far only been made in the context of RNAi. A likely explanation for a suppression of *mlt-3* RNAi in *bcc-1(ef48)* animals is an involvement of BCC-1 in the molecular process of RNA interference itself. Such a scenario is supported by findings suggesting that Bicaudal-C plays a role in loading the RISC complex in other species (Rothé et al. 2015). To rule out the possibility that loss of *bcc-1* leads to reduced RNAi activity in somatic tissues, a knockdown of genes otherwise not connected to *bcc-1* was performed. In order to examine this hypothesis more precisely, the *dumpy-10* (*dpy-10*) gene – unrelated to molting, but expressed in the same tissue– was targeted by RNAi. *dpy-10* encodes a collagen protein expressed in hyp7, the syncytial tissue in which BCC-1 was also detected. Loss of *dpy-10* results in a characteristic body size reduction, as well as a thicker (*dumpy*) body morphology, a phenotype inducible via RNAi (Zou et al. 2019).

To test whether the occurrence of Dumpy (Dpy) phenotypes is suppressed by *bcc-1* loss, the ORF of *dpy-10* was cloned into pL4440, transformed into RNAi feeding bacteria and administered to wild-type or *bcc-1(ef48)* worms in their first larval stage, analogous to *mlt-3* feeding experiments (**Figure 31, A**). Because Dpy phenotypes showed higher expressivity at 25° C than 20° C and for reason of efficiency, the experiments were conducted at 25° C and adult animals were scored already after two days (**Figure 32**). These experiments were conducted in collaboration with Richard Sachasa Petzsch.

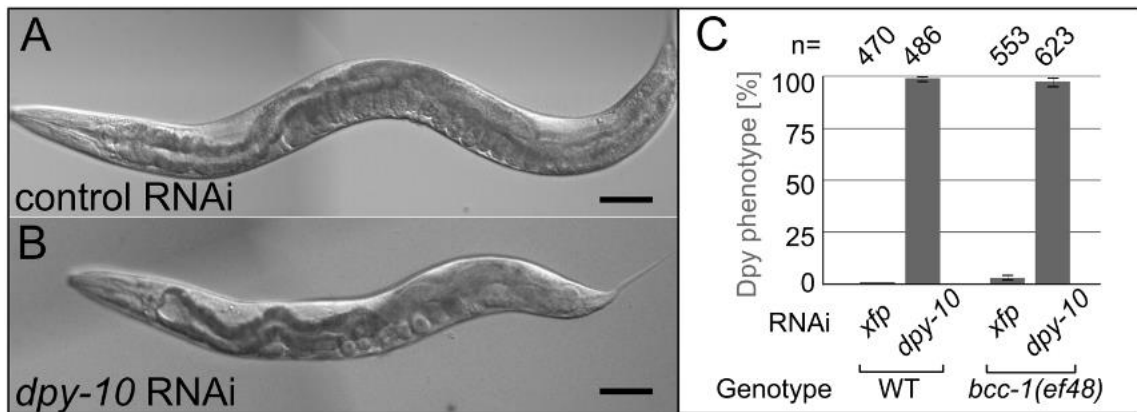


Figure 32: Loss of *bcc-1* does not suppress *dpy-10* induced phenotypes in RNAi experiments. (A and B) Feeding RNAi of *dpy-10* into L1 larvae induces the Dumpy (Dpy) phenotype in adult wild-type animals. DIC images after constant feeding of (A) *xfp* or (B) *dpy-10* dsRNA for 48 h at 25 °C. (C) Quantification of RNAi feeding results, conducted three times in collaboration with Richard Petsch. Error bars represent 95% confidence intervals.

In *bcc-1(ef48)* animals being fed control RNA, the amount of scored Dpy worms is basically zero (Figure 32, C), arguing that triggering the RNAi machinery in *bcc-1* mutants does not induce Dumpy phenotypes. Close to 100% of WT worms being fed dsRNA against *dpy-10* show the expected phenotype (Figure 32, B, C), demonstrating the effectiveness of the constructed feeding RNAi clones. When animals lacking full-length BCC-1 were fed dsRNA against *dpy-10*, the amount of Dpy worms (97.9%) was similar to wild-type (99.4%) (Figure 32, C), showing that loss of *bcc-1* does not suppress Dpy phenotypes. As loss of *bcc-1* does not lead to suppression of Dumpy phenotypes induced by RNAi, it can be concluded that *bcc-1* is not an essential component of the RNAi machinery. Conversely, the genetic connection between *bcc-1* and *mlt-3* demonstrated earlier (Figure 31, B) is therefore unrelated to the process of RNAi and more likely related to the actual molting process. This idea would also be consistent with the Yeast Two-Hybrid results shown in Figure 29, which argue for a direct physical interaction of BCC-1 and MLT-3.

Deletions or N-terminal tagging of *bcc-1* compromises the *in vivo* function of BCC-1

After having established how a protein null mutant of *bcc-1* performs in a quantifiable assay for BCC-1 function, it is now possible to test other generated alleles of *bcc-1* regarding their *in vivo* functionality. The molting assay described above is therefore extended to the deletion mutant *bcc-1(q754)*, removing parts of the central IDR and the C-terminal SAM domain of BCC-1 and N-terminally tagged alleles *bcc-1(ef52)* (expressing 2xFLAG::BCC-1) and *bcc-1(ef58)* (expressing 3xFLAG::mCherry::BCC-1). L1 worms were spotted onto RNAi plates targeting *mlt-3* and visually analyzed after 48 h at 25 °C.

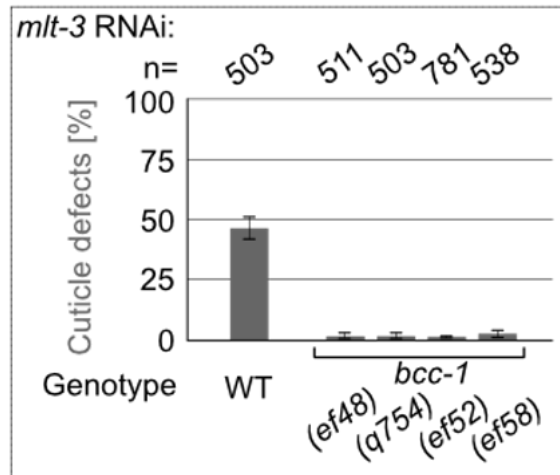


Figure 33: C-terminal deletion of IDR and SAM as well as N-terminal tags compromise BCC-1 function *in vivo*. Quantification of *mlt-3* RNAi feeding results. L1 worms were spotted onto RNAi plates targeting *mlt-3* and scored for cuticle defects after two days at 25 °C. Error bars represent 95% confidence intervals. Experiment conducted two times.

Surprisingly, all analyzed *bcc-1* alleles strongly suppressed molting defective phenotypes induced by *mlt-3* RNAi (**Figure 33**). The observed penetrance of suppression mediated by all tested alleles is comparable to a protein null mutation of *bcc-1* (**Figure 33**), arguing that BCC-1 protein function is strongly compromised when it is N-terminally tagged or missing C-terminal parts that include the SAM domain. While N-terminally tagged variants of BCC-1 were detected in western blots (**Figure 10**), expression of the protein predicted to be encoded by *bcc-1*(*q754*) could not be verified. The phenotypic suppression of molting defects in this strain might therefore not occur due to just a missing C-terminal part, but rather because of very low or missing protein abundance. The data suggests that N-terminally tagging BCC-1 can easily result in a strong loss of protein function.

bcc-1* also genetically interacts with the molting factors *nekl-3* and *mlt-2

After establishing a genetic connection between *bcc-1* and molting factor *mlt-3*, the question emerged whether this cause-and-effect relationship could be extended to other Bicaudal-C genes of *C. elegans* on the one hand and other molting factors on the other. To address these questions, RNAi experiments were performed in the background of *gld-3* mutants. Additionally, two molting genes other than *mlt-3* were targeted in RNAi experiments. If *bcc-1* loss was able to suppress molting phenotypes arising from other molting factors, it would indicate a more centralized role in the molting process rather than one only connected to a single factor. First, *nekl-3* was chosen because its gene product, NEKL-3, is suggested to be a direct physical interactor of MLT-3 (Lažetić and Fay 2017). Second, *mlt-2*

was selected because it encodes a protein essential for molting (MLT-2) that is reported to not colocalize to MLT-3 (Lažetić and Fay 2017). Lack of either aforementioned factor leads to cuticle defects similar to *mlt-3* loss (Lažetić and Fay 2017; Yochem et al. 2015). Therefore, it was evaluated whether these phenotypes could be alleviated through loss of *bcc-1* activity.

To conduct these series of experiments, the complete ORFs of *nekl-3* and *mlt-2* were cloned into pL4440 vectors. The transformed plasmids producing dsRNA were fed to wild-type worms in order to evaluate the penetrance and expressivity of the RNAi setup. As feeding L1 worms lead to a drastically lower percentage of molting defective adults when compared to *mlt-3* RNAi (**Figure 31**), the assay was modified and L4 worms were put onto RNAi plates to grow into adulthood. On the next day, animals were transferred to another RNAi plate to grow into adulthood. On the next day, animals were transferred to another RNAi plate where they were allowed to lay eggs for a few hours. Afterwards, adult worms were removed and the F1 generation was visually analyzed after three days at 20 °C (**Figure 34, A**).

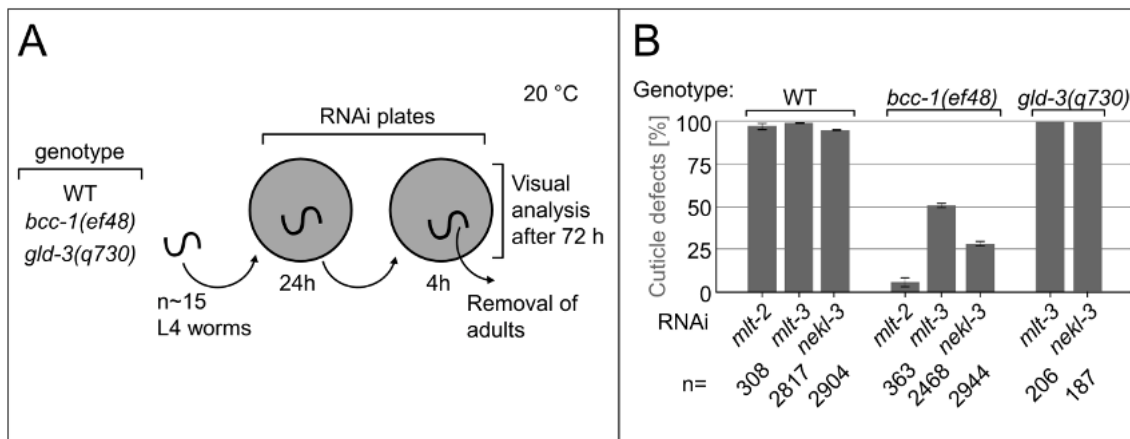


Figure 34: *bcc-1*, but not *gld-3*, genetically interacts with different molting factors. (A) Schematic overview of an adjusted molting assay. Larval stage 4 (L4) worms of either indicated genotype were placed onto RNAi plates targeting the three molting factors, *mlt-2*, *mlt-3* or *nekl-3*. After 24 hours, the now adult worms were transferred to a second RNAi plate and removed after having laid a sufficient number of embryos (typically between 150 and 300). Three days later the F1 generation was visually analyzed for molting phenotypes. (B) Quantification of experiments described in (A). *mlt-2* RNAi experiments were conducted only once and not with *gld-3* mutants. Other RNAi constructs and genotypes were tested in ≥ 2 experimental repetitions. n indicates total number of animals scored. Error bars represent 95% confidence intervals.

In **Figure 34**, wild-type animals treated with RNAi against either molting factor, exhibited molting defects in almost 100% of cases, with *nekl-3* achieving the lowest rate (**Figure 34**, left). In the previous RNAi regime (**Figure 31**), the observed rates of cuticle defects in wild-type animals after treatment with *mlt-3* RNAi were lower (47% as compared to 94,5% in **Figure 34**, **Figure 37**, B). Therefore, the modified setup appears to enhance

RNAi penetrance. By contrast, *bcc-1* mutant animals fed dsRNA against *mlt-2*, *mlt-3* or *nekl-3* displayed cuticle phenotypes in lower rates (6.0%, 50.7% and 28.2%, respectively) (**Figure 34**, B middle). This demonstrates that loss of *bcc-1* can lead to suppression of molting phenotypes resulting from reduced molting factors other than *mlt-3*. Lastly, *gld-3* mutants failed to suppress molting phenotypes after RNAi treatment against *mlt-3* or *nekl-3* in every animal (**Figure 34**, B to the left), suggesting no genetic connection of *gld-3* to any of the molting genes.

Taken together, this experiment demonstrates that in *C. elegans* a connection between *bcc-1* and multiple molting factors exists, that cannot be extrapolated to *gld-3*. Furthermore, as phenotypic suppression rates in *bcc-1* mutants were observed to be below 100%, the data also argues that the capability of *bcc-1* to suppress cuticle defects is limited. As the penetrance difference in molting defects induced by *mlt-3* RNAi between WT and *bcc-1* animals is only ~50%, the more effective RNAi condition against *nekl-3* was chosen for subsequent experiments to support a fine-tuned analysis of structure-functions.

N-terminally tagged *bcc-1* alleles retain partial function

As the generated tagged *bcc-1* alleles displayed molting suppression rates similar to a *bcc-1* protein null mutant (**Figure 33**), it was investigated whether the alleles exhibit residual function when RNAi is performed using the adjusted RNAi regime of **Figure 34** rather than the initial regime of **Figure 31**, A. Moreover, to putatively improve the *in vivo* functionality of mCherry tagged BCC-1 fusion protein, two more alleles containing a flexible region between the tags and the actual BCC-1 sequence were generated. One of them, *bcc-1(ef108)*, provides BCC-1 with a linker sequence of 10 glycines (**Figure 4**, variant 8). The other one, *bcc-1(ef122)*, extends BCC-1 with a defined linker sequence rich in glycines and serines (**Figure 4**, variant 9) taken from another tag used in proximity labeling ('Turbo ID') experiments (Artan et al. 2021). The generated strains were included in RNAi experiments targeting *mlt-3* and *nekl-3* (**Figure 35**).

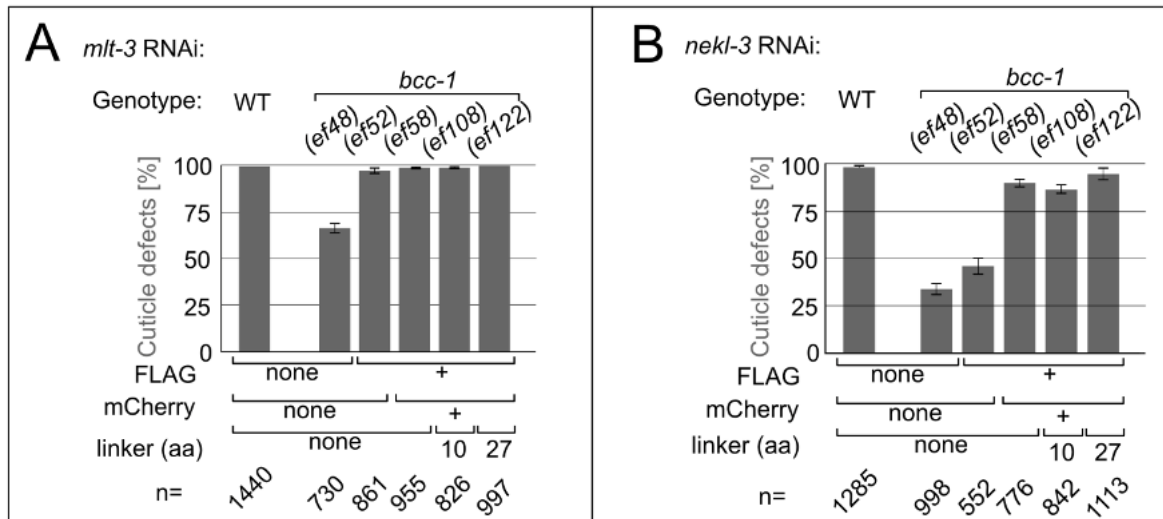


Figure 35: N-terminally tagged *bcc-1* retains partial function. L4 animals of indicated genotypes were RNAi-treated against the two molting factors, (A) *mlt-3* or (B) *nekl-3*. Indicated is the presence of a FLAG tag (FLAG), a fluorescence tag (mCherry) or additional linker sequences between BCC-1 and a tag with their respective amino acid lengths (aa) given below. F1 generation was visually analyzed for molting defective phenotypes after three days. Quantifications represent ≥ 2 independent repetitions. n means analyzed animals. Error bars represent 95% confidence intervals. Experiments were conducted in collaboration with Jacqueline Pinheiro.

When wild-type animals are treated with RNAi against *mlt-3* or *nekl-3*, 100% or 99% of animals showed cuticle defects (**Figure 35, A and B**), consistent with what has been observed in **Figure 34, B**. Furthermore *bcc-1*(*ef48*) mutants exhibited 64% or 34% cuticle defects when *mlt-3* or *nekl-3* was targeted (**Figure 35, A and B**), similar to what has been shown in **Figure 34, Figure 37, B**. Interestingly, animals carrying any other alleles of *bcc-1* showed an almost 100% cuticle defective rate when treated with *mlt-3* RNAi, ranging from 97% to 100% (**Figure 35, A**). This suggests a functionality of all tagged *bcc-1* alleles close to wild-type *bcc-1*, which is in sharp contrast to the results in **Figure 33**, where tagged *bcc-1* alleles behaved like a protein null allele. Moreover, the knockdown of *nekl-3* revealed a difference in cuticle defects between the allele *bcc-1*(*ef52*), encoding for a just FLAG tagged BCC-1 protein, and all considered N-terminally tagged *bcc-1* alleles (**Figure 35, B**). As *bcc-1*(*ef52*) animals displayed a molting deficiency rate of 46%, indicating loss of function almost as strong as the protein null allele *bcc-1*(*ef48*), animals with other tagged *bcc-1* alleles showed cuticle defects in 87% to 95% of cases (**Figure 35, B**), suggesting an almost wild type-like function. Regarding all alleles encoding for mCherry::BCC-1 fusion proteins, *bcc-1*(*ef122*) animals encoding for an additional 27 aa linker showed cuticle defect rates closest to WT, arguing this allele is tolerated better than the others.

In summary, the data argues that a RNAi feeding regime targeting *nekl-3* is more suitable for structure-function analysis than one targeting *mlt-3*. Additionally, this

experimental setup highlights that adding FLAG tags to the amino-terminal end of BCC-1 compromises its' *in vivo* function. However, the inclusion of mCherry seems to restore some functionality to an N-terminally FLAG tagged BCC-1 protein. Lastly, the mCherry tag seems to be slightly better tolerated if an additional 27 aa linker sequence is introduced before the BCC-1 sequence.

***bcc-1* function depends on an RNA-binding motif in a KH domain**

Knocking down *nekl-3* by feeding RNAi has revealed differences in functionality of differently tagged *bcc-1* alleles (**Figure 35, B**). This setup was therefore deemed adequate to perform structure-function analysis of BCC-1 *in vivo*. As frog Bicaudal-C has been shown to bind RNA via a particular GXXG motif in KH 2 (Dowdle et al. 2019), it was investigated if alteration of such a motif would result in compromised *bcc-1* activity. As such activity is quantifiable by rates of molting phenotypes in RNAi experiments, it was examined whether and which of two GXXG motifs that *C. elegans* possesses in KH2 (**Figure 2, Ce**) have a functional significance. To examine the importance of either GXXG motif, two additional alleles of *bcc-1* were generated using CRISPR/Cas9. One allele, *bcc-1(ef115)*, encodes a full-length BCC-1 protein with all four amino acids of the first GXXG loop (GXXG1) turned into alanines (**Figure 4, variant 4**). The second allele, *bcc-1(ef111)*, encodes a full-length BCC-1 protein with the second GXXG motif (GXXG2) modified by changing just the outer glycines into alanines (**Figure 4, variant 5**). The encoded protein has only these outer glycines altered, as changing the glycine within would interfere with the previous GXXG motif (**Figure 2**, see respective amino acid positions in *CeBCC-1*).

After generating strains containing the aforementioned *bcc-1* alleles, they were used in L4 regime RNAi feeding experiments alongside wild-type and *bcc-1(ef48)* animals serving as a benchmark for 100% or 0% activity (**Figure 36**). Upon RNAi against *nekl-3*, 92% (n=1619) of wild-type F1 progeny displayed cuticle defects compared to only 25% (n=1946) of *bcc-1(ef48)* protein null mutants (**Figure 36**). These values are similar to those measured before (**Figure 34, Figure 35, B**) and therefore allow for functional characterization of the two other alleles. While animals with alterations in the GXXG1 motif exhibited only 26% (n=1710) molting phenotypes, 80% (n=1336) of worms with changes in GXXG2 showed cuticle deficiencies (**Figure 36**). Hence, the data argues that the sequence encoding for GXXG1, but not GXXG2 is essential for the function of *bcc-1*.

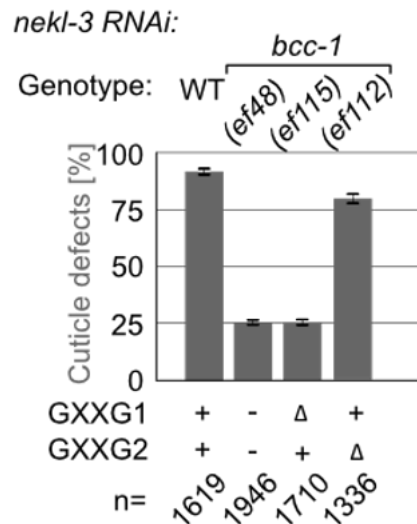


Figure 36: *bcc-1* requires the sequence of the first, but not the second GXXG motif. Wild-type (WT) worms or animals carrying indicated alleles of *bcc-1* were placed as L4 worms on RNAi plates targeting *nekl-3*. Alleles encode for BCC-1 proteins with two putative RNA-binding domains (GXXG1 and 2) being either wild-type (+), absent (-) or altered (Δ). F1 generation was visually analyzed for molting defective phenotypes after three days. Quantifications represent ≥ 3 experiments. n corresponds to analyzed animals. Error bars represent 95% confidence intervals. Experiments conducted in collaboration with Lisa Neuder.

The finding that function of *bcc-1* depends on a sequence encoding an RNA-binding motif in KH domain 2 indicates that BCC-1 is an RNA-binding protein. Furthermore, Bicaudal-C has been shown to recruit the CCR4-NOT deadenylation complex in flies (Chicoine et al. 2007). One molecular role of BCC-1 in the context of molting might therefore be the recruitment of deadenylation entities to target RNAs. In such a case, reduced deadenylation capability would suppress molting phenotypes induced by RNAi in a similar manner as loss of *bcc-1*. To test how loss of deadenylation entities affects molting phenotypes resulting from *nekl-3* RNAi, the assay displayed in **Figure 36** was extended to L4 animals with mutations in genes encoding the deadenylation enzymes PARN-1, PARN-2 and CCR-4. Such worm strains have been described before and were available in the lab (Nousch et al. 2013).

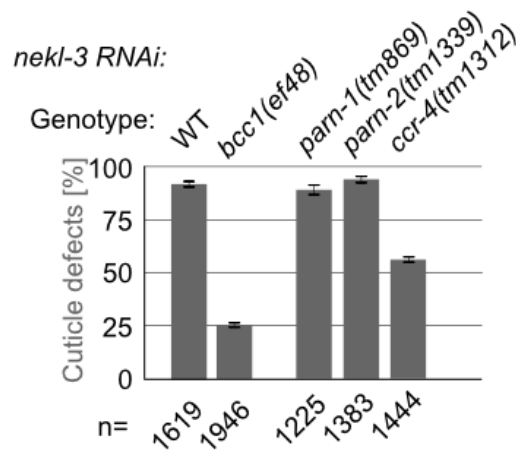


Figure 37: Loss of *ccr-4*, but not *parn-1* or *parn-2* activity suppresses *nekl-3* RNAi-induced molting defects. L4 worms of indicated genotype were used in RNAi feeding experiments targeting *nekl-3*. Animals are either wild-type (WT), mutant for *bcc-1* or have reduced deadenylation activity. F1 generation was visually scored for cuticle defects after three days. Three independent experiments were performed. Data for wild-type and *bcc-1(ef48)* is the same as in Figure 36 as all alleles were tested together. Error bars represent 95% confidence intervals. Experiments conducted in collaboration with Lisa Neuder.

In **Figure 37**, the same results for WT and *bcc-1* mutants are displayed as in the previous figure (**Figure 36**), as data from both figures was generated together. Animals mutant for *parn-1* or *parn-2* displayed 89% and 94% molting phenotypes, indicating no suppression of molting phenotypes, as these levels are comparable to wild-type animals (92%). In contrast, only 56% of *ccr-4* mutant animals exhibited cuticle defects, demonstrating that loss of *ccr-4* activity is able to suppress molting defects, similar to loss of *bcc-1*.

Taken together, the data suggests a connection of deadenylation processes to molting. As loss of either *parn* gene does not suppress cuticle defects, such a connection is somewhat specific to *ccr-4* activity. Suppression of molting phenotypes by either *bcc-1* or *ccr-4* furthermore argues for a connection between these two genes. Such a model is in line with findings from the *Drosophila*, where Bicaudal-C protein was found to be physically associated with the fly's CCR4-Not complex (Chicoine et al. 2007).

Discussion

This study revealed basic aspects of *bcc-1* and established a yet not defined role in osmoregulation and molting. First, using affinity purified antibodies, this study found the expression of several BCC-1 protein variants in wild-type animals. Confocal microscopy of *bcc-1* reporter strains and strains expressing endogenously tagged BCC-1 then revealed a predominant expression of *bcc-1* in the worms' hypodermis (**Figure 16, Figure 17**). Based on the established expression pattern, an *in vivo* implication of *bcc-1* in the process of osmoregulation (**Figure 21**) and molting (**Figure 31**) was established, using salt stress experiments and RNAi. Molecular insights into protein domains of BCC-1 and their consequences on the newly found role in molting are discussed below.

The conserved N- and C-terminus of BCC-1 contribute to its function

This study aimed to illuminate molecular aspects of BCC-1 as a member of the Bicaudal-C family. Utilizing the found phenomenon of *bcc-1* related molting phenotype suppression in RNAi experiments, the present thesis successfully developed a way of conducting comprehensive *in vivo* structure-function analysis of Bicaudal-C in a quantifiable manner. This revealed fresh insights into the *in vivo* importance of several BCC-1 protein regions, specifically the N-terminus containing KH-type domains associated with RNA-binding, the C-terminus as a likely protein-protein interaction surface and an IDR spacer that could be involved in the regulation of the protein.

The N-terminus of BCC-1 requires flexibility

Regarding the N-terminus, experiments using tagged BCC-1 variants revealed that while all created tagged alleles of *bcc-1* likely exhibit a reduced level of functionality (**Figure 33, Figure 35**), the insertion of 2xFLAG appears to have a greater detrimental effect on the protein's functionality compared to 3xFLAG::mCherry (**Figure 35**). Given the substantial size (~27kDa) of the fluorescent mCherry protein, it seems surprising that a mCherry::BCC-1 fusion protein retains more functionality than one with a smaller 2xFLAG (<1kDa) tag. In order to enhance the understanding of this potential impact of a FLAG tag incorporation into BCC-1, a 3D model of both the wild-type (WT) and 2xFLAG-tagged BCC-1 protein was generated using the Robetta algorithm (Baek et al. 2021). The resulting models (**Figure 38**) were subsequently visualized and annotated by color coding predicted domains using the software Chimera (Pettersen et al. 2004).

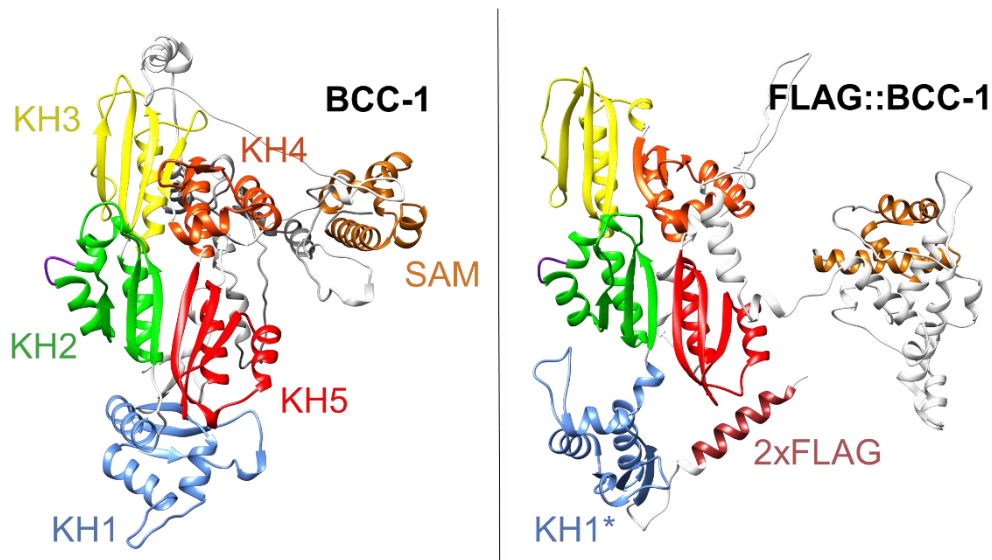


Figure 38: 3D modelling predicts a conformational change in KH-type (KH) domain 1 upon introduction of a 2xFLAG tag. Displayed is a Robetta 3D prediction derived from the primary sequence of BCC-1 (left) and BCC-1 fused to 2xFLAG (right). Colors were assigned to KHs and SAM according to predicted secondary structures. Conserved GXXG loop (GXXG1) in KH2 highlighted in purple.

According to the Robetta prediction, BCC-1 (left) exhibits a globular platform structure, consisting of four KH-type domains (KH2-5). Additionally, the algorithm predicts KH-type domains 2-5 displaying interconnectivity in contrast to KH-type domain 1, which is left out of the globular platform-like structure. The peculiar arrangement of KH-type domains 2-5 excluding KH-type domain 1, carries striking resemblance to the structural data of GLD-3 obtained through crystallography and SAXS (Nakel et al. 2010). While it should be taken into account that the prediction of BCC-1 is biased by GLD-3 being the sole Bicaudal-C protein structure present in the protein database, it is plausible to expect a significant structural resemblance between GLD-3 and BCC-1, as they are likely successors of a common ancestral protein. In the context of structure-function ties, Nakel et al. proposed that KH-type domain 1 of GLD-3 experiences a conformational change upon its interaction with the GLD-2 protein, resulting in enhanced stability of GLD-2's catalytic site (Nakel et al. 2015). A similar conformational rearrangement in KH-type domain 1 of BCC-1, potentially triggered by a yet unidentified mechanism, may account for the observed decrease in protein function following the introduction of a 2xFLAG tag. The model seen in the right panel of **Figure 38** displays a 3D representation of BCC-1, with 2x FLAG close to KH-type 1 at the N-terminus. In this model, KH-type 1 can be seen to undergo a rotation of about 90 degrees compared to the WT display. Consequently, it seems plausible that the introduction of the helically arranged 2xFLAG tag results in increased rigidity, hence imposing stereochemical limitations on KH-type 1 and further resulting in a partial diminishment of the protein's functional properties.

This observation aligns with the notion that the tagged *bcc-1(ef122)* allele performs most close to the wild type (**Figure 35, B**). This allele encodes a BCC-1 variant with a 27 amino acid linker preceding the beginning of KH-type 1 potentially providing additional flexibility. It should also be noted that Robetta predicts not only KH-type domain 1 but also the orientations of the IDR and the SAM domain differently after introduction of 2xFLAG to BCC-1. However, the low structural characteristics of the IDR enable a wide range of possible orientations, irrespective of minor, distant N-terminal variations. Additionally, the SAM retains its structural integrity consisting of five helices in both setups, not indicating a potential loss of function. Taken together, it appears that the presence of flexibility in the proximity to the N-terminus, which is restricted by the addition of 2xFLAG, may be a crucial need for BCC-1 to effectively carry out its intended function.

If BCC-1's function suffers from N-terminal tagging, it seems reasonable to assume that the same might be true for other Bicaudal-C proteins. A hypothesized loss of flexibility described above may result in fewer binding partners or weaker interactions. This may lead to different experimental outcomes, e.g. in co-immunoprecipitation experiments, which have been conducted using HA-tagged vertebrate Bicaudal-C (Dowdle et al. 2019; Rothé et al. 2015). While studies using HA-tagged Bic-C have the protein tagged in the IDR and not N-terminally, a loss-of-function still might have gone unnoticed. The possibility of this scenario is increased when the fact that the IDR of Bic-C protein GLD-3 has been suggested to be an interaction surface is taken into account (Eckmann, personal communication).

BCC-1 likely binds RNA *in vivo* and is associated with the Ccr4-Not complex

RNAi feeding experiments targeting *nekl-3* have demonstrated that the first GXXG motif, a putative RNA-binding domain in KH-type domain 2, is essential for the role of BCC-1 in molting (**Figure 36**). Notably, the crucial GXXG(1) motif is predicted as an actual loop (**Figure 38**, purple color) rather than adopting a secondary structure and is oriented outward. This observation aligns with the notion that the GXXG loop potentially interacts with external elements, such as RNA molecules. A study conducted by Dowdle et al. demonstrated the *in vivo* binding of RNA by Bicaudal-C in frogs, facilitated by the corresponding GXXG sequence containing identical amino acids located in KH-domain 2 (Dowdle et al. 2019). Interestingly, all studied Bicaudal-C proteins contain a highly conserved GXXG motif in KH-type domain 2 (**Figure 2**), with the exception of GLD-3, which possesses a SxxG loop and was shown to exhibit poor RNA affinity (Nakel et al. 2010). From an evolutionary perspective, it may be argued that the disappearance of GXXG in GLD-3 may have been

tolerated due to the presence of BCC-1 in the same system, which nevertheless retains the GXXG motif. Moreover, Bic-C proteins typically exhibit exactly 5 KH-type domains (Gamberi and Lasko 2012) arguing for a strong selection pressure presumably arising from 3D dimensional KH-type domain scaffolds as seen in **Figure 38**. Taken together, the data supports the idea of BCC-1 being an RNA-binding protein and further underscores the importance of an evolutionary conserved RNA-binding motif and adjacent KH-type domains for *in vivo* Bicaudal-C function.

Given that BCC-1 is an RBP, it remains to be answered if BCC-1 contributes to translational activation or repression. One finding of RNAi feeding against molting factors in this study involved the suppression of cuticle defective phenotypes not only through loss of *bcc-1*, but also through loss of *ccr-4* (**Figure 37**), a gene encoding for the deadenylase CCR-4. Notably, a suppressive effect has not been observed for either of the two *parn* loci (**Figure 37**) encoding for the physically different deadenylases PARN-1 or PARN-2. This supports the idea that a reduced occurrence of cuticle defects is specifically linked to the deadenylation process mediated by the Ccr4-Not complex, rather than being a generic consequence of altered deadenylation capability. While this interpretation infers a more significant connection between *bcc-1* and *ccr-4*, it is important to note that for *C. elegans* the Ccr4-Not complex is suggested to be the primary deadenylation factor (Nousch et al., 2013). This assumption is supported by evidence showing that the absence of certain components constituting the Ccr4-Not complex, but not other deadenylases, lead to significant impairments in deadenylation at the organismal level (Nousch et al., 2013). If the *parn* deadenylases are therefore considered to have minor relevance for deadenylation overall, it is possible that a connection between *parn-1/2* and *bcc-1* may have been overlooked as the impact on molting defect suppression would be weak.

If assumed that BCC-1's role in molting is connected to Ccr4-Not, the question arises as to why the suppression of molting is not as strongly seen when there is a functional loss of *ccr-4* compared to the loss of *bcc-1* (**Figure 37**). One plausible hypothesis is that the Ccr4-Not complex maintains residual function even in the absence of CCR-4, allowing for a continued interaction with BCC-1. This idea is substantiated by co-immunoprecipitation data, which reveals the consistent association of two central components, CCF-1 and NTL-1, even in the absence of CCR-4 (Nousch et al. 2013). The catalytic CCF subunit is, unlike CCR4, furthermore shown to be essential to the worm hinting at a more assisting role of CCR-4 in the complex altogether (Nousch et al. 2013). Regarding a hypothetical interaction between

BCC-1 and the Ccr4-Not complex, it may be inferred that BCC-1 might not just interact with CCR-4, but also with other constituents. Collectively, the findings of this work indicate that BCC-1 acts as an RBP recruiting the Ccr4-Not complex. As co-immunoprecipitation experiments suggested an *in vivo* association between Bic-C and the CCR4-NOT deadenylation complex in *Drosophila* (Chicoine et al. 2007), this work presents more empirical support for the association between Bic-C and deadenylation complexes. Since the bound RNA would be subjected to deadenylation, BCC-1 would be considered a translational repressor. Such a model is generally in line with Bic-C being thought to be a translational regulator, altering the fate of its mRNA targets (Gamberi and Lasko 2012). However, while mammalian Bic-C is suggested to be a repressor of (*dand5*) RNA through Ccr4-Not association (Maerker et al. 2021), in frogs the protein is hypothesized to upregulate its target (*pkd2*) RNA. Co-immunoprecipitation experiments investigating a putative association of BCC-1 and Ccr-4 Not constituents in *C. elegans* might be interesting. To investigate actual RNA targets of BCC-1, transcriptome analyses of worms expressing wild-type *bcc-1* and animals expressing *bcc-1(ef115)*, encoding a BCC-1 protein with altered RNA-binding capabilities, could provide additional insights.

BCC-1 functions likely through SAM-SAM interactions

Through Y2H experiments, this study revealed MLT-3 as a likely physical protein interactor of BCC-1 (**Figure 29**). This interaction is consistent with the suggested interaction of the mammalian homologs ANKS3 and BICC1 (Rothé et al. 2018). Beyond that, this study revealed that BCC-1 is able to interact with its mammalian counterpart, BICC1, as seen in **Figure 28**. In conjunction with the findings of Rothé et al., which indicate that BICC1 has the ability to undergo self-polymerization *in vitro* via its SAM domain (Rothé et al. 2015), the likelihood of a homo-polymerization of BCC1 molecules is increased. However, direct evidence of this interaction in the yeast system was not obtained due to the issue of BCC-1 autoactivation, as seen in **Figure 28**.

Another notable aspect is that both MLT-3 and BCC-1, like their vertebrate analogs, include a SAM domain, indicating that the observed physical connection is in fact facilitated by this domain prone to interact with itself. This assumption is further strengthened by the finding that no interaction could be demonstrated between BCC-1 or MLT-3 with the mammalian homolog of ANKS6, MLT-2 (**Figure 29**). With regard to the suggested interaction between ANKS6 and both ANKS3 and BCC-1 in mammals through a SAM-related manner as suggested by Rothé et al., it is noteworthy that the *C. elegans* protein MLT-

2 is not predicted to possess a SAM domain (Lažetić and Fay 2017; Rothé et al. 2018). One plausible hypothesis is that this absence of a SAM domain may account for the lack of interaction between MLT-2 and both BCC-1 and MLT-3. Taken together, the entirety of the data suggests that not only the binding of BICC1 to BCC-1 but also the binding of BCC-1 to MLT-3 is likely SAM-mediated.

In total, this study found implications for the *in vivo* relevance of N- and C-terminal structures of BCC-1, which seem to align with what has been suggested for Bicaudal-C in flies and vertebrates (Dowdle et al. 2022), making BCC-1 a typical Bic-C member not only in structure, but also in terms of function. A summary of presumed BCC-1 features in the form of a stick diagram is given in **Figure 39**.

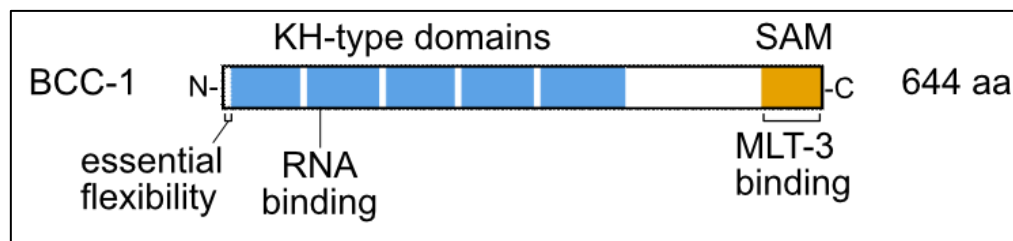


Figure 39: Summary of putative N-and C-terminal domain contributions of BCC-1. The N-terminal end of BCC-1 does not tolerate the rigidity introduced by e.g. a FLAG tag. KH-type domain 2 contains a GXXG motif which likely binds RNA and the SAM domain is a putative interaction surface for the MLT-3 protein.

BCC-1 appears to be the most trimmed protein with a mere 644 amino acids among Bicaudal-C protein in common model organisms (worms, flies, frog, zebrafish, mice). Interestingly, BCC-1 exhibits not only the shortest IDR, it also contains the shortest distance from the N-terminus to the first KH-type domain as well as the shortest distance between SAM and the C-terminal end. As it still has retained all structural features of typical Bic-C proteins, this indicates that BCC-1 was evolutionary condensed to a minimum to fulfill a molecular role that is likely also present in other species.

***bcc-1* and *gld-3* are rather complementary than redundant genes**

A primary objective of this thesis was to examine the relation between the two Bicaudal-C loci in *C. elegans*, *gld-3* and *bcc-1*. The expression pattern, structural characteristics, and biological functions of *gld-3* have been previously documented (Eckmann et al. 2002; Nakel et al. 2010; Eckmann et al. 2004). However, there remains a scarcity of published information regarding *bcc-1*. It is possible that *bcc-1* fulfills roles in the germline,

suggesting a potential redundancy to *gld-3*. Alternatively, it is possible that the two genes have undergone evolutionary changes in order to perform exclusive functions.

It was first investigated whether the expression of both *bic-c* genes overlaps in a temporal manner. By subjecting worms of different larval stages to western blotting, both isoforms of GLD-3 were found predominantly in adults and embryos (**Figure 12**), consistent with the idea that GLD-3 is maternally donated to embryos (Eckmann et al. 2002). In contrast, BCC-1 was found in all larval stages and adults, but not detected in the embryos (**Figure 12**), arguing that BCC-1 is not maternally donated. Additionally, GLD-3 expression was shown to be drastically reduced when worms exhibited only rudimentary germ line tissue (Eckmann et al. 2002). As BCC-1 expression was shown to be independent of the presence of germ line tissue (**Figure 14**), it can be concluded that BCC-1 is not predominantly a germ line protein.

This concept is further substantiated by the discovery that the absence of *bcc-1* does not diminish the number of viable progeny (**Figure 11**), while it has been demonstrated that *gld-3* is necessary for the survival of germ cells (and consequently, the size of the brood) (Eckmann et al., 2002). The observation that *bcc-1* mutants exhibit brood sizes comparable to those of wild-type worms stands in sharp contrast to previously reported RNAi experiments, which indicated a considerable reduction of 25% in brood size from wild-type (Haskell and Zinovyeva 2021). As the brood size experiments in the present study were conducted using a genetic allele of *bcc-1* instead of RNAi, an explanation for non-reduced brood could be residual function of the *bcc-1*(*ef48*) allele. However, as the protein encoded by this allele is consisting merely of the initial four amino acids, it likely is without any function. An alternative interpretation could be that the use of RNA interference against *bcc-1* may result to some degree of unintended targeting of *gld-3* transcripts. If the *gld-3* transcript is targeted alongside that of *bcc-1*, it is conceivable that the result could be a decrease in brood production. While the presence of *gld-3* could be enough to compensate for missing *bcc-1*, a role of the latter gene for normal brood size cannot be fully excluded. Yet, in the converse scenario, presence of *bcc-1* is not sufficient to make up for loss of *gld-3* (Eckmann et al. 2002).

Moreover, while *bcc-1* was not shown to fulfil a (germ line) role redundant to *gld-3*, it could still mean that *gld-3* has a function redundant to *bcc-1*. This study found *bcc-1* to be expressed in the hypodermis (**Figure 16, Figure 17**), a tissue currently not connected to *gld-3*. Furthermore, using RNAi this thesis unveiled a phenotype associated with the loss of *bcc-1* (suppression molting defects), which could not be attributed to the loss of *gld-3* as depicted in

Figure 34. In summary, the data presented in this study substantiates the hypothesis that *bcc-1* and *gld-3* exhibit unique functionalities and split their specific roles between the soma and germline. To further solidify this concept, the salt stress recovery rates of *gld-3* and *gld-3*; *bcc-1* double mutants might be insightful, as *bcc-1* was also found to have a role in osmoregulation, which might be overlapping with *gld-3*. To address the question whether *bcc-1* is at all expressed in germ line tissue, immunofluorescence using whole animals and/or solely gonads could prove useful.

***bcc-1* has a conserved role in osmoregulation**

One objective of this study was to elucidate biological functions of *bcc-1*. Remarkably, loss of *bcc-1* has not exhibited any overt defects in terms of developmental or reproductive aspects, at least within the framework of standard laboratory conditions. However, quantifiable effects of *bcc-1* loss were observed under more demanding circumstances; one being severe salt concentrations (**Figure 21, B**). As *bcc-1* protein null mutants exhibited a significantly lower recovery rate, a role in salt stress mediation can be inferred. This idea is consistent with confocal microscopy data demonstrating mCherry::BCC-1 to be expressed in cytosol of the hypodermis (**Figure 17, Figure 20**), a tissue involved in osmoregulation. Such a renal-related function would be in line with point mutations in human Bicaudal-C being associated with renal dysplasia (Kraus et al. 2012). Downregulation of Bic-C has furthermore been shown to result in kidney defects and cyst formation in the kidney equivalents of frogs and zebrafish (Tran et al. 2010; Bouvrette et al. 2010). Lastly, reduced Bic-C function in flies leads to aberrations in the Malpighian tubules (Gamberi et al. 2017). Together, a presumed function of *bcc-1* in salt-water balance seems conceivable.

Nonetheless, the only moderate reduction in salt stress recovery in *bcc-1* mutants and the absence of BCC-1 signal in the EC cell (**Figure 25**), which is the primary tissue involved in osmoregulation, suggests that the protein may not play a central role in the process of salt-water balance. Furthermore, while confocal microscopy reveals a relocalization of mCherry::BCC-1 upon exposure to high salt concentration, a similar effect was observed after heat shock treatments (**Figure 23**). In both scenarios, the otherwise homogeneously distributed mCherry::BCC-1 signal became distorted, less smooth and therefore more granular. *bcc-1* might therefore be associated with the regulation of stress in a broader sense rather than specifically salt stress. Studies in vertebrate cell culture indicate that Bicaudal-C is recruited into stress-induced foci known as P-bodies, essentially through its SAM domain (Maisonneuve et al. 2009). Whether the invertebrate BCC-1 protein is relocated upon stress

into similar structures remains elusive in this study, but the finding that mCherry::BCC-1 signal returns to a homogenous distribution eventually after stress conditions have been lifted (**Figure 24**) would be consistent with a concept of *bcc-1* regulating stress. Further insights into whether BCC-1 gets recruited into stress dependent foci could be obtained by confocal microscopy using strains expressing fluorescently tagged granule markers and mCherry::BCC-1. To investigate if such a relocalization is SAM-dependent, the expression pattern could be analysed of strains that have the SAM removed from *bcc-1(ef58)* using CRISPR/Cas9.

Molting emerges as a role Bicaudal-C

This study aimed to characterize *bcc-1* regarding its expression and putative functions. Developmental western blotting demonstrated BCC-1 expression in all stages except for embryos. Furthermore, using confocal microscopy, mCherry::BCC-1 expression was shown to be predominantly confined to *hyp7* in younger (L1) and older (L4) larvae (**Figure 19**, **Figure 17**). As one reoccurring task of larval *hyp7* is the secretion of the cuticle, a putative interaction of *bcc-1* in the process of molting was investigated and Y2H experiments revealed a likely physical interaction of BCC-1 and the molting factor MLT-3. As loss of *bcc-1* was able to suppress phenotypes resulting from loss of *mlt-3* or other molting factors (**Figure 34**), this study presents evidence for a role of *bcc-1* in molting that has been hinted at through the connection of *bcc-1* and the molting factor *rol-3* (Jones et al. 2013).

Since cell culture experiments suggest Bic-C to assemble microRNA-induced silencing complexes (Piazzon et al. 2012), one idea would be that RNAi itself might be compromised if worms lack *bcc-1* activity. However, loss of *bcc-1* did not suppress Dumpy phenotypes induced by RNAi (**Figure 32**) arguing that RNAi in somatic tissues is unaffected by *bcc-1* loss. This study therefore provides validation for the utilization of RNAi as a technique to explore the relationship between *bcc-1* and other genes while at the same time demonstrating that BCC-1 is not an essential part of the RNAi machinery in *C. elegans*.

Western blot analysis detected BCC-1 in hatched L1 larvae that lack access to food (**Figure 13**), but failed to detect the protein in embryos (**Figure 12**). This suggests that the expression of BCC-1 is likely initiated during later stages of embryonic development which are not well represented in western blot samples obtained by bleaching. In regards to molting this means that BCC-1 is present when the first cuticle needs to be shed, but not during its formation, indicating that BCC-1 is more closely associated with the processes of apolysis or ecdysis rather than the synthesis or secretion of the cuticle. Following this line of thought, it

should be noted that disorders related to all molting components mentioned in this study, namely *nekl-3*, *mlt-2*, *mlt-3* and *rol-3*, are characterized by only partial removal of the old cuticle rather than a deficiency in the formation of a new cuticle (Yochem et al. 2015; Lažetić and Fay 2017; Jones et al. 2013).

While experiments using yeast suggest a likely physical interaction of BCC-1 and MLT-3, an interaction between BCC-1 and MLT-2 could not be shown (**Figure 29**). Yet, in RNAi experiments, an alleviation of molting phenotypes is not only seen when *mlt-3* is targeted, but also when animals are RNAi treated against *mlt-2* (**Figure 34**). Microscopy data argues for a localization pattern of MLT-2 different from MLT-3 (Lažetić and Fay 2017). The results of this study therefore indicate that BCC-1 has a role in regulating the molting process, not solely through its direct interaction with MLT-3. This line of thought is consistent with the observation that deficiencies in cuticle shedding facilitated by a mutation in another epithelial but otherwise seemingly unrelated gene, *rol-3*, are also not seen in the background of *bcc-1* deletion mutant (Jones et al. 2013).

Although the precise function of *bcc-1* in the molting process remains vague, it is plausible that a correlation between *bcc-1* and several components involved in molting exists. BCC-1 might be associated with deadenylation complexes and functioning as a repressor of bound transcripts as discussed before. One simple explanation concerning its role in molting would therefore be that *bcc-1* functions as an inhibitor of molting binding pro-molting transcripts. In this particular setting, the reduction of pro-molting factors would be attenuated through the elimination of a repressor. An alternative scenario could involve the regulation of *bcc-1* by molting factors, in which a misregulation of *bcc-1* resulting from reduced molting factor activity would lead to observable skin aberrations. The absence of BCC-1 in the system would then remove the potential for such misregulation. If *bcc-1* suppresses the act of molting in any manner, it could be expected that the lack of *bcc-1* alone would lead to traits such as early molting or accelerated development into maturity compared to wildtype worms. However, such phenotypes have not been observed in this study or described in other studies where *bcc-1* was compromised (Jones et al. 2013; Haskell and Zinovyeva 2021). Moreover, the suppressive effect of *bcc-1* loss was weaker when feeding started in the parental generation (**Figure 31, Figure 34**)

. Together, this indicates that the repressive effect of *bcc-1* on molting is only seen in a narrow window of molting factor activity: If the genetic activity of a molting component (hence referred to as *mlt-x*) is normal, the molting process is occurring whether *bcc-1* is active

or not. Likewise, if *mlt-x* activity is drastically reduced, like it would be in a null mutant allele or through very efficient RNAi, molting will, irrespective of *bcc-1*'s presence, not happen. That loss of *bcc-1* promotes molting is only apparent when *mlt-x* activity is reduced to an amount somewhere above zero. In addition, *mlt-x* might regulate the function of *bcc-1*. A visualization of this concept is given in **Figure 41**.

If assumed that BCC-1 protein acts as a facilitator of molting, the question remains how it might fulfil this task. One naive concept proposes that the quantity of BCC-1 directly impacts the procedure of molting. In this setting, it could be expected that the quantity of BCC-1 is going to show fluctuation across repeated molting cycles. According to Hendriks et al. *bcc-1* RNA exhibits oscillations that may have resemblance to a molting cycle (Hendriks et al. 2014). However, this study did not identify any discernible alteration in protein abundance, at least during the initial larval stage (**Figure 13**). The likelihood of a regulation being implemented just through BCC-1 amount appears therefore to be limited. The fly system proposes an alternate concept, particularly phosphorylation as *in vitro* kinase assays suggest phosphorylation of Bicaudal-C by a (PNG) kinase (Hara et al. 2018). Similar to other generic Bicaudal-C proteins, BCC-1 possesses an area characterized by inherent lack of structure including a section that exhibits a notable abundance of serine amino acid residues serving as potential targets for phosphorylation events.

To evaluate whether BCC-1 might be subjected to phosphorylation, PhosphoSVM, a computational method employed for the prediction of phosphorylation sites derived from primary amino acid sequences, was utilized (Dou et al., 2014). The results, shown in **Figure 40**, show a substantial probability of phosphorylation within the intrinsically disordered region of BCC-1.

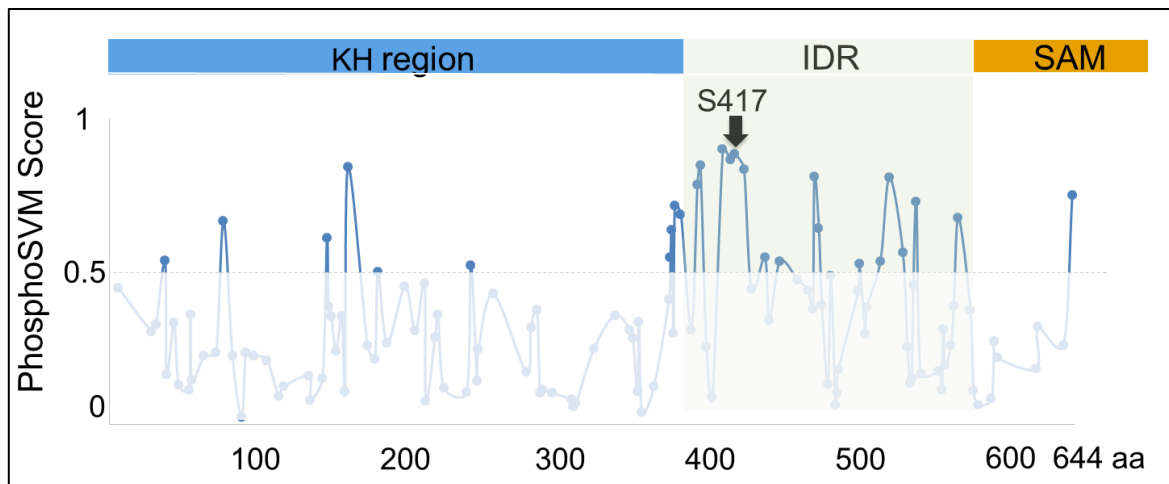


Figure 40: Phosphorylation likely occurs in the intrinsically disordered region (IDR) of BCC-1. PhosphoSVM Scores are listed for all amino acids (aa) of BCC-1, with corresponding domains listed above. Scores above 0.5 are considered to be likely targets for phosphorylation. A serine residue found phosphorylated by Zielinska et al. is indicated.

Additionally, a research endeavour aimed at characterizing the phosphoproteome through utilization of mass spectrometry documented the phosphorylation of a serine residue at position 417, suggesting that phosphorylation in the IDR of BCC-1 happens *in vivo* (Zielinska et al., 2009). Taken together, it appears reasonable to speculate that the control of molting to a certain degree might take place via phosphorylated BCC-1. A conceivable model could be that BCC-1, through its SAM-dependent binding to MLT-3, is brought into physical proximity of the kinase NEKL-3. As MLT-3 is suggested to also bind NEKL-3 (Lažetić and Fay 2017) the kinase could then regulate the activity of BCC-1 through phosphorylation presumably targeting serine residues in the IDR. As a result, phosphorylated BCC-1 would not negatively interfere with molting. By knocking down either *mlt-3* or *nekl-3* through RNAi, the amount of corresponding protein is reduced leading to a misregulation of BCC-1. In turn, this gives rise to molting phenotypes which can be suppressed by removing *bcc-1* activity and therefore the BCC-1 protein. An illustration of this hypothesis in the context of *mlt-3* knockdown is given in **Figure 41**.

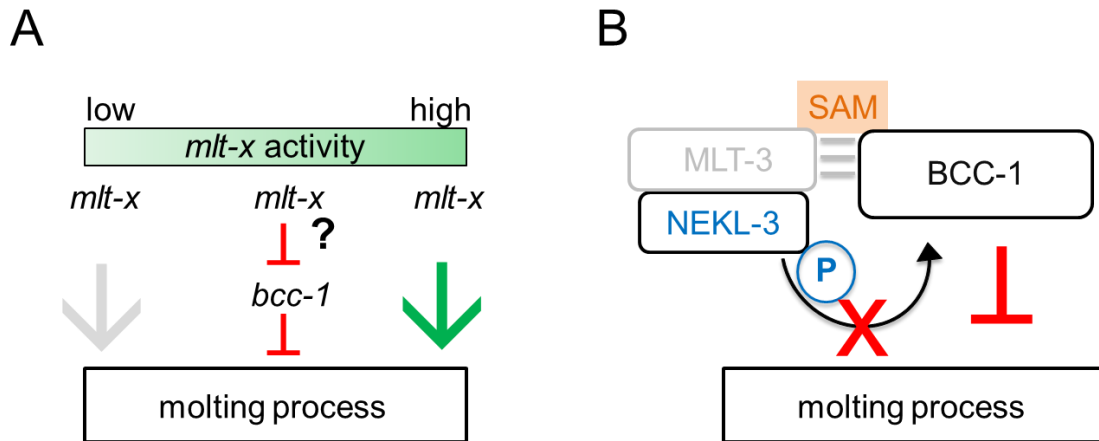


Figure 41: A hypothetical model explanation explaining *bcc-1* related suppression of molting. (A) On the genetic level, the activity of a molting factor, *mlt-x*, is required to induce molting. At reduced *mlt-x* levels, *bcc-1* represses molting but is unable to do so at full *mlt-x* activity. A potential regulation of *bcc-1* by *mlt-x* is indicated with a question mark. (B) Molecular realization on the level of gene products exemplified by BCC-1 and the molting factors MLT-3 and NEKL-3. The loss of MLT-3 leads to molting defects. If MLT-3 was present, it would simultaneously bind BCC-1 in a SAM-mediated manner and NEKL-3 resulting in the phosphorylation of BCC-1 by the kinase NEKL-3. Absence of either molting protein leads to unregulated, non-phosphorylated BCC-1 repressing the molting process. Removal of BCC-1 also restores the ability to molt.

The idea that BCC-1 is subjected to regulation through posttranslational modifications is reinforced by western blot results detecting multiple variants of BCC-1 (**Figure 7**, **Figure 9**, **Figure 12**). These variants are constantly detected throughout the worm's larval stages (**Figure 12**). Furthermore, the notion that only one BCC-1 band remains fairly stable over time (**Figure 9**) can be interpreted as PTMs being taken away, meaning that the protein has been post-translationally modified at some point.

The precise function and molecular aspects of *bcc-1* in the molting process remains a conundrum. However, it is noteworthy that although Bic-C proteins have been investigated in several metazoans, molting is a mechanism absent in most of them. Yet, with the majority of known animals undergoing molting events of some sorts, a biologically fundamental part of Bic-C in general likely has been neglected so far. As *bcc-1* is not essential to the worm, the gene can be altered in numerous further ways using CRISPR/Cas9. Combined with RNAi against molting factors this will allow for further characterization of functional domains of the BCC-1 protein. The substantial conservation of Bic-C and its protein interaction partners across several species, ranging from worms to mammals, enables the transfer of insights from BCC-1 to other systems regarding specific molecular mechanisms. Bicaudal-C is implicated in several medical conditions, with polycystic kidney disease being the most prominent. As

researching Bic-C using mammals is challenging in terms of time, labor, ethics and due to the essential nature of the protein, this study suggests *C. elegans* as a suitable model system to investigate somatic aspects of Bicaudal-C.

Literature

Aguinaldo, A. M. A., Turbeville, J. M., Linford, L. S., Rivera, M. C., Garey, J. R., Raff, R. A., & Lake, J. A. (1997): Evidence for a clade of nematodes, arthropods and other moulting animals. In *Nature* 387 (6632) pp. 489–493. DOI: 10.1038/387489a0

Antoine Cléry and Frédéric H.-T. Allain. (2013): From structure to function of RNA binding domains. In *Madame Curie Bioscience Database*

Arribere, Joshua A.; Bell, Ryan T.; Fu, Becky X. H.; Artiles, Karen L.; Hartman, Phil S.; Fire, Andrew Z. (2014): Efficient marker-free recovery of custom genetic modifications with CRISPR/Cas9 in *Caenorhabditis elegans*. In *Genetics* 198 (3), pp. 837–846. DOI: 10.1534/genetics.114.169730.

Artan, Murat; Barratt, Stephen; Flynn, Sean M.; Begum, Farida; Skehel, Mark; Nicolas, Armel; Bono, Mario de (2021): Interactome analysis of *Caenorhabditis elegans* synapses by TurboID-based proximity labeling. In *The Journal of Biological Chemistry* 297 (3), p. 101094. DOI: 10.1016/j.jbc.2021.101094.

Barr, M. M.; DeModena, J.; Braun, D.; Nguyen, C. Q.; Hall, D. H.; Sternberg, P. W. (2001): The *Caenorhabditis elegans* autosomal dominant polycystic kidney disease gene homologs *lov-1* and *pkd-2* act in the same pathway. In *Current biology : CB* 11 (17), pp. 1341–1346. DOI: 10.1016/s0960-9822(01)00423-7.

Barr, M. M.; Sternberg, P. W. (1999): A polycystic kidney-disease gene homologue required for male mating behaviour in *C. elegans*. In *Nature* 401 (6751), pp. 386–389. DOI: 10.1038/43913.

Barton, M. K.; Kimble, J. (1990): *fog-1*, a regulatory gene required for specification of spermatogenesis in the germ line of *Caenorhabditis elegans*. In *Genetics* 125 (1), pp. 29–39. DOI: 10.1093/genetics/125.1.29.

Baugh, L. Ryan (2013): To grow or not to grow: nutritional control of development during *Caenorhabditis elegans* L1 arrest. In *Genetics* 194 (3), pp. 539–555. DOI: 10.1534/genetics.113.150847.

Baek, M., DiMaio, F., Anishchenko, I., Dauparas, J., Ovchinnikov, S., Lee, G. R., Wang, J., Cong, Q., Kinch, L. N., Schaeffer, R. D., Millán, C., Park, H., Adams, C., Glassman, C. R., DeGiovanni, A., Pereira, J. H., Rodrigues, A. V., van Dijk, A. A., Ebrecht, A. C., ... Baker, D. (2021): Accurate prediction of protein structures and interactions using a

three-track neural network. In *Science* 373 (6557), pp. 871–876. DOI: 10.1126/science.abj8754

Bouvrette, Denise J.; Price, Sarah J.; Bryda, Elizabeth C. (2008): K homology domains of the mouse polycystic kidney disease-related protein, Bicaudal-C (Bicc1), mediate RNA binding in vitro. In *Nephron. Experimental nephrology* 108 (1), e27–34. DOI: 10.1159/000112913.

Bouvrette, Denise J.; Sittaramane, Vinoth; Heidel, Jerry R.; Chandrasekhar, Anand; Bryda, Elizabeth C. (2010): Knockdown of bicaudal C in zebrafish (*Danio rerio*) causes cystic kidneys: a nonmammalian model of polycystic kidney disease. In *Comparative medicine* 60 (2), pp. 96–106.

Bradford, Marion M. (1976): A rapid and sensitive method for the quantitation of microgram quantities of protein utilizing the principle of protein-dye binding. In *Analytical Biochemistry* 72 (1-2), pp. 248–254. DOI: 10.1016/0003-2697(76)90527-3.

Brenner, S. (1974): The genetics of *Caenorhabditis elegans*. In *Genetics* 77 (1), pp. 71–94. DOI: 10.1093/genetics/77.1.71.

Bull, A. L. (1966): Bicaudal, a genetic factor which affects the polarity of the embryo in *Drosophila melanogaster*. In *Journal of Experimental Zoology* 161 (2) pp. 221–241. DOI: 10.1002/jez.1401610207

Byerly, L.; Cassada, R. C.; Russell, R. L. (1976): The life cycle of the nematode *Caenorhabditis elegans*. I. Wild-type growth and reproduction. In *Developmental biology* 51 (1), pp. 23–33. DOI: 10.1016/0012-1606(76)90119-6.

Chicoine, Jarred; Benoit, Perrine; Gamberi, Chiara; Paliouras, Miltiadis; Simonelig, Martine; Lasko, Paul (2007): Bicaudal-C recruits CCR4-NOT deadenylase to target mRNAs and regulates oogenesis, cytoskeletal organization, and its own expression. In *Developmental cell* 13 (5), pp. 691–704. DOI: 10.1016/j.devcel.2007.10.002.

Chisholm, A. D., & Hsiao, T. I. (2012): The *Caenorhabditis elegans* epidermis as a model skin. I: development, patterning, and growth. In *WIREs Developmental Biology* 1 (6) pp. 861–878). DOI: 10.1002/wdev.79

Chow, K. L.; Hall, D. H.; Emmons, S. W. (1995): The *mab-21* gene of *Caenorhabditis elegans* encodes a novel protein required for choice of alternate cell fates. In *Development* 121 (11), pp. 3615–3626. DOI: 10.1242/dev.121.11.3615.

Cogswell, Cathy; Price, Sarah J.; Hou, Xiaoying; Guay-Woodford, Lisa M.; Flaherty, Lorraine; Bryda, Elizabeth C. (2003): Positional cloning of jcpk/bpk locus of the mouse. In *Mammalian genome : official journal of the International Mammalian Genome Society* 14 (4), pp. 242–249. DOI: 10.1007/s00335-002-2241-0.

Collart, M. A., & Panasenko, O. O. (2012): The Ccr4–Not complex. In *Gene* 492 (1) pp. 42–53. DOI: 10.1016/j.gene.2011.09.033

Conte, Darryl; MacNeil, Lesley T.; Walhout, Albertha J. M.; Mello, Craig C. (2015): RNA Interference in *Caenorhabditis elegans*. In *Current protocols in molecular biology* 109, 26.3.1-26.3.30. DOI: 10.1002/0471142727.mb2603s109.

Delestré, Laure; Bakey, Zeineb; Prado, Cécilia; Hoffmann, Sigrid; Bihoreau, Marie-Thérèse; Lelongt, Brigitte; Gauguier, Dominique (2015): ANKS3 Co-Localises with ANKS6 in Mouse Renal Cilia and Is Associated with Vasopressin Signaling and Apoptosis In Vivo in Mice. In *PLoS ONE* 10 (9), e0136781. DOI: 10.1371/journal.pone.0136781.

Deltas, C. C. (2001): Mutations of the human polycystic kidney disease 2 (PKD2) gene. In *Human mutation* 18 (1), pp. 13–24. DOI: 10.1002/humu.1145.

Dou, Yongchao; Yao, Bo; Zhang, Chi (2014): PhosphoSVM: prediction of phosphorylation sites by integrating various protein sequence attributes with a support vector machine. In *Amino acids* 46 (6), pp. 1459–1469. DOI: 10.1007/s00726-014-1711-5.

Dowdle, Megan E.; Kanzler, Charlotte R.; Harder, Cole R. K.; Moffet, Samuel; Walker, Maya N.; Sheets, Michael D. (2022): Bicaudal-C Post-transcriptional regulator of cell fates and functions. In *Front. Cell Dev. Biol.* 10, p. 981696. DOI: 10.3389/fcell.2022.981696.

Dowdle, M. E., Imboden, S. B., Park, S., Ryder, S. P., & Sheets, M. D. (2017): Horizontal Gel Electrophoresis for Enhanced Detection of Protein-RNA Complexes. In *Journal of Visualized Experiments* 125. DOI: 10.3791/56031

Dowdle, Megan E.; Park, Sookhee; Blaser Imboden, Susanne; Fox, Catherine A.; Houston, Douglas W.; Sheets, Michael D. (2019): A single KH domain in Bicaudal-C links mRNA binding and translational repression functions to maternal development. In *Development* 146 (10). DOI: 10.1242/dev.172486.

Eckmann, Christian R.; Crittenden, Sarah L.; Suh, Nayoung; Kimble, Judith (2004): GLD-3 and control of the mitosis/meiosis decision in the germline of *Caenorhabditis elegans*. In *Genetics* 168 (1), pp. 147–160. DOI: 10.1534/genetics.104.029264.

Eckmann, Christian R.; Kraemer, Brian; Wickens, Marvin; Kimble, Judith (2002): GLD-3, a bicaudal-C homolog that inhibits FBF to control germline sex determination in *C. elegans*. In *Developmental cell* 3 (5), pp. 697–710. DOI: 10.1016/S1534-5807(02)00322-2.

Fields, S.; Song, O. (1989): A novel genetic system to detect protein-protein interactions. In *Nature* 340 (6230), pp. 245–246. DOI: 10.1038/340245a0.

Frøkjær-Jensen, Christian; Davis, M. Wayne; Ailion, Michael; Jorgensen, Erik M. (2012): Improved Mos1-mediated transgenesis in *C. elegans*. In *Nature methods* 9 (2), pp. 117–118. DOI: 10.1038/nmeth.1865.

Frøkjær-Jensen, Christian; Davis, M. Wayne; Hopkins, Christopher E.; Newman, Blake J.; Thummel, Jason M.; Olesen, Søren-Peter et al. (2008): Single-copy insertion of transgenes in *Caenorhabditis elegans*. In *Nature genetics* 40 (11), pp. 1375–1383. DOI: 10.1038/ng.248.

Gamberi, Chiara; Hipfner, David R.; Trudel, Marie; Lubell, William D. (2017): Bicaudal C mutation causes myc and TOR pathway up-regulation and polycystic kidney disease-like phenotypes in *Drosophila*. In *PLoS Genetics* 13 (4), e1006694. DOI: 10.1371/journal.pgen.1006694.

Gamberi, C., & Lasko, P. (2012): The Bic-C Family of Developmental Translational Regulators. In *Comparative and Functional Genomics 2012* pp. 1–23). DOI: 10.1155/2012/141386

Garcia, L. R.; Mehta, P.; Sternberg, P. W. (2001): Regulation of distinct muscle behaviors controls the *C. elegans* male's copulatory spicules during mating. In *Cell* 107 (6), pp. 777–788. DOI: 10.1016/S0092-8674(01)00600-6.

Gerstberger, S., Hafner, M., & Tuschl, T. (2014): A census of human RNA-binding proteins. In *Nature Reviews Genetics* 15 (12) pp. 829–845. DOI: 10.1038/nrg3813

Gietz, R. Daniel; Woods, Robin A. (2006): Yeast transformation by the LiAc/SS Carrier DNA/PEG method. In *Methods in molecular biology (Clifton, N.J.)* 313, pp. 107–120. DOI: 10.1385/1-59259-958-3:107.

Gilleard, J. S.; Barry, J. D.; Johnstone, I. L. (1997): cis regulatory requirements for hypodermal cell-specific expression of the *Caenorhabditis elegans* cuticle collagen gene *dpy-7*. In *Molecular and Cellular Biology* 17 (4), pp. 2301–2311. DOI: 10.1128/MCB.17.4.2301.

Green, J. B., Gardner, C. D., Wharton, R. P., & Aggarwal, A. K. (2003): RNA Recognition via the SAM Domain of Smaug. In *Molecular Cell* 11 (6) pp. 1537–1548. DOI: 10.1016/s1097-2765(03)00178-3

Hahn-Windgassen, Annett; van Gilst, Marc R. (2009): The *Caenorhabditis elegans* HNF4alpha Homolog, NHR-31, mediates excretory tube growth and function through coordinate regulation of the vacuolar ATPase. In *PLoS Genetics* 5 (7), e1000553. DOI: 10.1371/journal.pgen.1000553.

Haskell, D., & Zinovyeva, A. (2021): KH domain containing RNA-binding proteins coordinate with microRNAs to regulate *Caenorhabditis elegans* development. In *G3 Genes/Genomes/Genetics* 11 (2) DOI: 10.1093/g3journal/jkab013

Hendriks, Gert-Jan; Gaidatzis, Dimos; Aeschimann, Florian; Großhans, Helge (2014): Extensive oscillatory gene expression during *C. elegans* larval development. In *Molecular cell* 53 (3), pp. 380–392. DOI: 10.1016/j.molcel.2013.12.013.

Hodgkin, J.; Barnes, T. M. (1991): More is not better: brood size and population growth in a self-fertilizing nematode. In *Proceedings. Biological sciences* 246 (1315), pp. 19–24. DOI: 10.1098/rspb.1991.0119.

Hwang, Woong Y.; Fu, Yanfang; Reyon, Deepak; Maeder, Morgan L.; Tsai, Shengdar Q.; Sander, Jeffry D. et al. (2013): Efficient genome editing in zebrafish using a CRISPR-Cas system. In *Nature biotechnology* 31 (3), pp. 227–229. DOI: 10.1038/nbt.2501.

Igual Gil, C., Jarius, M., von Kries, J. P., & Rohlfing, A.-K. (2017): Neuronal Chemosensation and Osmotic Stress Response Converge in the Regulation of aqp-8 in *C. elegans*. In *Frontiers in Physiology* 8 DOI: 10.3389/fphys.2017.00380

Johnstone, I. L., & Barry, J. D. (1996): Temporal reiteration of a precise gene expression pattern during nematode development. In *The EMBO Journal* 15 (14) pp. 3633–3639. DOI: 10.1002/j.1460-2075.1996.tb00732.x

Jones, Martin R.; Rose, Ann M.; Baillie, David L. (2013): The ortholog of the human proto-oncogene ROS1 is required for epithelial development in *C. elegans*. In *Genesis (New York, N.Y. : 2000)* 51 (8), pp. 545–561. DOI: 10.1002/dvg.22405.

Katzen, Federico (2007): Gateway(®) recombinational cloning: a biological operating system. In *Expert opinion on drug discovery* 2 (4), pp. 571–589. DOI: 10.1517/17460441.2.4.571.

Kedersha, N., Stoecklin, G., Ayodele, M., Yacono, P., Lykke-Andersen, J., Fritzler, M. J., Scheuner, D., Kaufman, R. J., Golan, D. E., & Anderson, P. (2005): Stress granules and processing bodies are dynamically linked sites of mRNP remodeling. In *The Journal of Cell Biology* 169 (6) pp. 871–884. DOI: 10.1083/jcb.200502088

Kim, C., Gingery, M., Pilpa, R. (2002): The SAM domain of polyhomeotic forms a helical polymer. In *Nat Struct Mol Biol* 9 pp. 453–457. DOI: 10.1038/nsb802

Knight, M. J., Leettola, C., Gingery, M., Li, H., & Bowie, J. U. (2011): A human sterile alpha motif domain polymerizome. In *Protein Science* 10, pp. 1697–1706. DOI:10.1002/pro.703

Krasnow, M. A., Saffman, E. E., Kornfeld, K., & Hogness, D. S. (1989): Transcriptional activation and repression by Ultrabithorax proteins in cultured Drosophila cells. In *Cell* 57 (6) pp. 1031–1043. DOI: 10.1016/0092-8674(89)90341-3

Kugler, J.-M., Chicoine, J., & Lasko, P. (2009): Bicaudal-C associates with a Trailer Hitch/Me31B complex and is required for efficient Gurken secretion. In *Developmental Biology* 328 (1) pp. 160–172. DOI: 10.1016/j.ydbio.2009.01.024

Lažetić, Vladimir; Fay, David S. (2017): Conserved Ankyrin Repeat Proteins and Their NIMA Kinase Partners Regulate Extracellular Matrix Remodeling and Intracellular Trafficking in *Caenorhabditis elegans*. In *Genetics* 205 (1), pp. 273–293. DOI: 10.1534/genetics.116.194464.

Leal-Esteban, L. C., Rothé, B., Fortier, S., Isenschmid, M., & Constam, D. B. (2018): Role of Bicaudal C1 in renal gluconeogenesis and its novel interaction with the CTLH complex. In *PLOS Genetics* 14 (7) p. e1007487). DOI: 10.1371/journal.pgen.1007487

Lee, Li-Wei; Lee, Chi-Chang; Huang, Chi-Ruei; Lo, Szecheng J. (2012): The nucleolus of *Caenorhabditis elegans*. In *Journal of biomedicine & biotechnology* 2012, p. 601274. DOI: 10.1155/2012/601274.

Leettola, C. N., Knight, M. J., Cascio, D., Hoffman, S., & Bowie, J. U. (2014): Characterization of the SAM domain of the PKD-related protein ANKS6 and its interaction with ANKS3. In *BMC Structural Biology* 14 (1). DOI: 10.1186/1472-6807-14-17

Lemaire, L. A., Goulley, J., Kim, Y. H., Carat, S., Jacquemin, P., Rougemont, J., Constam, D. B., & Grapin-Botton, A. (2015): Bicaudal C1 promotes pancreatic NEUROG3+ endocrine progenitor differentiation and ductal morphogenesis. In *Development* 142 (5) pp. 858–870. DOI: 10.1242/dev.114611

Lian, P., Li, A., Li, Y., Liu, H., Liang, D., Hu, B., Lin, D., Jiang, T., Moeckel, G., Qin, D., & Wu, G. (2014): Loss of Polycystin-1 Inhibits Bicc1 Expression during Mouse Development. In *PLoS ONE* 9 (3) p. e88816. DOI: 10.1371/journal.pone.0088816

Liu, K. S.; Sternberg, P. W. (1995): Sensory regulation of male mating behavior in *Caenorhabditis elegans*. In *Neuron* 14 (1), pp. 79–89. DOI: 10.1016/0896-6273(95)90242-2.

Lunde, B. M., Moore, C., & Varani, G. (2007): RNA-binding proteins: modular design for efficient function. In *Nature Reviews Molecular Cell Biology* 8 (6) pp. 479–490). DOI: 10.1038/nrm2178

Maerker, M., Getwan, M., Dowdle, M. E., McSheene, J. C., Gonzalez, V., Pelliccia, J. L., Hamilton, D. S., Yartseva, V., Vejnar, C., Tingler, M., Minegishi, K., Vick, P., Giraldez, A. J., Hamada, H., Burdine, R. D., Sheets, M. D., Blum, M., & Schweickert, A. (2021): Bicc1 and Dicer regulate left-right patterning through post-transcriptional control of the Nodal inhibitor Dand5. In *Nature Communications* 12 (1). DOI: 10.1038/s41467-021-25464-z

Mahone, M., Saffman, E. E., & Lasko, P. F. (1995): Localized Bicaudal-C RNA encodes a protein containing a KH domain, the RNA binding motif of FMR1. In *The EMBO Journal* 14 (9) pp. 2043–2055. DOI: 10.1002/j.1460-2075.1995.tb07196.x

Maisonneuve, Charlotte; Guilleret, Isabelle; Vick, Philipp; Weber, Thomas; Andre, Philipp; Beyer, Tina et al. (2009): Bicaudal C, a novel regulator of Dvl signaling abutting RNA-processing bodies, controls cilia orientation and leftward flow. In *Development* 136 (17), pp. 3019–3030. DOI: 10.1242/dev.038174.

Mattingly, Brendan C.; Buechner, Matthew (2011): The FGD homologue EXC-5 regulates apical trafficking in *C. elegans* tubules. In *Developmental biology* 359 (1), pp. 59–72. DOI: 10.1016/j.ydbio.2011.08.011.

Mercurio, F. A., Di Natale, C., Pirone, L., Vincenzi, M., Marasco, D., De Luca, S., Pedone, E. M., & Leone, M. (2019): Exploring the Ability of Cyclic Peptides to Target SAM Domains: A Computational and Experimental Study. In *ChemBioChem* 21 (5) pp. 702–711. DOI: 10.1002/cbic.201900444

Minegishi, K., Rothé, B., Komatsu, K. R., Ono, H., Ikawa, Y., Nishimura, H., Katoh, T. A., Kajikawa, E., Sai, X., Miyashita, E., Takaoka, K., Bando, K., Kiyonari, H., Yamamoto, T., Saito, H., Constam, D. B., & Hamada, H. (2021): Fluid flow-induced left-right asymmetric decay of Dand5 mRNA in the mouse embryo requires a Bicc1-Ccr4 RNA degradation complex. In *Nature Communications* Vol. 12 (1). DOI: 10.1038/s41467-021-24295-2

Mohler, J., & Wieschaus, E. F. (1986): DOMINANT MATERNAL-EFFECT MUTATIONS OF DROSOPHILA MELANOGASTER CAUSING THE PRODUCTION OF DOUBLE-ABDOMEN EMBRYOS. In *Genetics* 112 (4), pp. 803–822. DOI: 10.1093/genetics/112.4.803

Nakel, K., Bonneau, F., Eckmann, C. R., & Conti, E. (2015): Structural basis for the activation of the *C. elegans* noncanonical cytoplasmic poly(A)-polymerase GLD-2 by GLD-3. In *Proceedings of the National Academy of Sciences* 112 (28) pp. 8614–8619. DOI: 10.1073/pnas.1504648112

Nakel, K., Hartung, S. A., Bonneau, F., Eckmann, C. R., & Conti, E. (2010): Four KH domains of the *C. elegans* Bicaudal-C ortholog GLD-3 form a globular structural platform. In *RNA* 16 (11) pp. 2058–2067. DOI: 10.1261/rna.2315010

Nicastro, G., Taylor, I. A., & Ramos, A. (2015): KH–RNA interactions: back in the groove. In *Current Opinion in Structural Biology* 30, pp. 63–70. DOI: 10.1016/j.sbi.2015.01.002

Nelson, F. K.; Riddle, D. L. (1984): Functional study of the *Caenorhabditis elegans* secretory-excretory system using laser microsurgery. In *J. Exp. Zool.* 231 (1), pp. 45–56. DOI: 10.1002/jez.1402310107.

Nguyen, C. Q.; Hall, D. H.; Yang, Y.; Fitch, D. H. (1999): Morphogenesis of the *Caenorhabditis elegans* male tail tip. In *Developmental biology* 207 (1), pp. 86–106. DOI: 10.1006/dbio.1998.9173.

Nousch, Marco; Techritz, Nora; Hampel, Daniel; Millonigg, Sophia; Eckmann, Christian R. (2013): The Ccr4-Not deadenylase complex constitutes the main poly(A) removal activity in *C. elegans*. In *J Cell Sci* 126 (Pt 18), pp. 4274–4285. DOI: 10.1242/jcs.132936.

Page, A. (2007): The cuticle. In *WormBook*. DOI: 10.1895/wormbook.1.138.1

Park, S., Blaser, S., Marchal, M. A., Houston, D. W., & Sheets, M. D. (2016): A gradient of maternal Bicaudal-C controls vertebrate embryogenesis via translational repression of mRNAs encoding cell fate regulators. In *Development* DOI:10.1242/dev.131359

Parker, R., & Sheth, U. (2007): P Bodies and the Control of mRNA Translation and Degradation. In *Molecular Cell* 25 (5) pp. 635–646. DOI: 10.1016/j.molcel.2007.02.011

Peterson, A. J., Kyba, M., Bornemann, D., Morgan, K., Brock, H. W., & Simon, J. (1997): A Domain Shared by the Polycomb Group Proteins Scm and ph Mediates Heterotypic and Homotypic Interactions. In *Molecular and Cellular Biology* 17 (11), pp. 6683–6692). DOI: 10.1128/mcb.17.11.6683

Pettersen, E. F., Goddard, T. D., Huang, C. C., Couch, G. S., Greenblatt, D. M., Meng, E. C., & Ferrin, T. E. (2004): UCSF Chimera—A visualization system for exploratory research and analysis. In *Journal of Computational Chemistry* 25 (13), pp. 1605–1612). DOI:10.1002/jcc.20084

Piasecki, Brian P.; Sasani, Thomas A.; Lessenger, Alexander T.; Huth, Nicholas; Farrell, Shane (2017): MAPK-15 is a ciliary protein required for PKD-2 localization and male mating behavior in *Caenorhabditis elegans*. In *Cytoskeleton* 74 (10), pp. 390–402. DOI: 10.1002/cm.21387.

Piazzon, N., Maisonneuve, C., Guilleret, I., Rotman, S., & Constam, D. B. (2012): Bic1 links the regulation of cAMP signaling in polycystic kidneys to microRNA-induced gene silencing. In *Journal of Molecular Cell Biology* 4 (6), pp. 398–408. DOI: 10.1093/jmcb/mjs027

Pincus, Zachary; Mazer, Travis C.; Slack, Frank J. (2016): Autofluorescence as a measure of senescence in *C. elegans*: look to red, not blue or green. In *Aging* 8 (5), pp. 889–898. DOI: 10.18632/aging.100936.

Ponting, C. P. (1995): SAM: A novel motif in yeast sterile androsophilapolyhomeotic proteins. In *Protein Science* 4 (9) pp. 1928–1930. DOI: 10.1002/pro.5560040927

Protter, D. S. W., & Parker, R. (2016): Principles and Properties of Stress Granules. In *Trends in Cell Biology* 26 (9) pp. 668–679. DOI: 10.1016/j.tcb.2016.05.004

Putnam, A., Thomas, L., & Seydoux, G. (2023): RNA granules: functional compartments or incidental condensates? In *Genes & Development* 37 (9–10) pp. 354–376. DOI: 10.1101/gad.350518.123

Qiao, F., & Bowie, J. U. (2005): The Many Faces of SAM. In *Science's STKE* 2005 (286) DOI: 10.1126/stke.2862005re7

Ran, F. Ann; Hsu, Patrick D.; Wright, Jason; Agarwala, Vineeta; Scott, David A.; Zhang, Feng (2013): Genome engineering using the CRISPR-Cas9 system. In *Nat Protoc* 8 (11), pp. 2281–2308. DOI: 10.1038/nprot.2013.143.

Rastogi, Suchita; Borgo, Ben; Pazdernik, Nanette; Fox, Paul; Mardis, Elaine R.; Kohara, Yuji et al. (2015): *Caenorhabditis elegans* glp-4 Encodes a Valyl Aminoacyl tRNA Synthetase. In *G3 (Bethesda, Md.)* 5 (12), pp. 2719–2728. DOI: 10.1534/g3.115.021899.

Ripin, N., & Parker, R. (2023): Formation, function, and pathology of RNP granules. In *Cell* 186 (22) pp. 4737–4756. DOI: 10.1016/j.cell.2023.09.006

Rohlfing, Anne-Katrin; Miteva, Yana; Moronetti, Lorenza; He, Liping; Lamitina, Todd (2011): The *Caenorhabditis elegans* mucin-like protein OSM-8 negatively regulates osmosensitive physiology via the transmembrane protein PTR-23. In *PLoS Genetics* 7 (1), e1001267. DOI: 10.1371/journal.pgen.1001267.

Rothé, B., Fortier, S., Gagnieux, C., Schmuziger, C., & Constam, D. B. (2023): Antagonistic interactions among structured domains in the multivalent Bicc1-ANKS3-ANKS6 protein network govern phase transitioning of target mRNAs. In *iScience* 26 (6) p. 106855. DOI: 10.1016/j.isci.2023.106855

Rothé, Benjamin; Gagnieux, Céline; Leal-Esteban, Lucia Carolina; Constam, Daniel B. (2020): Role of the RNA-binding protein Bicaudal-C1 and interacting factors in cystic kidney diseases. In *Cellular Signalling* 68, p. 109499. DOI: 10.1016/j.cellsig.2019.109499.

Rothé, Benjamin; Leal-Esteban, Lucia; Bernet, Florian; Urfer, Séverine; Doerr, Nicholas; Weimbs, Thomas et al. (2015): Bicc1 Polymerization Regulates the Localization and Silencing of Bound mRNA. In *Molecular and Cellular Biology* 35 (19), pp. 3339–3353. DOI: 10.1128/MCB.00341-15.

Rothé, Benjamin; Leettola, Catherine N.; Leal-Esteban, Lucia; Cascio, Duilio; Fortier, Simon; Isenschmid, Manuela et al. (2018): Crystal Structure of Bicc1 SAM Polymer and Mapping of Interactions between the Ciliopathy-Associated Proteins Bicc1, ANKS3, and ANKS6. In *Structure* 26 (2), 209-224.e6. DOI: 10.1016/j.str.2017.12.002.

Saffman, E. E., Styhler, S., Rother, K., Li, W., Richard, S., & Lasko, P. (1998): Premature Translation of oskar in Oocytes Lacking the RNA-Binding Protein Bicaudal-C. In *Molecular and Cellular Biology* 18 (8), pp. 4855–4862. DOI:10.1128/mcb.18.8.4855

Seibel, Nicole Maria; Eljouni, Jihane; Nalaskowski, Marcus Michael; Hampe, Wolfgang (2007): Nuclear localization of enhanced green fluorescent protein homomultimers. In *Analytical Biochemistry* 368 (1), pp. 95–99. DOI: 10.1016/j.ab.2007.05.025.

Singh, R. N., & Sulston, J. E. (1978): Some Observations On Moulting in *Caenorhabditis Elegans*. In *Nematologica* 24 (1) pp. 63–71. DOI: 10.1163/187529278x00074

Snee, M. J., & Macdonald, P. M. (2009): Bicaudal C and trailer hitch have similar roles in gurken mRNA localization and cytoskeletal organization. In *Developmental Biology* 328 (2) pp. 434–444. DOI: 10.1016/j.ydbio.2009.02.003

Sun, Yinyan; Yang, Peiguo; Zhang, Yuxia; Bao, Xin; Li, Jun; Hou, Wenru et al. (2011): A genome-wide RNAi screen identifies genes regulating the formation of P bodies in *C. elegans* and their functions in NMD and RNAi. In *Protein & Cell* 2 (11), pp. 918–939. DOI: 10.1007/s13238-011-1119-x.

Timmons, L.; Fire, A. (1998): Specific interference by ingested dsRNA. In *Nature* 395 (6705), p. 854. DOI: 10.1038/27579.

Tran, Uyen; Pickney, L. Mary; Ozpolat, B. Duygu; Wessely, Oliver (2007): *Xenopus* Bicaudal-C is required for the differentiation of the amphibian pronephros. In *Developmental biology* 307 (1), pp. 152–164. DOI: 10.1016/j.ydbio.2007.04.030.

Tran, Uyen; Zakin, Lise; Schweickert, Axel; Agrawal, Raman; Döger, Remziye; Blum, Martin et al. (2010): The RNA-binding protein bicaudal C regulates polycystin 2 in the kidney by antagonizing miR-17 activity. In *Development (Cambridge, England)* 137 (7), pp. 1107–1116. DOI: 10.1242/dev.046045.

Valverde, R., Edwards, L., & Regan, L. (2008): Structure and function of KH domains. In *The FEBS Journal* 275 (11) pp. 2712–2726. DOI: 10.1111/j.1742-4658.2008.06411.x

Wang, L., Eckmann, C. R., Kadyk, L. C., Wickens, M., & Kimble, J. (2002): A regulatory cytoplasmic poly(A) polymerase in *Caenorhabditis elegans*. In *Nature* 419 (6904) pp. 312–316. DOI: 10.1038/nature01039

Wessely, O., & De Robertis, E. M. (2000): The *Xenopus* homologue of Bicaudal-C is a localized maternal mRNA that can induce endoderm formation. In *Development* 127 (10), pp. 2053–2062. DOI: 10.1242/dev.127.10.2053

Yochem, John; Lažetić, Vladimir; Bell, Leslie; Chen, Lihsia; Fay, David (2015): *C. elegans* NIMA-related kinases NEKL-2 and NEKL-3 are required for the completion of molting. In *Developmental biology* 398 (2), pp. 255–266. DOI: 10.1016/j.ydbio.2014.12.008.

Zielinska, Dorota F.; Gnad, Florian; Jedrusik-Bode, Monika; Wiśniewski, Jacek R.; Mann, Matthias (2009): *Caenorhabditis elegans* has a phosphoproteome atypical for metazoans that is enriched in developmental and sex determination proteins. In *Journal of proteome research* 8 (8), pp. 4039–4049. DOI: 10.1021/pr900384k.

Zhang, Y., Cooke, A., Park, S., Dewey, C. N., Wickens, M., & Sheets, M. D. (2013): Bicaudal-C spatially controls translation of vertebrate maternal mRNAs. In *RNA* 19 (11) pp. 1575–1582. DOI:/10.1261/rna.041665.113

Zhang, Y., Forinash, K. D., McGivern, J., Fritz, B., Dorey, K., & Sheets, M. D. (2009): Spatially Restricted Translation of the xCR1 mRNA in *Xenopus* Embryos. In *Molecular and Cellular Biology* 29 (13) pp. 3791–3802. DOI: 10.1128/mcb.01865-08

Zhang, Y., Park, S., Blaser, S., & Sheets, M. D. (2014):. Determinants of RNA Binding and Translational Repression by the Bicaudal-C Regulatory Protein. In *Journal of Biological Chemistry* 289 (11) pp. 7497–7504 DOI: 10.1074/jbc.m113.526426

Zou, Lina; Di Wu; Zang, Xiao; Wang, Zi; Wu, Zixing; Di Chen (2019): Construction of a germline-specific RNAi tool in *C. elegans*. In *Scientific reports* 9 (1), p. 2354. DOI: 10.1038/s41598-019-38950-8.

Appendix

Table S1: Materials used in this study

Item	Manufacturer	Cat. No.
Adenine	SERVA	10739.02
1 Kb Plus DNA Ladder	Thermo Fisher	10787018
2-Mercaptoethanol	SERVA	39563.01
3 M Sodium acetate solution pH 5.0	SERVA	39572.01
Acetic acid	Millipore	1.000.631.011
Acrylamide/Bis solution, 19:1 (40% w/v)	SERVA	10681.01
Agar (used for 6 cm NGM plates only)	ROTH	5210.2
Agar	VWR	J637-1KG
Agarose	ROTH	5210.02
Ammonium persulfate	AppliChem	5M012857
Ampicillin	Sigma-Aldrich	A9518-25G
Aqua-Phenol pH 4.5	ROTH	A980.2
ATP	SERVA	10920.02
Bacto Peptone	Thermo Fisher	211677
Bovine Serum Albumin Standard	Thermo Fisher	23209
Bromo-chloro-indolyl-galactopyranoside (X-Gal)	Thermo Fisher	B1690
Bromophenol blue	Thermo Fisher	A18469.18
CaCl ₂	ROTH	CN92.1
Chloroform	Millipore	1.070.242.500
Cholesterol	SERVA	17101
Coomassie Brilliant Blue R-250 Dye	SERVA	17525
CSM –Leu-Trp dropout mix	MP Biomedicals	4530-522
D-Glucose	ROTH	6780.2
D-Maltose	Merck	M5885
dNTP mix	Jena Bioscience	NU-1005S
DOB medium	MP Biomedicals	4025012
DTT	Thermo Fisher	R0861
EconoFit Profinity IMAC Column	Bio-Rad	12009298
EDTA	ROTH	8040.2
Ethanol	ROTH	P075.5
Ethanolamine	Sigma-Aldrich	E9508-100ML
Ethidium Bromide	ROTH	2218.2
Filter paper	Whatman	3030917
Gelatin	Fluka Analytical	04055-500G
Glycerol	VWR	19J044109
Glycine	Sigma-Aldrich	33226-1KG
HCl (37%)	ROTH	9277.2
Horse serum	Thermo Fisher	16050122
IPTG	SERVA	26600.06
Isopropanol	AppliChem	6P011742
Isopropyl-β-D-thiogalactopyranoside (IPTG)	SERVA	26600.06
Kanamycin	ROTH	T832.2

Item	Manufacturer	Cat. No.
KCl	ROTH	HN02.3
KH ₂ PO ₄	ROTH	3904.3
Lithium Acetate	AppliChem	A3478
MgCl ₂	Millipore	1.058.331.000
MgSO ₄	Millipore	1.058.861.000
Na ₂ HPO ₄	ROTH	P030.3
NaCl	ROTH	HN00.3
NaH ₂ PO ₄	ROTH	T877.1
NaOH	ROTH	6771.1
(NH ₄) ₂ SO ₄	Merck	1.01217.1000
Nitrocellulose membrane, 0.45µm	GE Healthcare	A10021531
Nonidet P 40 (NP40) substitute	Fluka BioChemika	74.385
PageRuler prestained protein ladder	Thermo Fisher	26616
Polyethylenglycol (PEG) 3350 solution	Sigma-Aldrich	88276-1KG-F
Ponceau S red staining solution	Fluka	09189-1L-F
Protease Inhibitor Cocktail	Roche Diagnostics	11836170001
RiboLock RNase Inhibitor	Thermo Fisher	EO0382
Salmon Sperm DNA solution	CloneTech	63440
Skimmed milk powder (TSI)	REWE	23078
Sodium azide	SERVA	30175.01
Sodium dodecyl sulfate (SDS)	SERVA	20765.03
Sodium hypochlorite solution (6-14% active chlorine)	Chemsolute	1305.1000
TEMED	Thermo Fisher	17919
Tetracycline	ROTH	HP63.1
Trichloroacetic acid (TCA)	Merck	T6399
TRIS	ROTH	4855.4
Triton X-100	Merck	1.086.031.000
Tryptone	AppliChem	0A011675
Tween-20	SERVA	37470.01
Xylene cyanol	Sigma-Aldrich	X4126-10G
Yeast extract	MP Biomedicals	103303

Table S2: worm strains used in this study

Strain no.	Genotype	Made via	Comment
EV261	<i>ccr-4(tm1312) IV</i>	mutagenesis	Nousch et al., 2013
EV448	<i>parn-1(tm869) V</i>	mutagenesis	Nousch et al., 2013
EV449	<i>parn-2(tm1339)II</i>	mutagenesis	Nousch et al., 2013
EV1003	<i>bcc-1(ef48) IV</i>	CRISPR/Cas9	provided by Ryuji Minasaki
EV1012	<i>bcc-1(ef52) IV</i>	CRISPR/Cas9	provided by Ryuji Minasaki
EV1113	<i>bcc-1(ef58) IV</i>	CRISPR/Cas9	provided by Ryuji Minasaki
EV1237	<i>bcc-1(ef58ef108) IV</i>	CRISPR/Cas9	provided by Kathrin Patsias
EV1242	<i>bcc-1(ef111) IV</i>	CRISPR/Cas9	made with Kathrin Patsias
EV1243	<i>bcc-1(ef112) IV</i>	CRISPR/Cas9	made with Kathrin Patsias
EV1271	<i>bcc-1(ef115) IV</i>	CRISPR/Cas9	made with Kathrin Patsias
EV1272	<i>bcc-1(ef116) IV</i>	CRISPR/Cas9	made with Kathrin Patsias
EV1058	<i>gld-3(q730) / mln1[mls14 dpy-10(e128)] II; bcc-1(ef48) IV</i>	crossing	first independent line

Strain no.	Genotype	Made via	Comment
EV1059	<i>gld-3(q730) / mln1[mls14 dpy-10(e128)] II; bcc-1(ef48) IV</i>	crossing	second independent line
EV1066	<i>bcc-1(ef48) IV; him-5(e1490) V</i>	crossing	first independent line
EV1067	<i>bcc-1(ef48) IV; him-5(e1490) V</i>	crossing	second independent line
EV1114	<i>efls234[Cbr-unc-119(+)+ bcc-1P::3xFLAG::GFP::bcc-1 3'UTR] II; unc-119(ed3) III</i>	MosSCI	provided by Kathrin Patsias
EV1115	<i>efls234 [Cbr-unc-119(+)+ bcc-1P::3xFLAG::GFP::bcc-1 3'UTR] II; unc-119(ed3) III</i>	MosSCI	provided by Kathrin Patsias
EV1123	<i>qpls11 I; bcc-1(ef58) IV</i>	crossing	first independent line
EV1124	<i>qpls11 I; bcc-1(ef58) IV</i>	crossing	second independent line
EV1128	<i>knuSi221[fib-1p::fib-1(genomic)::eGFP::fib-1 3' UTR + unc-119(+)] II; bcc-1(ef58 [mCherry::bcc-1]) IV</i>	crossing	first independent line
EV1128	<i>knuSi221[fib-1p::fib-1(genomic)::eGFP::fib-1 3' UTR + unc-119(+)] II; bcc-1(ef58 [mCherry::bcc-1]) IV</i>	crossing	second independent line
EV1130	<i>glp-4(bn2ts) I; bcc-1(ef48) IV</i>	crossing	first independent line
EV1131	<i>glp-4(bn2ts) I; bcc-1(ef48) IV</i>	crossing	second independent line
EV1217	<i>pha-1(e2123) III; bcc-1(ef48) IV; mgEx646 [mlt-10p::gfp-pest pha-1]</i>	crossing	first independent line
EV1218	<i>pha-1(e2123) III; bcc-1(ef48) IV; mgEx646 [mlt-10p::gfp-pest pha-1]</i>	crossing	second independent line
EV1207	<i>bcc-1(q754) IV</i>	mutagenesis	JK3346 (made by Christian Eckmann)
EV1228	<i>efSi250[Cbr-unc-119(+)+ Pdpi7::3xFLAG::GFP::bcc-1 3'UTR] II; unc-119(ed3) III</i>	MosSCI	provided by Maxie Rockstroh
EV1229	<i>efSi251[Cbr-unc-119(+)+ Pdpi7::3xFLAG::GFP::bcc-1 3'UTR] II; unc-119(ed3) III</i>	MosSCI	
PT8	<i>pkd-2(sy606)</i>	mutagenesis	provided by CGC

Table S3: Oligonucleotides designed and used in this work

Primer	Sequence	Used for
CE05828(bcc1F1)	CCATCGGTCATCATCATCTT	genotyping <i>bcc-1</i>
CE05829(bcc1R1)	TCGATTCGACCTGAATCAAT	genotyping <i>bcc-1</i>
CE05830(bcc1F2)	TACACATTTTACCCGCCATT	genotyping <i>bcc-1</i>
CE05831(bcc1R2)	AAGCAGAGGCATTTGTTTTG	genotyping <i>bcc-1</i>
CE06423(bcc-1_cF2)	GAATCAGCACGAACGCTTG	sequencing <i>bcc-1</i> ORF
CE06424(bcc-1_cF3)	GGTCAATGTGTCCGTTGAC	sequencing <i>bcc-1</i> ORF
CE06425(bcc-1_cF4)	TGTAGAGGAGCATCGGGAA	sequencing <i>bcc-1</i> ORF
CE06426(bcc-1_cF5)	CTGTTAGCTCTACCACCAA	sequencing <i>bcc-1</i> ORF
CE06427(bcc-1_cF6)	CCGATCGAGGAGAAATGCT	sequencing <i>bcc-1</i> ORF
CE06428(bcc-1_cF7)	AGCTTCATCCACTAATTATGG	sequencing <i>bcc-1</i> ORF
CE06429(bcc-1_cF8)	GCTTTTTTGCTGCTCGACG	sequencing <i>bcc-1</i> ORF
CE06430(bcc-1_cR1)	GCTGCCAGGAAACAGCTAT	sequencing <i>bcc-1</i> ORF
CE06431(bcc-1_cR2)	AACCATGGAAGGATCCGTG	sequencing <i>bcc-1</i> ORF
CE06432(bcc-1_cR3)	GAGGACCATTGTGGATGG	sequencing <i>bcc-1</i> ORF
CE06433(bcc-1_cR4)	CTCGTACTCCAGATGCCAT	sequencing <i>bcc-1</i> ORF
CE06434(bcc-1_cR5)	AATACTCCCGATGGAGGAC	sequencing <i>bcc-1</i> ORF
CE06435(bcc-1_cR6)	TGGCGTCTTGACTTCCTGT	sequencing <i>bcc-1</i> ORF
CE06436(bcc-1_cR7)	ACGTCCTCCCTTGCCAATA	sequencing <i>bcc-1</i> ORF
CE06437(bcc-1_cR8)	GACCTGTTATCATTGACTCC	sequencing <i>bcc-1</i> ORF

Primer	Sequence	Used for
CE06438(bcc-1_I3F)	acattattagtttcaattcagAGATTCGAACAAAA GCGATCA	to reintroduce intron 3 into <i>bcc-1</i> cDNA sequence
CE06439(bcc-1_I3R)	taaagtaagctaaaaccttacGAATATTTATTGG AATCTGGAAA	to reintroduce intron 3 into <i>bcc-1</i> cDNA sequence
CE06440(bcc-1_I4F)	ttaaaaaaagagaaaaattacagTCAATGTGTC CGTTGACAGT	to reintroduce intron 4 into <i>bcc-1</i> cDNA sequence
CE06441(bcc-1_I4R)	ttgaaaattattataaaattatacCCTCAAGTGT TTTAAAGCTTC	to reintroduce intron 4 into <i>bcc-1</i> cDNA sequence
CE06490(bcc1_RT_1_F)	ATGGCATCTGGAGTACGAGT	RT-PCR primer for <i>bcc-1</i>
CE06491(bcc1_RT_1_R)	GCATTTCTCCTCGATCGGCT	RT-PCR primer for <i>bcc-1</i>
CE06492(bcc1_RT_2_F)	CTCCGCCATTGAATCTCCA	RT-PCR primer for <i>bcc-1</i>
CE06493(bcc1_RT_2_R)	AAATTGCCTGCGTTGCTTTT	RT-PCR primer for <i>bcc-1</i>
CE06531(pk2_s6061F)	cacTTCACCACACAAACAG	genotyping <i>pkd-2(sy606)</i>
CE06532(pk2_s6062F)	TCGCATTGTACAGAGCAAAG	genotyping <i>pkd-2(sy606)</i>
CE06533(pk2_s6063F)	CACGTGATCCTCTGTCGA	genotyping <i>pkd-2(sy606)</i>
CE06534(pk2_s6061R)	gatgtgataaccactacacc	genotyping <i>pkd-2(sy606)</i>
CE06535(pk2_s6062R)	gaaccaccgacctctgt	genotyping <i>pkd-2(sy606)</i>
CE06536(pk2_s6063R)	atgattgtgccgtatagtcg	genotyping <i>pkd-2(sy606)</i>
CE06537(pk2_606s1F)	gcatgacaaccataatgttc	genotyping <i>pkd-2(sy606)</i>
CE06538(pk2_606s2F)	caataactatctaagactaacia	genotyping <i>pkd-2(sy606)</i>
CE06539(pk2_606s3F)	aaggattggtgagactgtttt	genotyping <i>pkd-2(sy606)</i>
CE06540(pk2_606s1R)	TGCGGACGAGCGATGGG	genotyping <i>pkd-2(sy606)</i>
CE06541(pk2_606s2R)	GAGCATGGCCCCTCGTTT	genotyping <i>pkd-2(sy606)</i>
CE06542(pk2_606s3R)	ctgttcagcgagccgtc	genotyping <i>pkd-2(sy606)</i>
CE06543(pk2-2_606IR)	gtttcatggcatttatgggg	genotyping <i>pkd-2(sy606)</i>
CE06544(pk2-2_606IF)	ccggtggtgttaaaatcgg	genotyping <i>pkd-2(sy606)</i>
CE06733(bcc-1_Y2H_F)	ATTCCCGGGGGGTATGCTCCGAGAGGA TACAGTAAT	to introduce XmaI site into <i>bcc-1</i>
CE06734(bcc-1_Y2H_R)	ATTCTCGAGCTAGACTGCATATCCGTTA AGTCG	to introduce XhoI site into <i>bcc-1</i>
CE06735(mlt-2_Y2H_F)	ATTCCCGGGGGGTATGAGCGGTGCTGC AGC	to introduce XmaI site into <i>mlt-2</i>
CE06736(mlt-2_Y2H_R)	ATTCTCGAGCTACAGTGATCGGCTAAGA A	to introduce XhoI site into <i>mlt-2</i>
CE06737(mlt-3_Y2H_F)	ATTCCCGGGGGGTATGTCGTTTCGTGTC CGTTT	to introduce XmaI site into <i>mlt-3</i>
CE06738(mlt-3_Y2H_R)	ATTCTCGAGTCAAACATGTGAGGAACT TTTAAACT	to introduce XhoI site into <i>mlt-3</i>
CE06911(dpy10RNAi_F)	ATTCCCGGGGGGTGAAAAACAACGCC AAAGAA	to introduce XmaI site into <i>dpy-10</i>
CE06912(dpy10RNAi_R)	ATTCTCGAGCTACTTTCTACCGTAACCTT	to introduce XhoI site into <i>dpy-10</i>
CE06825(NEKL3_Y2H_F)	ATTCCCGGGGGGTATGGACAAAATTT GAACATC	to introduce XmaI site into <i>nekl-3</i>
CE06826(NEKL3_Y2H_R)	ATTCTCGAGTTAGAATTGCGTTGAAGGA	to introduce XhoI site into <i>nekl-3</i>
CE06839(bcc1SGdSAM1)	agTGTTCTCTGCATCAACGTGTTTTAGAG CTAGAAATAGCAAGTTA	CRISPR/Cas-9 sg template – removal of SAM from <i>bcc-1</i>
CE06840(bcc1SGdSAM2)	ACTTCCATATAATCTACAATGTTTTAGAG CTAGAAATAGCAAGTTA	CRISPR/Cas-9 sg template – removal of SAM from <i>bcc-1</i>
CE06841(bcc1SGdSAM3)	TTATTTACGGATCCTTCCAGTTTTAGAG CTAGAAATAGCAAGTTA	CRISPR/Cas-9 sg template – removal of SAM from <i>bcc-1</i>
CE06842(bcc1SGGxxG1)	TCACACATTATTGGCAAGGGGTTTTAGA	CRISPR/Cas-9 sg template –

Primer	Sequence	Used for
	GCTAGAAATAGCAAGTTA	alteration of GXXG in <i>bcc-1</i>
CE06843(<i>bcc1</i> SGGxxG2)	ATTATTGGCAAGGGAGGACGGTTTTAGA GCTAGAAATAGCAAGTTA	CRISPR/Cas-9 sg template – alteration of GXXG in <i>bcc-1</i>
CE06844(<i>bcc1</i> rT_SAM1)	CCTAGAAATGgtttgaattctcaagggtttaagttt atttcaaaaagttgaagTGTCTCTGCATaAAgcT taaTTTTCGATTCCGAACCTCACTTCCATATA ATCTACAATGGGATATTAATTATTTTCACG GATCCTT	CRIPR/Cas9 repair template – removal of SAM from <i>bcc-1</i>
CE06845(<i>bcc1</i> rT_SAM2)	atttcaaaaagttgaagTGTCTCTGCATCAACG TCGGTTTTCGATTCCGAACCTCACTTCCAT AaAAgCTtCAATaaaATATTAATTATTTTCAC GGATCCTTCCATGGTTCTTGCACAACCTT GGATGCAGTGAATACATGA	CRIPR/Cas9 repair template – removal of SAM from <i>bcc-1</i>
CE06846(<i>bcc1</i> rT_GxxG)	cagAAAGAGCGAGTTTTCGTTGAAAATGG AACTTCATCATTCTCTCACTCACACATT ATTGGCAAaGcAGGACGTGcAATTCAGA AAGTGATGAAAATGACGTCATGCCATAT ACATTTTCCAGATTCCAATAAATATTC	CRISPR/Cas-9 repair template – alteration of GXXG in <i>bcc-1</i>
CE06847(<i>bcc1</i> rT_IDR1)	GCAAACCTGAAATGGCATCTGGAGTACG AGTATTTTTGACTCCGCCATTGAATCT CCAAAATgaCaAGcTtCAGAttACTCTCCG CTCGCGGCTTCGATTTTGAAGGAGCAA AGGATATTAGCAAAAATAGgtaaggaa	CRISPR/Cas-9 repair template – stop after KH 5 in <i>bcc-1</i>
CE06854(<i>bcc1</i> SGdIDR1)	aaggaaaatctgaaggttacGTTTTAGAGCTAGA AATAGCAAGTTA	CRISPR/Cas-9 sg template –stop after KH 5 in <i>bcc-1</i>
CE06947(RT_10xG_1)	ACTACACCATCGTCGAGCAATACGAGC GTGCCGAGGGACGTCCTCCACTGGAG GAATGGACGAaCTCTACAAGggaggaggag gaggaggaggaggaggaggaCGAGAAGATACA GTAATCCAACCTCCAGATGGAAGA	CRISPR/Cas-9 repair template – introduction of 10x glycin linker in <i>bcc-1</i>
CE06948(sgRNA_A_10G)	GTAGAGCTCGTCCATTCTCGTTTTAGA GCTAGAAATAGCAAGTTA	CRISPR/Cas-9 sg template – introduction of 10x glycin linker in <i>bcc-1</i>
CE06895(<i>rec_bcc-1</i> _F)	aatGGTACCgATGCTCCGAGAGGATACA GTAAT	to introduce KpnI site into <i>bcc-1</i> (rBCC-1)
CE06896(<i>rec_bcc-1</i> _R)	CAGGTGCGACTCTCGAGCTA	to introduce XhoI site into <i>bcc-1</i> (rBCC-1)
CE06409(FLGmChr1)	CTTGTAGAGCTCGTCCATT	for genotyping <i>bcc-1</i> (<i>ef58</i>)

Table S4: List of enzymes used in this study

Enzyme	Manufacturer	Cat. No.	Buffer	Buffer Cat. No.
BamHI-HF	NEB	R3136S	rCutSmart	B6004S
DpnI	NEB	R0176S	rCutSmart	B6004S
EcoRI-HF	NEB	R3101S	rCutSmart	B6004S
EcoRV-HF	NEB	R3195S	rCutSmart	B6004S
HindIII-HF	NEB	R3104S	rCutSmart	B6004S
KpnI	NEB	R3142S	rCutSmart*	B6004S
Lambda protein phosphatase (APP)	NEB	P0753S	NEBuffer Pack for Protein MetalloPhosphatases (PMP) + MnCl ₂	B0761SVIAL + B1761SVIAL
PstI	NEB	R0140S	r3.1	B6003S
PvuII	NEB	R0151S	rCutSmart	B6004S
SspI	NEB	R3132S	rCutSmart	B6004S
SpeI	NEB	R3133S	rCutSmart	B6004S

Enzyme	Manufacturer	Cat. No.	Buffer	Buffer Cat. No.
XhoI	NEB	R0146S	rCutSmart	B6004S
XmaI	NEB	R0180S	rCutSmart	B6004S
Taq polymerase	Eckmann lab	-	PCR buffer	-
Phusion polymerase	Thermo Fisher	F530S	HF-buffer	F518L
T4 DNA ligase	Thermo Fisher	EL0013	T4 DNA ligase buffer	46300018
T4 Polynucleotide Kinase (PNK)	NEB	M0201S	T4 PNK reaction buffer	B0201S
TEV protease	Thermo Fisher	12575023	TEV-buffer + 1mM DTT	12575023

*manufacturer recommends a different but unavailable buffer

Table S5: Single guide (sg)RNAs and repair templates for CRISPR/Cas9-based alleles

Genotype	sgRNA Plasmid	ssDNA oligo repair template	Repair template
<i>bcc-1(ef48) IV</i>	pSG16*	CE05833(<i>bcc1sg2</i>)	CE05835(<i>bcc1fix2</i>)
<i>bcc-1(ef52) IV</i>	pSG16*	CE05833(<i>bcc1sg2</i>)	CE05947(<i>bcc1Fv2</i>)
<i>bcc-1(ef58) IV</i>	pSG16**	CE05833(<i>bcc1sg2</i>)	SC45, SC46
<i>bcc-1(ef58ef108) IV</i>	pSG57	CE06948(<i>sgRNA_A_10G</i>)	CE06947(<i>RT_10xG_1</i>)
<i>bcc-1(ef111) IV</i>	pSG55	CE06843(<i>bcc1SGGxxG2</i>)	CE06846(<i>bcc1rT_GxxG</i>)
<i>bcc-1(ef115) IV</i>	pSG55	CE06843(<i>bcc1SGGxxG2</i>)	CE07118(<i>bcc-1_rT_4A</i>)

*made by Dr. Ryuji Minasaki **made by Dr. Kathrin Patsias

Table S6: List of kits used in this study

Kit	Manufacturer	Cat. No.
AcTEV™ Protease	Thermo Fisher	12575023
CloneJET PCR Cloning Kit	Thermo Fisher	K1231
RevertAid	Thermo Fisher	K1621
Wizard® Plus SV Minipreps DNA Purification System	Promega	A1460
Wizard® SV Gel and PCR Clean-Up System	Promega	A9282

Table S7: MosSCI co-injection markers

Plasmid	Description	Purpose
pCFJ601	<i>eft-3P::transposase</i>	Mos Transposase enzyme
pGH8	<i>rab-3P::mCherry</i>	Pan-neuronal expressing transformation marker
pMA122	<i>hspP::peel-1</i>	Heat-induced negative selection marker
pCFJ90	<i>myo-2P:: mCherry</i>	Pharynx muscle expressing transformation marker
pCFJ104	<i>myo-3P:: mCherry</i>	Body muscle expressing transformation marker

Table S8: Transgenes used to generate MosSCI-based strains

Strain no.	Genotype	Transgene
EV1114 (line: <i>efSi233</i>)	<i>efIs23x[Cbr-unc-119(+)] + bcc-1P::3xFLAG::GFP::bcc-1 3UTR] II;</i>	pNJ294
EV1115 (line: <i>efSi234</i>)	<i>unc-119(ed3) III</i>	
EV1128 (line: <i>efSi250</i>)	<i>efSi25x[Cbr-unc-119(+)] + Pdpiy7::3xFLAG::GFP::bcc-1 3UTR] II;</i>	pGG23

Strain no.	Genotype	Transgene
EV1129 (line: <i>efSi251</i>)	<i>unc-119(ed3) III</i>	

Table S9: Plasmids for non-genome editing used in this study

Backbone	Insert	Reference
General cloning		
pL4440	none	preexisting
pLexKn2	none	preexisting
pACT2	none	preexisting
pETm41	none	preexisting
pJET	none	preexisting
pJET	<i>bcc-1</i> ORF	made in this study
	<i>mlt-2</i> ORF	made in this study
	<i>mlt-3</i> ORF	made in this study
	<i>dpy-10</i> ORF	made in this study
	<i>nekl-3</i> ORF	made in this study
Expression of recombinant BCC-1		
pETm41	<i>bcc-1</i> ORF	made in this study
RNAi feeding constructs		
pL4440	<i>fog-1</i> ORF	preexisting
	<i>bcc-1</i> ORF	made in this study
	<i>mlt-2</i> ORF	made in this study
	<i>mlt-3</i> ORF	made in this study
	<i>dpy-10</i> ORF	made in this study
	<i>nekl-3</i> ORF	made in this study
	<i>bcc-1</i> ORF	made in this study
Yeast Two-Hybrid		
PCR blunt	<i>bicc1</i> ORF	preexisting
pBTM116	<i>gld-3</i> ORF	preexisting
pLexKn2	<i>bcc-1</i> ORF	made in this study
	<i>mlt-2</i> ORF	made in this study
	<i>mlt-3</i> ORF	made in this study
	<i>nekl-3</i> ORF	made in this study
	<i>bicc1</i> ORF	made in this study
pACT2	<i>gld-2</i> ORF	preexisting
	<i>bcc-1</i> ORF	made in this study
	<i>mlt-2</i> ORF	made in this study
	<i>mlt-3</i> ORF	made in this study
	<i>nekl-3</i> ORF	made in this study
	<i>bicc1</i> ORF	made in this study

Table S10: Microbe strains used in this study

Strain	Genotype	Used for
--------	----------	----------

Strain	Genotype	Used for
<i>Escherichia coli</i>		
OP50	<i>ura-, strR, rnc-, (delta)attB::FRT-lacI-lacUV5p-T7</i>	standard feeding of <i>C. elegans</i>
DH5 α	<i>F- ϕ80lacZΔM15 Δ(lacZYA-argF)U169 recA1 endA1 hsdR17(rK-, mK+) phoA supE44 λ-thi-1 gyrA96 relA1</i>	cloning using heat shock transformation
XL1blue	<i>recA1 endA1 gyrA96 thi-1 hsdR17 supE44 relA1 lac [F proAB lacIqZΔM15 Tn10 (TetR)]</i>	cloning using heat shock transformation
HT115(DE3)	<i>F-, mcrA, mcrB, IN(rrnD-rrnE)1, rnc14::Tn10(DE3 lysogen: lacUV5 promoter -T7 polymerase</i>	RNAi feeding of <i>C. elegans</i>
BL21(DE3)	<i>F- ompT hsdS(rB- mB-) dcm+ Tetr gal endA Hte [argU ileY leuW CamR]</i>	expressing recombinant BCC-1
<i>Saccharomyces cerevisiae</i>		
L40	<i>MATa his3Δ200 trp1-901 leu2-3112 ade2 LYS2::(4lexAop-HIS3) URA3::(8lexAop-lacZ) GAL4</i>	Yeast Two-Hybrid

Table S11: Antibodies used in this thesis

ID	Type	Target	Host	Dilution	Origin
α -FLAG M2	primary	FLAG-Tag	mouse	1:500	Sigma-Aldrich
α -tubulin C4	primary	actin	mouse	1:100.000	MP Biomedicals
α -tubulin [B-5-1-2]	primary	tubulin	mouse	1:40.000	Sigma-Aldrich
α -GLD-3 [A23-1]	primary	GLD-3(L+S)	mouse	1:500	preexisting
rb24.420	primary (raw serum)	BCC-1	rabbit	undiluted	preexisting
rb7BF5	primary (raw serum)	BCC-1	rabbit	undiluted	preexisting
α -BCC-1	primary (purified serum)	BCC-1	rabbit	1:100	made in this study
α -GFP [3H9]	primary	GFP	mouse	1:1000	Chromotek
α -HA [12CA5]	primary	HA-Tag	mouse	1:500	Santa Cruz
α -LexA [D-19]	primary	LexA	mouse	1:500	Santa Cruz
α -rabbit (IRDye® 680cw)	secondary	rabbit IgG	goat	1:10.000	LI-COR
α -rabbit (IRDye® 800cw)	secondary	rabbit IgG	goat	1:10.000	LI-COR
α -mouse (IRDye® 680cw)	secondary	mouse IgG	goat	1:10.000	LI-COR
α -mouse (IRDye® 800cw)	secondary	mouse IgG	goat	1:10.000	LI-COR

Eidesstattliche Erklärung

Hiermit erkläre ich, dass ich die vorliegende wissenschaftliche Arbeit selbständig und ohne fremde Hilfe verfasst habe. Ich erkläre weiterhin, dass andere als die von mir angegebene Quellen und Hilfsmittel nicht benutzt und die den benutzten Werken wörtlich oder inhaltlich entnommenen Stellen als solche kenntlich gemacht wurden.

Mit dieser Arbeit bewerbe ich mich erstmals um die Erlangung des Doktorgrades.

Halle (Saale), den 10.12.2023

Robin Selle

Curriculum vitae

Name, Surname: Selle, Robin
Date and place of birth: 06.08.1989, Halle (Saale)
Nationality: German
E-Mail: robin.selle@genetik.uni-halle.de
Phone: 0157 357 978 97

Education

since 03/2020 PhD student in developmental genetics
Martin Luther University Halle-Wittenberg
10/2010-03/2013 Master in Biochemistry
Martin Luther University Halle-Wittenberg
10/2007-09/2010 Bachelor in Biology
Martin Luther University Halle-Wittenberg

Work experience

12/2017 - 07/2019 GMP-Officer
Bayer AG in Wuppertal
07/2014 - 11/2017 Subject Matter Expert (Fermentation)
Bayer Health Care in Wuppertal